Aus der

Orthopädischen Universitätsklinik mit Poliklinik Tübingen

Characterization of stiffness as a biomarker in osteoarthritis and in bone- and soft tissue cancers

Inaugural-Dissertation
zur Erlangung des Doktorgrades
der Medizin

der Medizinischen Fakultät
der Eberhard Karls Universität
zu Tübingen

vorgelegt von

Daniel, Cyril

2025

Dekan:	Professor Dr. B. Pichler
1. Berichterstatter:	Professor Dr. M. Ebinger
2. Berichterstatter:	Professorin Dr. D. Alexander-Friedrich
Tag der Disputation:	23.09.2025

Table of contents

List of abbreviations and acronyms ____ 2

1 Introduction ____ 3

1.1 Atomic force microscopy (AFM) ____ 4

1.2 Biomechanical properties of articular cartilage ____ 6

1.3 Biomechanical properties of bone- and soft-tissue cancers ____ 10

1.4 Aim of the thesis ____ 14

2 Results ____ 16

2.1 Addressing practical issues in atomic force microscopy-based micro-indentation on human articular cartilage explants ____ 16

2.2 An exploratory study of cell stiffness as a mechanical label-free biomarker across multiple musculoskeletal sarcoma cells ____ 39

3 Discussion ____ 51

3.1 Cartilage stiffness: a biological marker throughout the course of osteoarthritis ____ 51

3.2 Mechanical- and cytoskeletal characterization of bone- and soft-tissue cancer cell lines ____ 59

3.3 Conclusion ____ 65

4 Summary ____ 66

5 Zusammenfassung ____ 68

6 References ____ 70

7 Declaration of contribution ____ 90

8 Acknowledgements ____ 91

9 Appendix ____ 92

List of abbreviations and acronyms

Abbreviation	Definition
ADAMTS	A disintegrin and metalloproteinase with thrombospondin motifs
AFM	Atomic force microscopy
BC	Big cluster
BW	Bodyweight
CAF	Cancer-associated fibroblast
CD	Cluster of differentiation
DMD	Disease modifying drug
DS	Double string
ECM	Extracellular matrix
ELISA	Enzyme-linked immunosorbent assay
FBG	Fiber Bragg grating
HCC	Hepatocellular carcinoma
LCSC	Liver cancer stem-like cell
MMP	Matrix metalloproteinase
MSC	Mesenchymal stem cell
OA	Osteoarthritis
PCM	Pericellular matrix
qPCR	Quantitative polymerase chain reaction
SC	Small cluster
SKMC	Skeletal muscle cell
SS	Single string

1 Introduction

Biomechanical properties of living tissues are of prime importance for their survival, correct function and performance (Aszódi et al., 2006; Fletcher and Mullins, 2010; Lo et al., 2000). Proper interaction with the environment, protection from stress and fulfillment of the basic physiological functions are all processes that are closely linked to biomechanics (Mammoto et al., 2012; Provenzano and Keely, 2011). Inadequate mechanical stimulation and disturbed biomechanical properties in a tissue may lead to disease and degeneration.

In order for an organism to interact correctly with the permanent exposure to mechanical stimuli, it should be capable of protecting itself from harmful mechanical stress, sensing its environment in terms of mechanical inputs, and generating the appropriate response to those stimuli. Hence, the different living tissues have developed specific architectures and compositions that enable an adequate interaction with the environment. The cells and their surrounding connective tissue are structured in such a manner that they can naturally maintain their 3D shapes and withstand basic mechanical stress without suffering any damage (Ingber et al., 2014). Additionally, the cells possess a broad range of mechanical sensors, which enable them to discern fine mechanical stimuli and react appropriately, in a process called mechanosensing. This in turn permits the tissue involved to remodel itself in both the short and long term (Martino et al., 2018).

The complex processes that underlie mechanosensing and tissue remodeling are prone to dysregulation and can lead to disease development. Monitoring and comparing the organism´s responses to mechanical stimuli under healthy and impaired conditions can deliver important information about the pathophysiology of a disease. Several factors that play a key role in the protection from mechanical stress and the assimilation of mechanical inputs can be identified. The first of them is the extracellular matrix (ECM), which plays a relevant role in withstanding mechanical stress as a result of the particular nature and arrangement of its structural proteins. The ECM is principally composed of collagens and proteoglycans (Eyre, 2004; Iozzo and Schaefer, 2015), which exist as different subtypes and have been well characterized among the different connective tissues (Badylak, 2007). The second principal actor is the cytoskeleton, which confers the cell its own framework. The cytoskeleton is composed of actin, intermediate filaments, microtubules, and the numerous protein associated with these three main scaffold

elements (Fletcher and Mullins, 2010). Finally, assuring the link between the ECM and the intracellular milieu, a large group of regulators exist (cell-ECM adhesion molecules, sensor proteins (i.e. mechanoreceptors), signaling pathways, gene expression regulators), which enable adaptative processes and coordinate the cell response to acute or chronic mechanical stimulation (Jin et al., 2020; Lee et al., 2014; Lin et al., 2022).

A wide range of research tools are available to display and monitor those different actors. For instance, the structural components of the cell or the ECM can be directly displayed using different imaging/microscopy technics or quantified at the protein levels. Moreover, the activity of the mechanoreceptors can be monitored, and the gene expression profile of cells submitted to different mechanical stimuli can be determined. Putatively, these different components may be used as biomarkers for diagnostic or be targeted for therapeutical purposes.

The ability of a tissue or cell to resist deformation is referred to as stiffness, whereas its ability to recover its shape after the deformation generated by the applied force is referred to as elasticity. In the literature, both terms are employed to describe the mechanical properties of tissues, cells and materials. For increased consistency, the term stiffness will be preferred throughout this thesis. To measure this parameter, different devices have emerged and continuously been improved during recent decades (Cykowska et al., 2022). At the present time, atomic force microscopy (AFM) is considered the gold standard to measure the stiffness with a precision down to the nanoscale (Allison et al., 2010; Gerber and Lang, 2006).

1.1 Atomic force microscopy (AFM)

Invented in 1986, AFM (Binnig et al., 1986) is a powerful technique that allows topographic imaging, force measurement and sample manipulation up to the nanoscale level. The principle of AFM relies on the interaction between a probe – also known as a cantilever – and the surface of the investigated sample. The tip of the cantilever can consist of different materials and exhibit different forms (e.g. pyramidal, spherical, conical, needle-like or tip-less). Several operating modes are available (Dufrêne et al., 2017), the choice of which depends on the experimental design and the nature of the sample. For imaging, the device may be used in contact mode, where the cantilever is

directly driven over the sample´s surface, deflecting according to the relief, revealing detailed topography. Similar results can be achieved in dynamic mode, a procedure during which the cantilever is oscillating over the surface of the sample. The dynamic mode has the advantage of inflicting less damage on the inspected surface and hence allows a better preservation of the sample's integrity. Topographic maps realized with AFM are of high-resolution. For example, topographic scans in contact mode can reveal the relief of single membrane proteins with a resolution <1 nm (Müller et al., 1995). Regarding its force measurement capabilities (force spectroscopy), AFM has been used to investigate the physical properties of a broad range of surfaces, from artificial materials in industry to biological tissue (Karoutsos, 2009; Nandi and Ainavarapu, 2021). For this purpose, the device is typically used in contact mode. However, in this case the cantilever is not displaced over the surface of the sample (x-, y-axis) but is slowly moved vertically (i.e. on the z-axis) until its tip comes in direct contact with the surface of the sample. The bending of the cantilever resulting from the force applied at its tip can be quantified using a laser beam that reflects on the cantilever´s surface and reaches a photodiode sensor (Figure 1 in appendix). The movement of the laser beam on the photo diode is initially measured in volts and is converted into newtons after calibration of the device. The cantilever is extended into the investigated sample until a given force (i.e. "setpoint" in nN) or indentation depth is reached. The output of a measurement is a force-distance curve, depicting the extension of the cantilever up to the setpoint and its retraction. The fit of the curve using mathematical models permits calculating the Young's modulus, which is representative of the stiffness of the examined sample.

The Young´s modulus (E) is dependent of the stress applied on the surface of the sample (σ in Pa) with regard to the resulting strain (ε dimensionless) (equation 1).

$$E = \frac{\sigma}{\varepsilon} \tag{1}$$

In the case of a spherical indenter, the use of the classical Hertz model is the most established method to calculate the Young´s modulus. (Krieg et al., 2019) (equations 2 and 3).

$$F = \frac{E}{1 - v^2}\left[\frac{a^2 + R_s^2}{2} ln \frac{R_s + a}{R_s - a} - aR_s\right] \quad (2)$$

$$\delta = \frac{a}{2} ln \frac{R_s + a}{R_s - a} \quad (3)$$

Where F = force; E = Young's modulus; v = Poisson's ratio; δ = indentation; a = radius of contact circle; R_s = radius of sphere.

AFM was used in the framework of this thesis to investigate the stiffness of articular cartilage and malignant cells. In both cases, a cantilever with a spherical tip was used and the Hertz fit model was applied for the data analysis.

1.2 Biomechanical properties of articular cartilage

Healthy cartilage is a fundamental requirement for a well-functioning joint. Hyalin cartilage covers the surface of bones where they come into contact with each other. Its remarkable mechanical properties allow for a well-balanced force transfer and a smooth friction between the two surfaces in contact. Among the different joints of the human body, a broad range of degree of freedom and applied strain grades can be observed, leading to a varied demand on cartilage as a function of its localization. For example, the glenohumeral joint is known as the most mobile joint of the human body, and as a drawback of this attribute it is commonly subjected to dislocation and lesion of the periarticular apparatus (ligaments, tendons, labrum, etc.) (Quillen et al., 2004). On the other side, the large joints of the lower limb are qualified as "load bearing" since they support the whole body weight (BW) (e.g. knee and hip) and may be subjected to tremendous forces. As an example, cartilage of the knee can be exposed to forces up to 3x the BW during daily activities like stair climbing and up to 20x BW during the most demanding exercises (e.g. jumping) (D'Lima et al., 2007; Lee et al., 2017). Beside the scope of acute traumatic and sport injuries, those joints are typically prone to lesions of a degenerative nature occurring at later age and impacting the cartilage at the localization where the load transfer is at his highest, eventually leading to osteoarthritis (OA).

OA is a common disease principally affecting articular cartilage but also extending to the whole joint as it slowly progresses. At first, the cartilage surface erodes, prompting a

superficial fibrillation of the tissue. Subsequently, fissures appear, protruding into the deeper layers. Eventually a full thickness erosion of the cartilage is observed, whereby the subchondral bone is exposed to friction. The whole locale environment is turned into an inflamed-like milieu, supporting further degeneration (Scanzello 2017). The bone is also subjected to remodeling processes, with the formation of subchondral sclerosis, cysts, and osteophytes.

As previously mentioned, OA mainly affects the elderly, and notably women are more commonly affected than men. In Germany, the prevalence of the disease has been evaluated at 17.9% of the total adult (>18 years old) population. In the 18-29 years age group, OA affects 0.9% of women and 0.4% of men. By comparison, in the ≥ 65 years age group, 48.1% of woman and 31.2% of men are affected (Fuchs et al., 2017). From an etiologic point of view, OA is considered the result of the wear that the joint has experienced throughout its life, whereby factors such as genetics, physical activity habits and BW are thought to play an important role (Guilak, 2011). Nonetheless, OA can also appear at younger age, following a traumatic injury, a joint misalignment or any state leading to a repetitive and "unnatural" stress on a specific joint (typically by competitive sport or the practice of particular professions). At some point, the disease may evolve into a severe disabling condition due to the high levels of pain and joint movement restriction, leading to a pronounced decrease in the quality of life and a substantial economic burden (Safiri et al., 2020). At present, the diagnosis of OA mainly relies on clinical examination and imaging (Hunter and Bierma-Zeinstra, 2019). Established in 1957, the Kellgren-Lawrence score (Kellgren and Lawrence, 1957) remains one of the standard tools to assess OA via radiographs. Because of the broad availability of X-rays and the relative simplicity of the classification proposed, the Kellgren-Lawrence score is an attractive option for a rapid evaluation of the disease´s state. However, the inability of the score to detect OA at an early stage has been pointed out (Felson et al., 2011). For more accuracy, several authors propose the implementation of more specific yet more expensive and time-consuming methods such as MRI and diagnostic arthroscopy (Luyten et al., 2012). The most widespread classification in order to categorize OA-related lesions arthroscopically is the one that was developed by Outerbridge in the early-1960s (Outerbridge, 1961) and has since been adapted (Slattery and Kweon, 2018). It is based on haptic sensing and visual assessment of cartilage surface during arthroscopic

procedure and enables an orienting estimation of the cartilage integrity. However, due to the fact that this technique strongly relies on the individual perception of the examiner, the Outerbridge classification is criticized for being only moderately reliable (Cameron et al., 2003).

The therapeutical options to treat OA are limited. They range from a conservative strategy in the earlier stage of the disease (pain relief, physical therapies) to the use of endoprosthesis when the joints have already reached a high level of destruction. Regenerative approaches are either reserved for focal defects (Makris et al., 2015) or clinically show rather inconclusive results when applied to the whole joint (Sahin and Yesil, 2023). A rapidly growing panel of potential disease-modifying drugs (DMDs) is raising hope to provide a significant improvement of the actual therapeutical management of OA. DMDs are a large group of molecules including – among others – signaling pathways regulators, growth factors, and enzyme inhibitors (Rodriguez-Merchan, 2023). Their usage aims to influence the homeostasis within the joint in order to turn the inflammatory/catabolic processes into favorable conditions for cartilage regeneration. Clinical trials show heterogenous results depending on the DMD tested, with a clear breakthrough remaining unmet at the present time. Several authors have emphasized the fact that the potence of DMDs may not be uncovered until the selection of the patients for the clinical trials is revised. It is thought that most of those therapeutical agents are only able to reverse the course of OA if the disease is addressed at an early stage (Cai et al., 2021). This indicates that new diagnostic methods are needed, not only relying on macroscopic aspects of cartilage degeneration (like radiographs and arthroscopy evaluation does), but also detecting the fine alterations that are representative of OA onset. To this end, a deep understanding of the tissue at the cellular and molecular level is needed.

Articular cartilage is organized in a specific three-dimensional structure. The 3-5mm thick coat of tissue covering the bone can be divided in three distinct layers. The upmost layer is the superficial zone, in which the collagen fibers are oriented tangentially (i.e. bending and ending their course almost parallel to the surface) and the concentration of the chondrocytes is at its highest (Ulrich-Vinther et al., 2003). Then comes the transitional zone, which is the thickest of all and hence contributing the most to the cartilage's total volume. The orientation of the collagen fibers here is predominantly perpendicular to the

surface and the chondrocytes become more sparsely scattered. As the third zone, the deep zone delimits the final territory where the cartilage displays its classical organization with the group of chondrocytes being embedded in a soft ECM of collagen and proteoglycans. Beyond, the cells begin to be surrounded by hydroxyapatite crystals. This switch in the matrix composition is termed “mineralization” and is indicative of the zone of calcified cartilage. This zone and the deep zone are separated by a clear, histologically visible delimitation, termed the tide mark. Eventually the ECM consists exclusively of mineralized substance and chondrocytes are replaced by osteoblasts, whereby the subchondral bone is reached.

At the microscopical level, hyalin cartilage presents the peculiar architecture of connective tissue. The ECM represents the main part of the substance and contains the sparsely scattered chondrocytes, which constitute <10% of the total volume (Ulrich-Vinther et al., 2003). In the direct vicinity of the chondrocytes, a specialized version of the ECM is deployed: the pericellular matrix (PCM). The chondrocytes are grouped in small assemblies, which together with their surrounding PCM are histologically referred to as chondrons.

At the molecular level, the ECM is composed principally of collagen type II (Eyre, 2002) and the proteoglycan aggrecan (Hardingham and Fosang, 1992). Both molecules are secreted by the chondrocytes themselves and play an important role in withstanding compressive load, hence conferring cartilage its particular elastic properties (Eschweiler et al., 2021). The PCM displays a modified molecular composition, as collagen type VI and IX are predominant here (Poole et al., 1992; Poole et al., 1997) and additional specific molecules have been identified in this region (e.g. the proteoglycans perlecan and biglycan, and the glycoproteins fibrillin-1 and fibronectin-1) (Keene et al., 1997; Melrose et al., 2008; Miosge et al., 1994). The PCM has been shown to be involved in the regulation of the metabolism of the chondrocytes (Zhao et al., 2020), in mechanosensing and mechanotransduction (Guilak et al., 2006; Vincent et al., 2007). The PCM seems to be particularly altered in osteoarthritic cartilage (Guilak et al., 2018).

During OA, the previously described architecture is disrupted and interestingly the spatial organization of the chondrocytes is remodeling. The group of cells display different patterns that are specific for the grade of the cartilage degeneration. In healthy cartilage of the knee joint, the chondrocytes of the superficial zone are typically organized in small

groups of few aligned cells, whereby these formations are referred as to single strings (SS) (Rolauffs et al., 2008). As the cartilage starts to degenerate, the cells then appear to form double strings (DS) (Rolauffs et al., 2010). Subsequently, with disease progression, the cells build small clusters (SC) and big clusters (BC) (i.e. groups of >20 chondrocytes) in highly degenerated areas (Danalache et al., 2021; Rolauffs et al., 2008). Eventually a complete loss of the organization can be observed, with the chondrocytes being randomly spread across the volume of the cartilage surface, without exhibiting any recognizable pattern. This end stage is referred as to "diffuse" arrangement (Felka et al., 2016).

Interestingly, it has been shown that the stiffness of articular cartilage at the microscopic level is decreasing with progressing degeneration. This stiffness loss – measured with AFM – remarkably correlates with the cellular patterns displayed at the surface of the cartilage (Danalache et al., 2020). Articular cartilage containing SS at its surface (i.e. healthy tissue) displays the highest stiffness. The stiffness is then gradually decreasing over DS, SC and reaches its lowest value by the BC. This observation is true for both the ECM and the PCM (Danalache et al., 2019). Hence, not only the chondrocytes organization but also the stiffness of the tissue appears to be a reliable biomarker capable of providing precious indications about the actual OA stage and may be used as a highly sensitive tool to explore the pathophysiology of cartilage degeneration.

1.3 Biomechanical properties of bone- and soft-tissue cancers

Cancer is broadly defined as a pathologic cell transformation that leads to uncontrolled growth, as well as invasion and destruction of the surrounding healthy tissue. Originally these alterations are the result of uncompensated pathogenetical mechanisms, which lead to mutations in the DNA sequences at the single cell level. These cells and their descendants can then modify themselves in order to grow faster, escape the immunosurveillance and break the anatomical boundaries. The malignant cells display an altered gene expression, molecular pathways activity and surface-receptor exposition.

Major efforts have been driven to understand the molecular biology of tumors. Over recent decades, in addition to the well-known significant contributors to cancer initiation (e.g. p53 (Vousden and Lane, 2007), Wnt (Kikuchi, 2003) or Ras (Bos, 1989)), a growing number of new tumor suppressors or oncogenes have been discovered. For example, within lung carcinomas, the cancer category accounting for the most victims due to

neoplastic disease in Germany (RKI, 2023), in the adenocarcinoma subgroup alone more than fifteen genes have been reported to be mutated in over 1% of the investigated tumors (Wadowska et al., 2020). For the EGFR gene alone, which has been shown to be altered in 30-40% of lung adenocarcinomas, more than twenty different common mutations including insertions, deletions, substitutions and amplification are well known (Tsiambas et al., 2016). The characterization of a tumor is crucial for the complete medical management from diagnosis to treatment, and is furthermore an important predictor for the overall prognosis. For many cancer types, the preference for the chemotherapeutical choice is dictated by the genetic profile of the tumor. As a consequence, the field of oncology is increasingly evolving towards the discipline of personalized medicine (Riedl et al., 2023).

Aside from genetical and molecular features, neoplastic material can also be characterized based on its mechanical aspect. As a tumor develops, its mechanical properties increasingly deviate from those of the healthy tissue, at both the macroscopic and microscopic level. Macroscopically, a stiffness increase is typically observed (Butcher et al., 2009; Paszek et al., 2005). This feature is indeed commonly used clinically for primal screening/diagnostic of numerous cancer entities. The most eloquent examples are prostate and breast cancers, in which cases the presence of the tumor is often revealed by the physician's palpation (Fiorica, 2001; Naji et al., 2018). Different imaging techniques such as magnetic resonance elastography or sonography based procedures also exist and enable quantifying the stiffness of the tissue at different stages of the disease in a non-invasive manner to make assumptions about the type of the tumor, its advancement or the response to treatment (Payen et al., 2020; Pepin and McGee, 2018; Yuan et al., 2022). The enhanced stiffness observed on the overall tumor mass is principally due to reorganization at the ECM level (Deng et al., 2022). A modified secretion of matrix components from the tumor cells and the action of the cancer-associated fibroblasts (CAFs) are the leading mechanisms causing such changes (Anderson and Simon, 2020).

While looking closely at the mechanical features of tumorous tissues, strong heterogeneity can be observed. When probed at the microscopic level using AFM, tumor biopsies of breast cancer display distinct stiffness peaks within the same tumor. Indeed, the stiffness values even reach beyond both sides of the range of the usual stiffness observed in healthy tissue (i.e. tumorous material displays not only stiffer but also softer

areas compared to a control) (Plodinec et al., 2012). This is due to the fact that the different microscopical components of the tumor mass themselves exhibit very distinct mechanical properties. If it is true that neoplastic ECM is typically stiffer than that of the healthy stroma, malignant cells have been shown to be of a particularly soft nature. For instance, malignant metastatic cells of non-small cell carcinoma of the lung have been shown to be almost four times softer compared to normal mesothelial cells of the same patients (Cross et al., 2007). HeLa cells (cervical cancer) have a Young´s modulus of about 2.5 kPa, whereas healthy cervical cells' stiffness is measured around 5.5 kPa (Hayashi and Iwata, 2015). The MCF-7 cells that are representative of invasive breast ductal carcinoma have been shown to be 1.4 to 1.8 times softer than normal cells from the mammary gland (Li et al., 2008). It is thought that the loss of stiffness dispenses an advantage to cancer cells, increasing their chances regarding survival, invasion and metastatic potential (Makale, 2007). The plasticity of the cell is thereby enhanced, allowing it to carry out its malignant role, namely to find a way through the stroma of the surrounding tissue, or manage to pass through the endothelium of the blood vessel to reach the bloodstream. Indeed, it is often the case that when investigating the biomechanical properties of a pallet of cancer cell lines belonging to a given tumor entity, an inverse correlation between the invasive potential and the stiffness of the cells is observed (Abidine et al., 2015; Omidvar et al., 2014; Xu et al., 2012). In an experiment where spheroids of malignant cells were deposed into an artificial 3D matrix, and the subsequent invasion was monitored, Wullkopf et al. (2018) showed that a decreasing gradient of the cell´s viscoelasticity exists from the center of the spheroid until the tip of the invading branches. This observation suggests that even within a particular population belonging to the same cell line, the cells displaying the most aggressive behavior are once again those with the lower stiffness (Wullkopf et al., 2018). Under certain circumstances, the stiffness of the malignant cells is an adaptable parameter and it strongly relies on interaction with the microenvironment. Differences in the stiffness of the surrounding matrices not only dictate cell growth and survival (Tilghman et al., 2010) but also influence the own stiffness of the developing neoplastic cells (Wullkopf et al., 2018).

The initial efforts of understanding cancer mechanobiology have been logically turned towards the cancer entities that are the most prominent in the field of oncology. The malignant diseases displaying the highest incidence and the highest mortality, leading to

the greatest economic burden, or simply benefiting from existing and well-established cell lines are the most prominently addressed. Concretely, publications treating breast, prostate, lung, bladder, colorectal or ovarian cancers account for the large majority of the available literature on the subject (Butcher et al., 2009; Deng et al., 2018; Vasudevan et al., 2023).

Soft-tissue sarcomas and bone cancers are rather seldom tumor types. Bone cancers – which encompass the three main entities of osteosarcoma, chondrosarcoma and Ewing sarcoma – are estimated to represent less than 1% of all diagnosed cancers every year (Ferguson and Turner, 2018). Soft-tissue sarcomas – a group of more than 80 indexed subtypes (according to the WHO classification (Gronchi et al., 2021)) – form a very diverse ensemble that is difficult to follow epidemiologically. Their incidence is thought to variate between 1.8 and 5.0 per 100,000 persons per year (S3-Leitlinie „Adulte Weichgewebesarkome“, 2022). Despite their relatively low prevalences, bone and soft-tissue sarcomas remain clinically highly relevant, since they are associated with poor outcome. The five-year survival rates are estimated to hold around 62% and 58%, respectively (Stiller et al., 2013). In addition, children are particularly affected by both diseases. Bone cancers and soft-tissue sarcomas each represent approximately 5% of all malignant conditions at young age (Deutsches Kinderkrebsregister, 2019). Notably osteosarcoma and Ewing sarcoma have a peak incidence between 10 and 25 years old and when not lethal they often require limb amputation, leading to dramatic disability in young patients (Esiashvili et al., 2008; Mirabello et al., 2009).

Given the fact that bone and soft-tissue sarcomas are neoplastic transformations of connecting and supporting tissues, it may be suspected that biomechanics plays an even more significant role in the biology of those tumors. However, little is known about this topic presently. In contrary to the main cancer entities mentioned earlier, the literature concerning the mechanobiology of mesenchymal tumors is not extensive. Some studies have addressed the question of the mechanical relevance of the microenvironment in the development of bone cancers (e.g. Deng et al., 2023; Jiang et al., 2019)), although works investigating the biomechanics of the cells themselves are not frequent. Similarly, the number of publications dedicated to soft-tissue sarcomas remains limited. It is probable that musculoskeletal sarcomas behave like “classical” tumors regarding several of their physiological aspects, although it remains unclear whether and to what extent the

knowledge accumulated from breast, lung or bladder neoplasia can be directly transferred to the field of bone and soft-tissue cancers. Overall, the mechanobiology of mesenchymal cancers appears to be largely unexplored and currently the need for the mechanical characterization of those tumors remains unfilled.

1.4 Aim of the thesis

There is accumulating evidence suggesting that the biomechanical properties of tissues/cells play a crucial role in the balance between health and disease. In consequence, the need for mechanical characterization of biological systems and the development of reliable models to study them is growing. To this end, the AFM still represent a milestone in the field of applied biomechanics. The precision and the reliability of the data delivered by this device make it the gold standard for force measurement and investigating the mechanical properties of a large range of biological constructs.

In the present thesis, we introduce two studies that focus on the mechanical characterization of tissue and cells using AFM.

The first study aimed to establish an in-vitro model for studying articular cartilage biomechanical properties. One of the main objectives was to process cartilage in order to obtain samples with properties close to native cartilage, as can be found in the joint. 1mm thick cartilage discs were generated from femoral condyles of patients having underwent total knee arthroplasty. These discs were sorted according to their predominant chondrocyte organization pattern (SS, DS, SC, BC, diffuse) and their stiffness was then assessed with AFM micro-indentation. This work is presented as a methodological protocol, where the different steps for tissue preparation, sorting and indentation measurements are thoroughly detailed. A particular focus is placed on the possible complications that may arise using this technique and solutions to overcome them are proposed. The reproductivity of the sample preparation process, the stability of the sample during AFM measurements and the determination of adapted indentation probes with regard to the investigated tissue surface represented central concerns. The principal objective was to establish an effective method to generate cartilage samples of high quality, which represent histologically and biomechanically different stages of OA.

In the second study, the mechanical and cytoskeletal alterations of neoplastic cells of the musculoskeletal system were analyzed. Five different cell lines of bone and soft-tissue sarcomas (chondrosarcoma, osteosarcoma, Ewing sarcoma, fibrosarcoma and rhabdomyosarcoma) were investigated and compared to their related healthy controls (chondrocytes, osteoblasts, MSCs, fibrocytes and skeletal muscle cells (SKMCs) respectively). The cells were submitted to AFM indentation measurements, and their F-actin and β-tubulin distribution profiles were displayed using fluorescent labeling. The protein amount and gene expression levels of F-actin and β-tubulin were determined. Since the structure and biomechanics of cancer cells and tissue are known to be implicated in tumor genesis, development, neighboring tissue infiltration and metastasis, the characterization and comparison of the different malignant entities is a crucial step towards the comprehension of such versatile diseases.

These works have already been published and will be presented in the following order:

1. **Daniel, C**; Alexander, D; Umrath, F; Danalache, M (2022): Addressing practical issues in atomic force microscopy-based micro-indentation on human articular cartilage explants. In *Journal of visualized experiments, JoVE* (188). DOI: 10.3791/64371.
2. **Daniel, C**; Traub, F; Sachsenmaier, S; Riester, R; Mederake, M; Konrads, C; Danalache, M (2023): An exploratory study of cell stiffness as a mechanical label-free biomarker across multiple musculoskeletal sarcoma cells. In *BMC cancer* 23 (1), p. 862. DOI: 10.1186/s12885-023-11375-3.

https://app.jove.com/t/64371/addressing-practical-issues-atomic-force-microscopy-based-micro

https://link.springer.com/article/10.1186/s12885-023-11375-3

2 Results

2.1 Addressing practical issues in atomic force microscopy-based micro-indentation on human articular cartilage explants

jove

Addressing Practical Issues in Atomic Force Microscopy-Based Micro-indentation on Human Articular Cartilage Explants

Cyril Daniel[1], **Dorothea Alexander**[2], **Felix Umrath**[1,2], **Marina Danalache**[1]

[1] Laboratory of Cell Biology, Department of Orthopaedic Surgery, University Hospital Tübingen [2] Department of Oral and Maxillofacial Surgery, University Hospital Tübingen

Corresponding Author

Cyril Daniel
cyril.daniel@med.uni-tuebingen.de

Citation

Daniel, C., Alexander, D., Umrath, F., Danalache, M. Addressing Practical Issues in Atomic Force Microscopy-Based Micro-indentation on Human Articular Cartilage Explants. *J. Vis. Exp.* (188), e64371, doi:10.3791/64371 (2022).

Date Published

October 28, 2022

DOI

10.3791/64371

URL

jove.com/video/64371

Abstract

Without a doubt, atomic force microscopy (AFM) is currently one of the most powerful and useful techniques to assess micro and even nano-cues in the biological field. However, as with any other microscopic approach, methodological challenges can arise. In particular, the characteristics of the sample, sample preparation, type of instrument, and indentation probe can lead to unwanted artifacts. In this protocol, we exemplify these emerging issues on healthy as well as osteoarthritic articular cartilage explants. To this end, we first show *via* a step-by-step approach how to generate, grade, and visually classify *ex vivo* articular cartilage discs according to different stages of degeneration by means of large 2D mosaic fluorescence imaging of the whole tissue explants. The major strength of the *ex vivo* model is that it comprises aged, native, human cartilage that allows the investigation of osteoarthritis-related changes from early onset to progression. In addition, common pitfalls in tissue preparation, as well as the actual AFM procedure together with the subsequent data analysis, are also presented. We show how basic but crucial steps such as sample preparation and processing, topographic sample characteristics caused by advanced degeneration, and sample-tip interaction can impact data acquisition. We also subject to scrutiny the most common problems in AFM and describe, where possible, how to overcome them. Knowledge of these limitations is of the utmost importance for correct data acquisition, interpretation, and, ultimately, the embedding of findings into a broad scientific context.

Introduction

Due to the ever-shrinking size of electronic devices and systems, the rapid development of micro- and nano-based technology and equipment has gained momentum. One such device is atomic force microscopy (AFM), which can scan

biological surfaces and retrieve topographic or biomechanical information at both nano- and micrometer scales[1,2]. Among its vast features, this tool can be operated as a micro- as well as a nano-indenter to obtain information about the mechanical properties of various biological systems[3,4,5,6]. The data are collected by physical contact with the surface through a mechanical probe, which can be as small as about 1 nm at its tip[7]. The resulting deformation of the sample is then displayed based on the indentation depth of the cantilever tip and the force applied on the sample[8].

Osteoarthritis (OA) is a long-term degenerative chronic disease characterized by deterioration of the articular cartilage in the joints and surrounding tissues, which can lead to complete exposure of the bone surfaces. The burden of OA is substantial; currently, half of all women and one-third of all men aged 65 and over suffer from OA[9]. Traumas, obesity, and the resulting altered biomechanics of the joint[10] determine the articular cartilage degeneration, which is viewed as a common end result. The pioneering study of Ganz et al. posited that the early steps of the OA process may involve the biomechanical properties of cartilage[11], and since then researchers have confirmed this hypothesis[12]. Likewise, it is generally accepted that the biomechanical properties of the tissue are functionally orchestrated by the ultrastructural organization as well as cell-cell and cell-matrix crosstalk. Any alterations can dramatically impact the overall tissue biomechanical functioning[13]. To date, OA diagnosis is clinical and is based on plain film radiography[14]. This approach is two-sided: firstly, the lack of a defined degenerative cut-off threshold to formulate the diagnosis of OA makes the condition difficult to quantify, and, secondly, imaging methods lack sensitivity and standardization and cannot detect localized cartilage damage[15,16,17]. To this end, the assessment of the mechanical properties of the cartilage has the decisive advantage that it describes a parameter that changes during the course of OA regardless of the etiology of the disease and has a direct influence on tissue functionality at a very early stage. Indentation instruments measure the force by which the tissue resists the indentation. This is, in fact, not a new concept; the earliest studies date back to the 1980s and 1990s. In this period, numerous studies suggested that indentation instruments designed for the arthroscopic measurements of articular cartilage could be well suited to detect degenerative changes in the cartilage. Even 30 years ago, some studies were able to demonstrate that indentation instruments were able to detect *in vivo* changes in the cartilage surface during tissue degeneration by conducting compressive stiffness measurements during arthroscopy[18,19,20].

AFM indentation (AFM-IT) of the articular cartilage provides information about a pivotal mechanical property of the tissue, namely, stiffness. This is a mechanical parameter that describes the relation between an applied, nondestructive load and the resultant deformation of the indented tissue area[21]. AFM-IT has been shown to be capable of quantifying age-dependent modifications in stiffness in macroscopically unaffected collagen networks, thus, differentiating between the pathological changes associated with OA onset (grade 0 on the Outerbridge scale in articular cartilage)[22]. We have previously shown that AFM-ITs, on the basis of spatial chondrocyte organization as an image-based biomarker for early cartilage degeneration, allow for not only quantifying but also actually pinpointing the earliest degenerative mechanical changes. These findings have already been confirmed by others[23,24]. Hence, AFM-IT acts as an interesting tool to diagnose and identify early degenerative changes. These changes can be already measured at a cellular level,

reshaping the understanding of the OA pathophysiological process.

In this protocol, we demonstrate a complete histological and biomechanical grading procedure of articular cartilage explants, from native cartilage explant preparation to AFM data acquisition and processing. Through a step-by-step approach, we show how to generate, grade, and visually classify articular cartilage tissue according to different stages of degeneration by means of 2D large mosaic imaging, followed by micro-AFM indentations.

Even though, currently, AFM-IT is one of the most sensitive tools to measure biomechanical changes in cartilage[7], like any other instrumental technique, it has limitations and practical peculiarities[25] that can lead to erroneous data acquisition. To this end, we subject to scrutiny the most common problems that arise during AFM measurements of the cartilage explants and describe, where possible, how to minimize or overcome them. These include topographical aspects of the samples and the difficulties to stabilize them in an AFM-compatible environment, physical peculiarities of the tissue's surface, and the resulting difficulties in performing AFM measurements on such surfaces. Examples of erroneous force-distance curves are also presented, emphasizing the conditions that may cause them. Additional limitations inherent to the geometry of the cantilever tip and the use of the Hertz model for the data analysis are also discussed.

Protocol

Femoral condyles collected from patients undergoing total knee arthroplasty at the University Hospital of Tübingen, Germany, were used. Only articular cartilage samples from patients with degenerative and posttraumatic joint pathologies were included in this study. Departmental, institutional, as well as local ethical committee approval were obtained before the commencement of the study (Project no.674/2016BO2). Written informed consent was received from all patients before participation.

NOTE: A flowchart of the experiment steps in their chronological order is given in **Figure 1**.

1. Tissue processing and generation of cartilage discs

1. Tissue preparation
    1. Following post-operative resection, place the cartilage samples in a container filled with Dulbecco's modified Eagle's medium (DMEM) supplemented with 5% (v/v) penicillin-streptomycin. Make sure the samples are completely submerged in the medium. The duration between surgical resection and further processing of the cartilage should not exceed 24 h. Ensure that, throughout the entire processing, the samples are fully submerged in media to avoid sample drying.
    2. Cut the cartilage away from the bone using a scalpel.
2. Cartilage disc generation
    1. Generate cartilage discs of 4 mm in diameter using a biopsy punch.

        NOTE: It is important to select and resect the areas of the condyle where the cartilage layer thickness exceeds 1 mm. This might be problematic, especially around loadbearing zones, where the cartilage layer typically loses its thickness due to wear and tear processes or degeneration.

2. Place the previously generated 4 mm cartilage discs on a custom-made cutting device and fix and hold the cartilage discs stable by means of a spatula. When placing the cartilage discs on the cutting device, care must be taken. Position the samples so that the cartilage's topmost layer (the superficial zone of the articular cartilage) does not face the blade
3. Cut the cartilage discs with a razor blade. Disc-shaped cartilage samples of 4 mm x 1 mm are, thus, generated. To prevent sample drying, perform tissue cutting as quickly as possible.
4. Collect each disc with the help of a spatula and place the generated cartilage discs into 1.5 mL tubes containing 1 mL of DMEM supplemented with 5% (v/v) penicillin-streptomycin. Place approximately 15 discs in one tube.

3. Cryotome sectioning of the cartilage discs (for perpendicular slices)

NOTE: This step is optional, and it can be employed if a side-view visualization of the cellular pattern distribution within the cartilage discs is desired. It can be used as a verification method as the distribution of cellular pattern is a 3D feature of articular cartilage[26]. Optical sectioning and 3D reconstructions of the entire cartilage discs using a confocal microscope can also be used, removing, thus, the need to section the samples as described in the protocol.

1. Cover the cartilage disc with water-soluble embedding medium and place it on its edge on the cryotome knob (with the surface of the disc perpendicular to the surface of the knob). In the cryotome device, the embedding medium freezes at low temperatures.
2. Using a standard cryotome, section the tissue sideways at a 60 µm thickness until the middle of the disc is reached (i.e., when cryosections reach a length of 4 mm) and collect the slices. By sectioning the disc explant perpendicularly, all zones of the cartilage (superficial, middle, and deep) can be visualized.
3. Collect the sections on a glass slide and remove the water-soluble embedding medium by washing three times with phosphate-buffered saline (PBS).

2. Cartilage disc sorting as a function of the cellular spatial pattern

1. Staining of the disc-shaped cartilage samples
    1. Place one cartilage disc (section 1.2) in each well of a 96-well plate and add 130 µL of cell permeable fluorescence dye at a dilution of 1:1,000 to each well.
    2. Visually inspect the entire plate and make sure that only one disc is placed in each well. Incubate the plate for 30 min in the standard cell culture incubator at 37 °C.
2. Staining of the 60 µm cartilage slices
    1. Gently place the cartilage disc sections (section 1.3) on glass microscope slides with the help of forceps.
    2. Cover the cartilage sections with mounting medium containing nuclear DAPI counterstaining and gently place coverslips that are suitable for fluorescence microscopy.
    3. Seal the edges of each coverslip with regular transparent nail polish and allow to dry for 3 min.

3. Top-down and side-view cartilage sorting and imaging

NOTE: Each disc must be examined under a fluorescent microscope. The aim of this step is to sort the discs based on their predominant cellular pattern (single strings, double strings, small clusters, big clusters, or diffuse).

1. Place the 96-well plate on the plate holder of the fluorescence microscope.
2. Select the appropriate fluorescence filter of either Em 495 nm/Ex 515 nm (for top-down imaging of the cartilage discs prepared in section 2.1.) or Em 358 nm/Ex 461 nm (for side-view imaging of the cartilage sections prepared in section 2.2) and the 10x objective.

   NOTE: Using the 10x objective allows the whole circumference of the disc to be inspected, and samples with inhomogeneous or improper staining can be excluded. However, using only the top-down view may result in the perception of changes in cellular organization as a result of analysis of the deeper tissue layers made visible to top-down observation by superficial erosion. As an example, an ascending string following the collagen arcades could be perceived as a single cell or scattered cells (diffuse pattern)[26]. As a result, both sides of the discs must be inspected to ensure proper cellular pattern selection.
3. Determine visually the cellular pattern displayed in each cartilage disc. It is unlikely that a disc will have only one type of cellular pattern. For the portion of the disc where the chondrocyte arrangement does not match the pattern of interest, only accept the samples if the undesired pattern is at the very periphery, where AFM measurements are not taking place (i.e., up to 0.5 mm from the disc border), and ensure that this does not exceed 10% of the total surface of the disc[27,28].

4. Image acquisition of the entire cartilage discs

1. Select the 10x objective of the microscope and position it underneath the preselected well containing an individual cartilage disc. Focus on the disc to see the cellular pattern.
2. Select the **Navigator Function** to get an overview of the entire well. Use the left mouse button and drag to navigate to a different stage position. With the mouse wheel, zoom in and out.

   NOTE: At this point, a preview of the well with the entire sample can be seen by double-clicking on each area of interest sequentially.
3. Select a square that encompasses the area of interest to be scanned; at this point, all single tiles that compose the mosaic will become visible.
4. Adjust the exposure/light intensity so that the cells can be clearly visualized from the background. At this point, the picture's brightness/contrast has been adjusted for all the tiles and can no longer be customized individually for each tile.

   NOTE: As the cells near the disc's edge often emit a higher fluorescence signal than the cells in the center, the exposure/light intensity settings must be adapted.

   1. To evaluate if the exposure time is appropriate for a particular channel, examine the distribution of the signal in the histogram. By using the automatic exposure mechanism included in the microscope's image software, visualize all the cells residing within the disc.

5. Select the software's **Focus Map Point** option, and then select each individual tile by left-clicking in the center of it.
6. Select the option **Focus Map**. A window is displayed with all the previously selected tiles. Double-click on a tile in the list to display and bring it into proper focus.
7. Click **Set Z** to save the focal plan and proceed to the next tile. After adjusting the focal plan for each individual tile, begin image acquisition by pressing **Start Scan**.
    1. If the scan is displaying darker horizontal and/or vertical bars, this may be due to improper and uneven illumination of the single frames. Resolve this by using the **Linked Shading** option incorporated in the software prior to the actual scan.
8. Save, export, and correctly annotate the images.

3. Biomechanical approach of cartilage explants

1. Sample preparation for AFM measurements
    1. Fix each preselected cartilage disc containing a cellular pattern (section 2) in Petri dishes by means of biocompatible glue.Add sufficient sample glue on the top, bottom, left, and right sides of the disc.
    2. Cover the discs with 2.5 mL of Leibovitz's L-15 medium without L-glutamine. Add the Leibowitz medium gently onto the samples to avoid sample detachment from the surface due to waves created by the medium.
2. Loading of the samples into the AFM
    1. Position the Petri dish in the AFM device's sample holder and turn on the Petri dish heater set to 37 °C. Allow the tissue culture dish to reach the desired temperature. This is done to exclude possible artifacts caused by temperature variation.
3. AFM-cantilever calibration
    1. Initialize the software setup as previously described by Danalache et al.[29].
    2. Select a suitable glass block cantilever holder for liquid measurements and carefully place it on the AFM head. A locking mechanism secures the glass block in the AFM head. Ensure that the glass block's reflective surface is straight and parallel to the AFM holder.
    3. Place the cantilever on the surface of the glass block cantilever holder with care. The cantilever itself should rest on the polished optical plane, in the center of the glass block.
    4. Carefully place a silicone skirt (silicone membrane) on the base of the cantilever holder in order to prevent medium condensation in the AFM head.
    5. Lower the cantilever in 100 µm steps using the stepper motor function until it is completely submerged in the medium.
    6. Run a scanner approach with the approach parameters described by Danalache et al.[29]. Retract the cantilever by 100 µm once the bottom of the Petri dish is reached.
    7. Calibrate the cantilever using the exact steps and run the parameters described by Danalache et al.[29]. At the end of the calibration, the vertical deflection is saved and displayed in newton (N)

units of force rather than volts (V)-the unit of the original registration by the photodiode detector. In the experiments here, a set point of 4.47 nN resulted after calibration.

8. Using the stepper motor function, retract the cantilever to 1,000 µm.

4. Identifying the desired cartilage measurement site under the AFM

NOTE: Due to the 1 mm thickness of the cartilage discs, the cantilever is not visible in the field of view while navigating over the sample.

1. Use the CCD camera of the microscope to identify the cantilever. The AFM cantilever should be positioned in a sample-free area of the Petri dish.
2. Start a scanner approach with the cantilever on a clean, sample-free area of the Petri dish, using the same parameters described by Danalache et al.[29].
3. Further retract the cantilever 1.5 mm away from the bottom of the plate with the stepper motor control. This step is crucial in order to avoid a direct collision between the cantilever and the sample.
4. Switch from brightfield to fluorescence view and visually identify the top of the disc.
5. Move the AFM sample holder exactly 2 mm toward the middle of the disc. This point is considered to be the center of the cartilage disc.
6. Run a scanner approach and, once the surface of the cartilage disc is reached, retract the cantilever by 100 µm.

5. Force-distance curve measurements

1. Focus on the cells positioned in the desired measurement site. Click the Run button to start the measurements and the generation of force-distance curves in the targeted position.
2. Acquire five force-distance curves on each measurement site. Retract the cantilever by 500 µm and move the cantilever to the next measuring site.

NOTE: The retraction of the cantilever is a crucial step, as the cartilage disc surface is not homogenous and has irregularities. A high hillock on the surface of the sample can result in a dramatic collision, leading to unwanted cantilever tip/sample damage. We recommend selecting a minimum of five different measurement sites dispersed across the surface of the disc and acquiring a minimum of five force-distance curves at each site.

3. Inspect the force-distance curves and save them.

6. Estimation of Young's moduli using the Hertz fit model

1. Open the generated force-distance curves to be analyzed (.jpk file) in the data analysis software using the **Open a Batch of Spectroscopy Curves** option.
2. Select the **Hertz fit model** and then select the **Elasticity fit** option.
    1. The elasticity fit option automatically performs the following computations on the selected force-distance curve: calculates the baseline and subtracts from the whole curve to remove the baseline offset (the baseline is brought back to zero on the y-axis); determines the contact point by detecting the point where the force-distance curve crosses the zero force-line (the contact point is set to zero on the x-axis); calculates the tip-sample separation (the height signal of the piezo accounting for the bending of

the cantilever is subtracted); and fits the force-distance curve automatically with the selected model. If desired, each of these steps can also be carried out independently.

3. Adapt using the following fit parameters: Poisson ratio of 0.5 and the appropriate cantilever tip radius.
   NOTE: When using a cantilever with a spherical cantilever tip, the Hertz fit model should be used. The cantilever used in this study had a spherical tip with a radius of 5 µm. We recommend fitting the force-distance curve until the maximum applied force is reached (setpoint).
4. Check visually the force-distance curve fit to ensure correctness. This step has to be done for each of the force-distance curves analyzed.

7. Indentation depth determination
   NOTE: Depending on the data analysis tool being used, this process may differ. The experimenter can easily read the indentation depth by following a series of steps that are included in the data analysis program.
   1. Open each of the generated force-distance curves in the data analysis software and select the **Hertz fit Model** as the analysis process.
   2. Apply the **Subtract Baseline Offset** option to zero the vertical deflection axis (y-axis) and select the **Offset + Tilt** function.
   3. Use the **Find Contact Point** function to automatically identify the contact point, which is automatically brought to an x-coordinate of zero.
   4. Subtract the distance accounting solely for cantilever deflection from the raw piezo height during the indentation using the **Vertical Tip Position** function.
   5. Select the **Elasticity Fit** option to display the processed force-distance curve and select the area of the graph so that it lines up with the most negative value on the **Vertical Tip Position Axis** (x-axis).
   6. Read and document the indentation from the X Min box in the parameter tab. Save and document the results.

4. Statistical analysis

1. Open the statistical software. Select **New Dataset** from the drop-down menu.
2. Open the **Variable View** tab after selecting the **DataSet** file. Define the numerical variables for each cellular pattern category: single strings = SS, double strings = DS, small clusters = SC, big clusters = BC, diffuse and the Young's moduli.
3. In the data view tab, enter the measured Young's moduli data for each of the corresponding cellular pattern categories. Analyze the data distribution by selecting Analyze from the menu bar, and then **Exploratory Data Analysis**.
4. Select **Young's Moduli** as the dependent variable and **Cellular Pattern** as the factor list. A box plot used for the results section is displayed among the results in the output file.
5. To conduct a statistical analysis, choose **Dependent Samples** in the nonparametric test section of the analyze menu bar tab. Select **Young's Moduli** as **Test Fields** and **Cellular Pattern** as **Groups** under the fields tab. Press **Run**.
   NOTE: The results are displayed in the output file. For the statistical analysis, a Friedman test is performed.

6. Incorporate the nonparametric test's *p*-values into the box plot that was created in step 4.4. Save the results by clicking **File** in the menu bar and selecting **Save**.

Representative Results

Using a self-made cutting device, we were able to explant and generate small (4 mm x 1 mm) cartilage discs from fresh human condyles containing a single cellular spatial pattern[30] of single strings (SS, **Figure 2A**), double strings (DS), small clusters (SC), big clusters (BC; **Figure 2A**), and diffuse (**Figure 2B**). A representative cartilage explant is depicted in **Figure 3A**. The selection of discs displaying only one type of pattern was done using top-down fluorescence imaging (**Figure 2**). The topographic variation of the cartilage surface disc was further illustrated by side-view imaging of 60 µm thick sections generated from the cartilage discs (**Figure 2C**). On the surface of the explanted osteoarthritic cartilage discs, superficial fibrillation and matrix clefting were present (**Figure 3B**,**C**). This was particularly notable in the discs representative of advanced OA progression-represented by the presence of BC (**Figure 2A**). Following post-fluorescence sorting, the stiffness of the discs was assessed by AFM micro-indentations. To this end, the generated cartilage discs were successfully fixed in the AFM Petri dish by means of biocompatible glue (**Figure 3D**) to avoid sample drifting during the measurements (**Figure 3E**). The amount of glue used has to be adjusted. An insufficient amount of glue will result in disc instability, while adding too much glue may lead to an unwanted spreading of the glue either under and/or over the cartilage disc. The latter leads to measurement artifacts and poor identification of the disc under the fluorescence microscope. Inadequate glue application or sudden movements of the sample during fixation are frequent issues that cause the tissue to detach from the Petri dish and should be avoided.

A representative gradual stiffness reduction alongside the cellular pattern arrangement is displayed in **Figure 4A**. The stiffness values were higher in the discs containing SS (median of 2.6 kPa)-representative of uncompromised heathly cartilage areas. With OA onset and progression, the AFM measurements showed a strong stepwise decrease in stiffness of 42% in DS (1.5 kPa), 77% in SC (0.6 kPa), and, ultimately, 88% in advanced stages represented by BC (0.3 kPa; **Figure 4A**). The discs containing a diffuse pattern displayed an elevated elasticity with an important variation of the Young's modulus single values. For all of the cartilage discs with assigned predominant cellular pattern organization, the indentation depth associated with the employed setpoint (4.477 nN) was found to be inversely proportional to stiffness (**Figure 4B**). A representative generated force-distance curve is shown in **Figure 4C**, and a Hertz fit as well as the identification of the contact point is shown in **Figure 4D**.

The correct fit depends on, among other factors, the correct determination of the baseline. If the automatic baseline detection is erroneous (for example, because of a turbulent baseline), the fit can also be determined manually, and it allows the user to select a more representative baseline for the measurements. However, if the generated force-distance curve does not allow a proper fit, it has to be discarded. **Figure 5** shows examples of incorrect force-distance curves. Generating suitable force-distance curves on osteoarthritic articular cartilage explants can be difficult due to the tissue's irregular surface, on the one hand (examples are shown in **Figure 5A**,**B**), and the sample's instability caused by improper sample fixation (examples displayed in **Figure 5C**,**D**). Artifacts may be caused by multiple probe-sample

contact points (due to the uneven surface of degenerated cartilage) or unwanted tissue movement (visible through changes in the focal plane). These artifacts can be seen in the generated force-distance curves and are indicative of either a suboptimal contact between the AFM cantilever and the cartilage surface or improper sample fixation to the Petri dish (see **Figure 5A-D**).

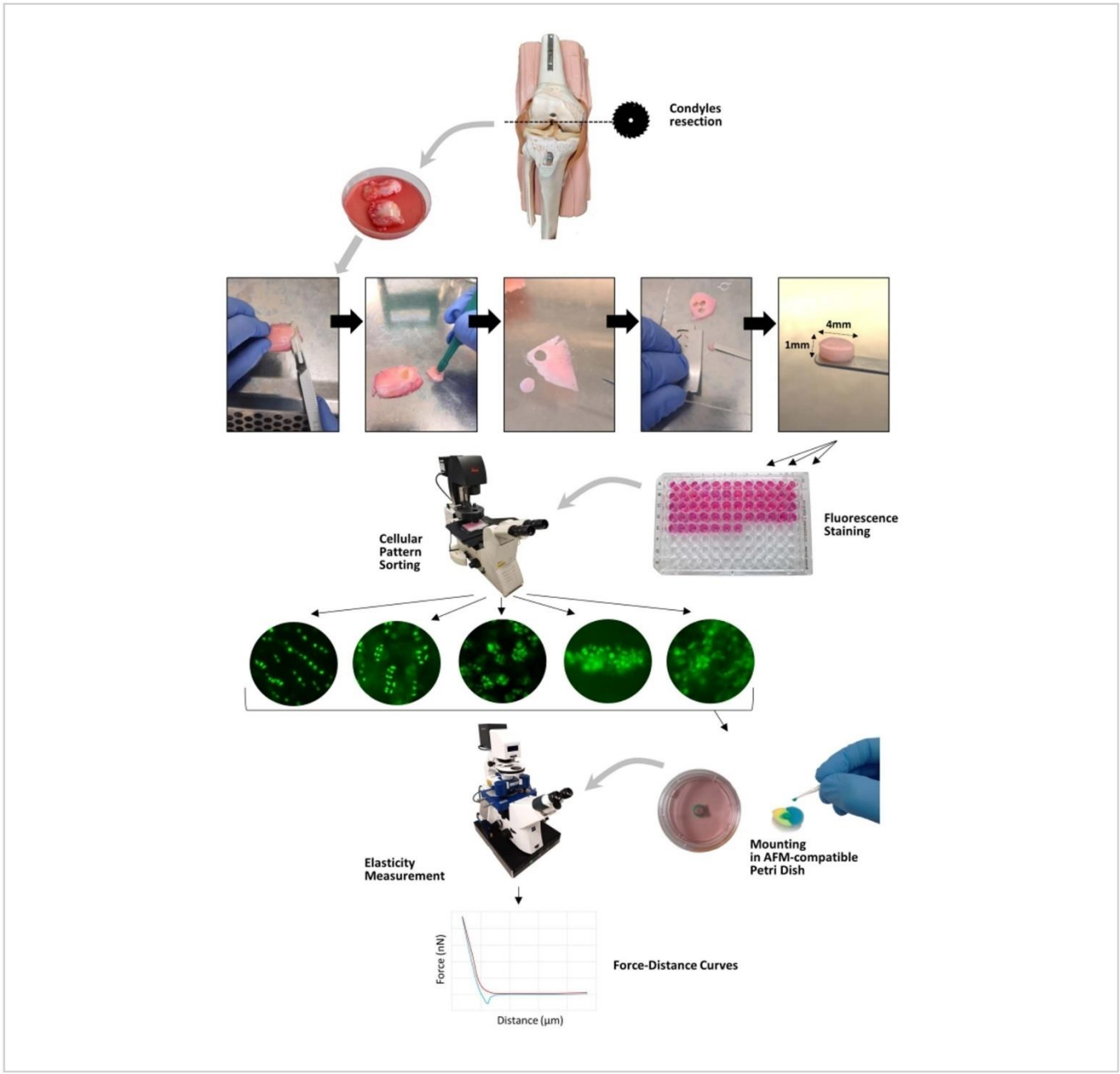

Figure 1: Flow chart of the experimental procedure. Summary of the experimental steps in chronological order, starting from intraoperatively resected cartilage samples to the generation of 4 mm x 1 mm cartilage discs, fluorescence staining

and sorting of the discs on the basis of the cellular pattern organization by means of top-down and side-view imaging, and, ultimately, elasticity assessment by means of atomic force measurements. Please click here to view a larger version of this figure.

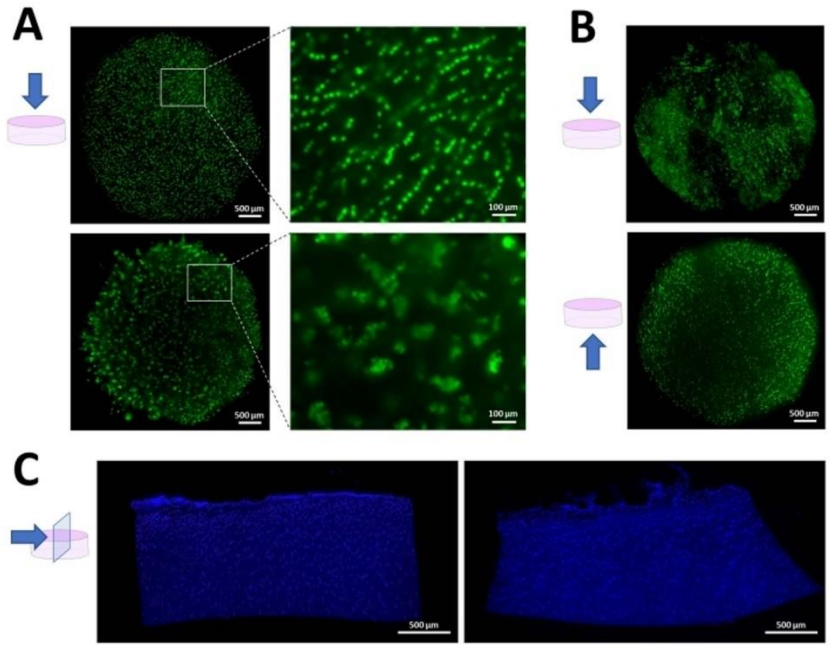

Figure 2: Fluorescence imaging of representative cartilage discs. (**A**) Mosaic 2D images and a zoomed exemplary field of cartilage discs stained with cell membrane permeable dye at 100x magnification. The top disc displays a representative single strings disc, while the lower one is representative of a big cluster disc (bottom). (**B**) Mosaic picture of a diffuse pattern disc seen from the surface (top), and the same disc imaged from the underside (bottom). (**C**) Side view of nuclear staining of 60 µm slices of cartilage discs. The white scale bar represents 500 µm for the mosaic pictures (larger field of view, A [left panel], B, C) and 100 µm for the zoomed in, focused pictures (A[right panel]). Please click here to view a larger version of this figure.

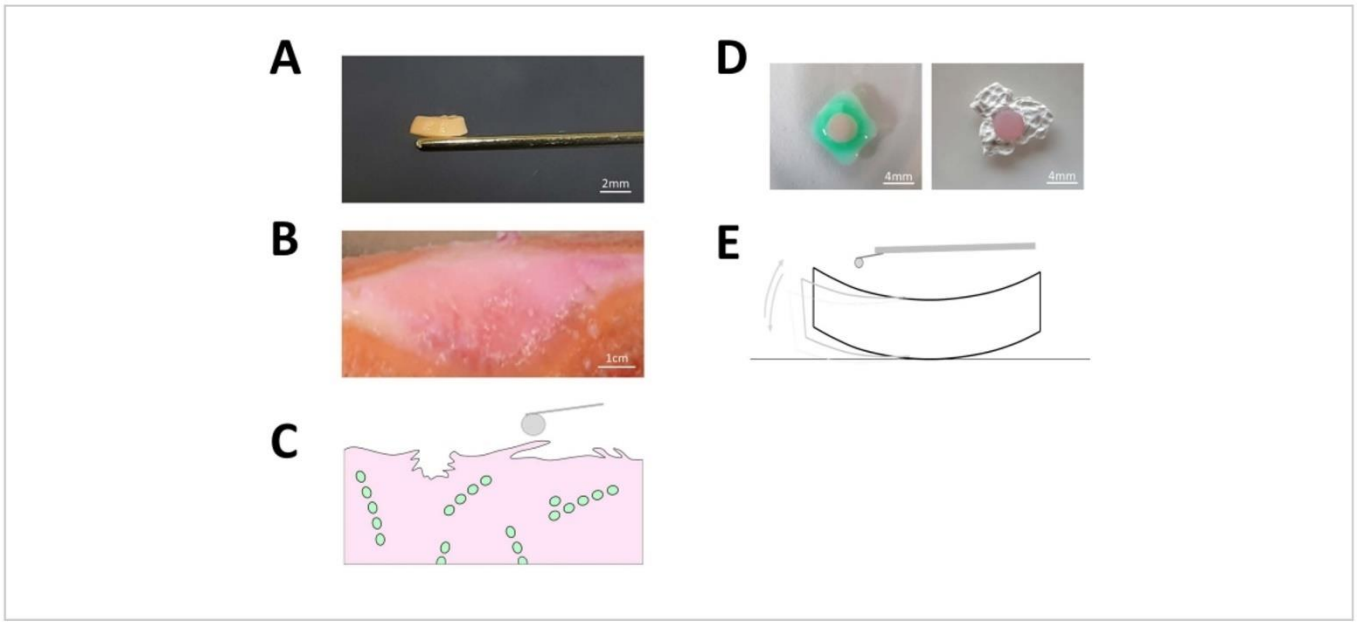

Figure 3: Explanted articular cartilage discs. (**A**) Representative image of a generated 4mm x 1mm cartilage disc explant from fresh human articular cartilage. The scale bar depicted in white represents 2mm. (**B**) Representative image of native osteoarthritic cartilage where the tissue surface presents macroscopically visible superficial fibrillation and clefting. The scale bar depicted in white represents 1,000 mm. (**C**) Schematical depiction of the fibrillated cartilage surface. (**D**) Prior to the AFM measurements, each of the cartilage disc explants was properly fixed by means of bio-compatible sample glue to the surface of the AFM Petri dish to avoid artifacts due to sample drifting during the actual indentation measurements as shown in (**E**). The white scale bar represents 4 mm. Please click here to view a larger version of this figure.

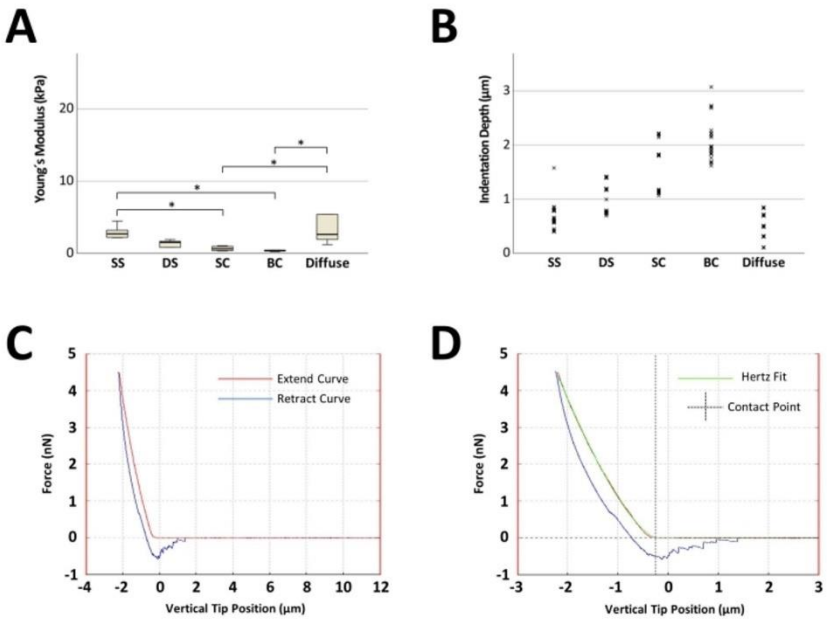

Figure 4: Representative results of atomic force microscopy measurements of articular cartilage discs sorted on the basis of their predominant cellular pattern organization. (**A**) Boxplot displaying the median of the computed Young's moduli of five discs, one for each cellular pattern, originating from one patient. A total of 25 measurements were performed on each disc (five measurements for five distinct measurement sites). The black line inside the rectangle represents the median value, the lower and upper extremities of the rectangle represent the first and third quartiles, respectively, and the error bars represent the lowest and highest values for each group. (**B**) Point-plot depicting the 125 indentation depth points for each cellular pattern. (**C**) Exemplary force-distance curves acquired with the AFM with a computed Young's modulus of 0.4 kPa. (**D**) A representative Hertz fit and contact point determination for the force-distance curve shown in (**C**). The x-axis displays the vertical tip position (which is the distance crossed by the piezo, with the length accounting for the cantilever bending being automatically subtracted from the contact part of the force-distance curve). *$p < 0.05$. For statistical analysis, the Friedman test was used. Abbreviations: SS = single strings; DS = double strings; SC = small clusters; BC = big clusters. Please click here to view a larger version of this figure.

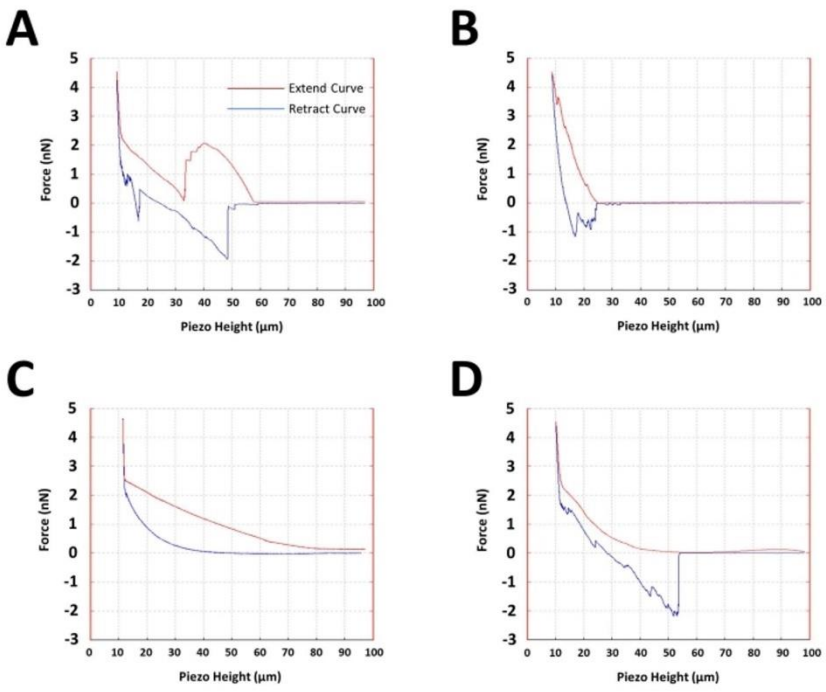

Figure 5: Examples of erroneous force-distance curves. (**A**) The force-distance curve shows a massive deviation followed by recovery near to the baseline level before a continuous indentation of the surface is observed. This phenomenon can be attributed to a relatively large obstacle (e.g., large surface clefts protruding from the topmost layer of the cartilage). (**B**) The extended force-distance curve shows multiple small peaks. These curves are thought to be caused by micro-scale irregularities on the cartilage surface (e.g., fibrillation). Both (**C**) and (**D**) display force-distance curves with biphasic courses. Both force-distance curves are representative of poor sample fixation and sample drift. It is also quite common in these cases to see a sudden change in the focal plane. Please click here to view a larger version of this figure.

Discussion

As a progressive and multifactorial disease, OA triggers structural and functional changes in the articular cartilage.Throughout the course of OA, impairments in mechanical features are accompanied by structural and biochemical changes at the surface of the articular cartilage[27,31]. The earliest pathological events occurring in OA are proteoglycan depletion coupled with collagen network disruption[32,33,34]. Such early subtle surface changes are difficult to pinpoint and identify with bulk testing, because the mechanical behavior is averaged over the whole tissue depth. Additionally, a still unaddressed question is whether functional changes at the organ and tissue levels relate to micro- or nano-scale structural and functional changes. To this end, AFM is considered to be one of the most sensitive methods, capable of detecting the earliest biomechanical changes occurring with OA onset[7]. It allows stiffness measurements on both micro- and nanometer scales in native

samples, providing information on the mechanical properties of articular cartilage[35,36]. In this protocol, using micro-AFM indentations, we measured the elastic properties of healthy and osteoarthritic articular cartilage human explants. The results showed that the cartilage explants are highly representative of early local OA events with a notable gradual decrease in stiffness occurring in pattern-specific cartilage explants. Furthermore, the results are in line with previous published research that showed a notable stiffness decrease alongside the cellular pattern organization[23,24,27,37].

Corroborated native human models that mimic various aspects of OA pathogenesis and progression are currently needed to address the shortfalls of translational research and the challenges of translating *in vitro* data to a clinical setting.To date, no model can accurately represent the complex native human cartilage compartment, let alone the age-related joint tissues which are prone to OA in response to disease-initiating stimuli[38]. The most commonly used explant-based models thus far were of bovine or cattle origin and applied either a strong inflammatory cytokine treatment or mechanical loading[39,40,41].This protocol, on the other side, demonstrates how to generate small (4 mm x 1 mm) explanted disc-shaped human cartilage samples, which are indicative of the individual stages of specific OA events. The cartilage explants are sorted and stage assigned using the cellular spatial organization as an image-based biomarker[30,42]. Since early changes in biomechanical properties can be already identified and quantified as soon as double strings start arising[23,27], at a stage where the cartilage surface still appears macroscopically intact[26], this explant-based model allows the investigation of a local native cartilage compartment and may provide insightful information on early OA. Furthermore, this cartilage model could be useful in investigating the cells and matrix response to mechanical and inflammatory alterations in a 3D native local habitat[38,39]. Being relatively simple and easy to generate, these cartilage explants can be also used to study OA heterogeneity, which is a limiting factor in developing and testing disease-modifying OA drugs[43]. It also has to be noted that scalability and dependency on patients undergoing joint replacement surgery are two of the model's shortcomings.

It is well known that articular cartilage presents a peculiar behavior depending on the scale level that is tested. As indicated by Loparic et al., at the micro-scale, the cartilage behaves as a nonstructured and uniform material[35], and such an approach gives an approximation of localized overall cartilage stiffness. With respect to whether micro- or nano-indentations are better suited, a 2004 study by Stolz et al.[44] compared both micro- and nano-scale indentations in assessing the structure-mechanical properties of articular cartilage. The authors emphasized that for micro-scale spherical indentation of the articular cartilage, the nano-scale fine structural components (i.e., individual collagen fibers and proteoglycans) commonly share the task of load bearing. In such, the aggregate mechanical properties differ markedly from those of the individual nanocomponents. The same authors proposed that a combination of micro- and nano-indentations could be used to assess the overall local stiffness profiles of articular cartilage, as well as the stiffness related to the fine structural components[44].

Numerous AFM-based indentation experiments have used sharp pyramidal cantilever tips (radius = 15-20 nm)[22,36,44] for assessing cartilage mechanics. Although the nanoindentations with sharp cantilevers are currently regarded to be more suitable for assessing the finest mechanical properties, spherical cantilever tips produce results that are more consistent and easier to model

and interpret when testing soft biological samples[44,45]. Furthermore, Stolz et al. demonstrated that AFM nano-indentations of enzymatically (i.e., elastase) degraded articular cartilage are not possible because the tissue becomes so sticky that tip-sample adhesion dominates the force-distance curves, rendering the data unfeasible[44].

In the present AFM measurements, a cantilever with a spherical cantilever tip of 5 µm radius was used. The cantilever choice was motivated by the intention to average the mechanical properties of the tissue over a fairly large surface while minimizing the inflicted damage on the cartilage surface. The relationship between the cantilever-applied force and the resulting sample indentation was fitted with the Hertz fit model. When using spherical indenters, the Hertz fit model is recommended, with the attractive forces acting between the cantilever tip and the sample surface being neglected[46]. The equations for the Hertzian model are shown in Eq.1 and Eq.2.

$$F = \frac{E}{1-v^2}\left[\frac{a^2+R_s^2}{2} ln \frac{R_s+a}{R_s-a} - aR_s\right] \quad \text{Eq.1}$$

$$\delta = \frac{a}{2} ln \frac{R_s+a}{R_s-a} \quad \text{Eq.2}$$

Where F = force; E = Young's modulus; v = Poisson's ratio; δ = indentation; a = radius of contact circle; and R_S = radius of sphere.

The model ultimately computes the cellular/tissue elasticity[47], formally expressed as the Young's modulus (E). The Hertz fit model takes into consideration several characteristics such as the tip shape and size, indentation, and sample deformability. If these requirements are not ideally met, the model may provide an inaccurate estimate of the Young's modulus[46].

The Hertz fit model assumes that the strain and elastic stress depend linearly on the elastic modulus, which implies that the indentation in the sample remains much smaller than the sample thickness itself[46]. This assumption was easily met in this setup, where the cartilage explants had a 1 mm thickness compared to indentations of few micrometers.

Articular cartilage can be modeled as a porous viscoelastic material[48,49]. The viscoelastic behavior results from friction between the intracellular/cytoplasmic or matrix constituents such as molecules, organelles, and the collagen-proteoglycan network[50,51]. As the name implies, viscoelastic materials combine two distinct properties: viscous-the material deforms slowly when subjected to an external load- and elastic-the material returns to its initial configuration once the applied load is removed[52,53]. The viscoelastic behavior is manifested as a hysteresis between the approach (extended) and retraction curves in the force-distance curves[46,52], similar to the ones obtained in this study (**Figure 4C**). Furthermore, a characteristic of viscoelastic materials is that their mechanical properties depend on the deformation rate, with the material's stiffness increasing with the rate at which loading is applied (indentation speed)[54]. Thus, by selecting different loading rates, a family of force-distance curves is generated, each of which represents the mechanical properties of the tested sample at each loading rate[52]. So, when attempting to compare the outcomes of various works, it is critical to take all of the indentation parameters into account. Overall, when measuring at the micrometer scale (as in this study with a 5 µm spherical cantilever tip), articular cartilage behaves as a nonstructured and uniform material, generating a cumulative elastic modulus that includes both elastic and viscous contributions to stiffness due to the poroviscoelastic nature of the tissue[35].

Another assumption of the Hertzian model is that the indentation depth is lower than the radius of the spherical cantilever tip[55]. The indentation depth represents the maximum displacement of the cantilever tip after first contact with the sample. At maximum load, the maximum indentation depth is the overall displacement of the sample and the cantilever tip. Bueckle's guideline states a maximum indentation depth of 10% of the overall thickness of a sample with the same structure throughout[56], else, the results vary according to the depth-to-thickness ratio. For a cantilever tip radius of 5 µm, the cartilage explants in this study were indented at 1.1 µm on average, with a few peaks of 3 µm in a few instances, particularly for the highly degenerated cartilage explants.In this case, a compromise was sought, as, in the experimental setting, relatively high forces associated with large indentations are required to neutralizethe surface irregularities of degenerated cartilage.A milder indentation would result in the examination of superficial fibrillation and collagen fissuring, both of which are common features of highly degenerated cartilage[57].

Crucial for the Hertz fit model is also the correct identification of the point at which the cantilever tip comes into direct contact with the sample, generically termed the contact point. However, this might turn out to be problematic when indenting too sticky or too soft samples, as it may result in multiple probe-sample contact points[58,59]. In fact, as nicely emphasized by A-Hassan et al., for soft biological tissues, the accurate determination of the point of contact is one of the most vexing problems[60]. This effect was also observed in the native osteoarthritic cartilage explants, as, depending on the stage of degeneration, the tissue surface loses its native mechanical characteristics and is often uneven, presenting superficial fibrillation and clefting (**Figure 3B**,**C**). This phenomenon was particularly noted in the cartilage explants where the dominant cellular pattern was big clusters (**Figure 2C**). These inhomogeneities in the cartilage surface might lead to multiple probe-sample contact points and, thus, erroneous results. Vast deflections were observed in some cases, followed by a rapid recovery of the baseline before the final stretch of the force-distance curve (**Figure 5A**). This could be attributed to a large obstacle in the cantilever tip's path (e.g., advanced fibrillation areas with fraying and splitting cartilage). In other instances, the final slope of the force-distance curve was scattered with smaller irregularities (**Figure 5B**), indicating contact with successively smaller hindrances (e.g., micro-fibrillation of the tissue). In such cases, the measurement site must be remeasured or even changed to ensure data reliability and reproducibility. To this end, it is also important to carefully inspect the force-distance curve output of the AFM for the correct identification of the contact point. This is a crucial point to be aware of, as it has been shown that an incorrect identification of the contact point by 50 nm results in an incorrect estimation of the value of *E* by an order of magnitude[61]. Several studies have begun to use automated approaches to determine the contact point of force-distance curves, with the goal of bypassing subjective user input when estimating the contact point by visual inspection and improving accuracy. This becomes even more crucial when dealing with a large number of force-displacement curves, such as those generated in cell mechanics mesurements[47,62]. Although several strategies have been proposed to automate the contact point determination[47,63,64,65], the optimal strategy is highly dependent on experimental conditions and factors such as the model used to analyze the data, the shape of the probe, the (non-)adhesive mechanical interaction between the cantilever tip and the sample, as well as the (non-)Hertzian behavior of the sample[63].

Sample drift is another common issue that may cause artifacts and erroneous contact point determination (**Figure 3E**). It basically means that the sample is not properly mounted in the sample holder (Petri dish) and the sample is moving during the AFM measurements. The effect is particularly pronounced when moving the AFM cantilever to a new measurement site. This aspect can be easily observed during the actual measurements by a sudden change in the focal plane. The resulting force-distance curves typically have a biphasic extended slope, with a mild rise at first, corresponding to the narrowing of the empty space between the bottom of the disc and the Petri dish as the disc is pushed down by the cantilever (see **Figure 3E**), followed by a firmer inclination in the second section of the slope, indicating that the disc is being further indented now that it is in direct contact with the bottom of the Petri dish (**Figure 5C**,**D**). To overcome the distortions, one can try to better fix the samples by using an adequate sample adhesive (**Figure 3D**), keeping the temperature constant by turning off external sources of heat (lights) to avoid thermal drifting, and conducting fast scanning measurements.In the experiments here, we observed a cantilever deflection drift that occurred within the first 15 min of the cantilever's immersion in media (due to sudden changes in temperature). After this time lapse, the drift is usually negligible. As a result, we advise the experimenter to carefully examine the baseline after cantilever immersion and to begin measuring once it has stabilized.The duration of this process can vary greatly depending on the cantilever used.

Another critical parameter for any AFM measurement is the set point, which is, simplistically, a measure of the force applied by the cantilever to the sample. For the contact mode (as used in this study), the set point represents a certain deflection of the cantilever. When performing several scans or several site repetitions, like in the protocol here, the cantilever tip can adsorb particles from the sample surface, thus making it sometimes necessary to remove the cantilever, properly clean it[66], and then recalibrate before proceeding with the measurements.

While AFM micro-indentations provide new and interesting data collection opportunities, in particular in the context of osteoarthritic cartilage, the consistency and reproducibility of the data produced are heavily dependent on several parameters, as outlined above.When using this approach to assess the mechanical changes caused by cartilage tissue degeneration, some pilot measurements on various spatial patterns must first be performed in order to scale up the results to the specific experimental design.Pilot AFM measurements should be performed with the most standardizable procedure taking enough samples (e.g., five discs) of the same pattern to provide an indication of the extent of data variability. This is particularly important when attempting to quantify and assess the earliest relevant OA stiffness changes (i.e., between single strings and double strings, **Figure 4A**). In fact, in a previous study, using a similar approach, we showed that a sample size of 30 human specimens was required to assess biomechanical changes in the matrix as a function of the spatial organization of the cells[37].

Furthermore, many of the steps presented in this protocol are susceptible to human error and heavily rely on the operator's experience.Given all of the factors that can influence the actual AFM results, the absolute *E* values reported in this study are not generalizable and are rather specific to this experimental setup. However, the relationship presented here between the various Young's moduli and the cellular pattern-based cartilage explants (the more pathologic the spatial pattern, the lower the elastic modulus [EM] of the cartilage)

is unaffected, as the findings are consistent with previous studies showing stiffness changes as a function of cellular pattern organization[23,37].

Overall, this step-to-step protocol demonstrates the functionality of standardized 3D native articular cartilage explants, which are not only representative of OA-driven cellular reorganization events ranging from onset to advanced progression but are also associated with a gradual decrease in stiffness. The explants may reflect a reliable biomimetic model for studying OA onset and progression, allowing the testing and development of different treatment modalities *ex vivo*. The use of such a human explant model in combination with AFM-based biomechanical assessment could result in a paradigm shift for biomedical research and the pharmaceutical industry, paving the way for new ways to identify greatly needed effective OA drugs.

Disclosures

The authors have nothing to disclose.

Acknowledgments

We thank the orthopedic surgeons from the Department of Orthopaedic Surgery of the University Hospital of Tuebingen for providing the tissue samples.

References

1. Allison, D. P., Mortensen, N. P., Sullivan, C. J., Doktycz, M. J. Atomic force microscopy of biological samples. *Wiley Interdisciplinary Reviews. Nanomedicine and Nanobiotechnology.* **2** (6), 618-634 (2010).
2. Deng, X. et al. Application of atomic force microscopy in cancer research. *Journal of Nanobiotechnology.* **16** (1), 102 (2018).
3. Radmacher, M. Studying the mechanics of cellular processes by atomic force microscopy. *Methods in Cell Biology.* **83**, 347-372 (2007).
4. Charras, G. T., Horton, M. A. Single cell mechanotransduction and its modulation analyzed by atomic force microscope indentation. *Biophysical Journal.* **82** (6), 2970-2981 (2002).
5. Rabinovich, Y. et al. Atomic force microscopy measurement of the elastic properties of the kidney epithelial cells. *Journal of Colloid and Interface Science.* **285** (1), 125-135 (2005).
6. Dufrêne, Y. F. Using nanotechniques to explore microbial surfaces. *Nature Reviews Microbiology.* **2** (6), 451-460 (2004).
7. Cykowska, A., Danalache, M., Bonnaire, F. C., Feierabend, M., Hofmann, U. K. Detecting early osteoarthritis through changes in biomechanical properties - A review of recent advances in indentation technologies in a clinical arthroscopic setup. *Journal of Biomechanics.* **132**, 110955 (2022).
8. Gavara, N. A beginner's guide to atomic force microscopy probing for cell mechanics. *Microscopy Research and Technique.* **80** (1), 75-84 (2017).
9. Fuchs, J., Kuhnert, R., Scheidt-Nave, C. 12-Monats-Prävalenz von Arthrose in Deutschland. *Journal of Health Monitoring.* **2**, 55-60 (2017).
10. Felson, D. T. Osteoarthritis of the knee. *New England Journal of Medicine.* **354** (8), 841-848 (2006).
11. Ganz, R., Leunig, M., Leunig-Ganz, K., Harris, W. H. The etiology of osteoarthritis of the hip. *Clinical Orthopaedics and Related Research.* **466** (2), 264-272 (2008).

12. Saxby, D. J., Lloyd, D. G. Osteoarthritis year in review 2016: Mechanics. *Osteoarthritis and Cartilage.* **25** (2), 190-198 (2017).

13. Buckwalter, J. A., Mankin, H. J. Articular cartilage: Degeneration and osteoarthritis, repair, regeneration, and transplantation. *Instructional Course Lectures.* **47**, 487-504 (1998).

14. Braun, H. J., Gold, G. E. Diagnosis of osteoarthritis: Imaging. *Bone.* **51**(2), 278-288 (2012).

15. Guermazi, A., Roemer, F. W., Burstein, D., Hayashi, D. Why radiography should no longer be considered a surrogate outcome measure for longitudinal assessment of cartilage in knee osteoarthritis. *Arthritis Research & Therapy.* **13** (6), 247 (2011).

16. Guermazi, A. et al. Different thresholds for detecting osteophytes and joint space narrowing exist between the site investigators and the centralized reader in a multicenter knee osteoarthritis study--Data from the Osteoarthritis Initiative. *Skeletal Radiology.* **41** (2), 179-186 (2012).

17. Bedson, J., Croft, P. R. The discordance between clinical and radiographic knee osteoarthritis: A systematic search and summary of the literature. *BMC Musculoskeletal Disorders.* **9** (1), 116 (2008).

18. Dashefsky, J. H. Arthroscopic measurement of chondromalacia of patella cartilage using a microminiature pressure transducer. *Arthroscopy.* **3** (2), 80-85 (1987).

19. Berkenblit, S. I., Frank, E. H., Salant, E. P., Grodzinsky, A. J. Nondestructive detection of cartilage degeneration using electromechanical surface spectroscopy. *Journal of Biomechanical Engineering.* **116** (4), 384-392 (1994).

20. Appleyard, R. C., Swain, M. V., Khanna, S., Murrell, G. A. The accuracy and reliability of a novel handheld dynamic indentation probe for analysing articular cartilage. *Physics in Medicine and Biology.* **46** (2), 541-550 (2001).

21. Hsieh, C. H. et al. Surface ultrastructure and mechanical property of human chondrocyte revealed by atomic force microscopy. *Osteoarthritis and Cartilage.* **16** (4), 480-488 (2008).

22. Stolz, M. et al. Early detection of aging cartilage and osteoarthritis in mice and patient samples using atomic force microscopy. *Nature Nanotechnology.* **4** (3), 186-192 (2009).

23. Tschaikowsky, M. et al. Proof-of-concept for the detection of early osteoarthritis pathology by clinically applicable endomicroscopy and quantitative AI-supported optical biopsy. *Osteoarthritis and Cartilage.* **29** (2), 269-279 (2021).

24. Tschaikowsky, M. et al. Hybrid fluorescence-AFM explores articular surface degeneration in early osteoarthritis across length scales. *Acta Biomaterialia.* **126**, 315-325 (2021).

25. Eaton, P., Batziou, K. Artifacts and Practical Issues in Atomic Force Microscopy. In *Atomic Force Microscopy: Methods and Protocols,.* edited by Santos, N. C., Carvalho, F. A., 3-28. Springer. New York, NY (2019).

26. Danalache, M. et al. Exploration of changes in spatial chondrocyte organisation in human osteoarthritic cartilage by means of 3D imaging. *Scientific Reports.* **11**, 9783 (2021).

27. Danalache, M. et al. Changes in stiffness and biochemical composition of the pericellular matrix as a function of spatial chondrocyte organisation in

osteoarthritic cartilage. *Osteoarthritis and Cartilage.* **27** (5), 823-832 (2019).

28. Danalache, M., Erler, A. L., Wolfgart, J. M., Schwitalle, M., Hofmann, U. K. Biochemical changes of the pericellular matrix and spatial chondrocyte organization-Two highly interconnected hallmarks of osteoarthritis. *Journal of Orthopaedic Research.* **38** (10), 2170-2180 (2020).
29. Danalache, M., Tiwari, A., Sigwart, V., Hofmann, U. K. Application of atomic force microscopy to detect early osteoarthritis. *Journal of Visualized Experiments.* (159), e61041 (2020).
30. Rolauffs, B. et al. Proliferative remodeling of the spatial organization of human superficial chondrocytes distant from focal early osteoarthritis. *Arthritis and Rheumatism.* **62** (2), 489-498 (2010).
31. Wilusz, R. E., DeFrate, L. E., Guilak, F. Immunofluorescence-guided atomic force microscopy to measure the micromechanical properties of the pericellular matrix of porcine articular cartilage. *Journal of The Royal Society Interface.* **9** (76), 2997-3007 (2012).
32. Guilak, F., Ratcliffe, A., Lane, N., Rosenwasser, M. P., Mow, V. C. Mechanical and biochemical changes in the superficial zone of articular cartilage in canine experimental osteoarthritis. *Journal of Orthopaedic Research.* **12**(4), 474-484 (1994).
33. Billinghurst, R. C. et al. Enhanced cleavage of type II collagen by collagenases in osteoarthritic articular cartilage. *The Journal of Clinical Investigation.* **99** (7), 1534-1545 (1997).
34. Wu, P. J. et al. Detection of proteoglycan loss from articular cartilage using Brillouin microscopy, with applications to osteoarthritis. *Biomedical Optics Express.* **10** (5), 2457-2466 (2019).
35. Loparic, M. et al. Micro- and nanomechanical analysis of articular cartilage by indentation-type atomic force microscopy: Validation with a gel-microfiber composite. *Biophysical Journal.* **98** (11), 2731-2740 (2010).
36. Moshtagh, P. R., Pouran, B., Weinans, H., Zadpoor, A. The elastic modulus of articular cartilage at nano-scale and micro-scale measured using indentation type atomic force microscopy. *Osteoarthritis and Cartilage.* **22**, S359-S360 (2014).
37. Danalache, M., Jacobi, L. F., Schwitalle, M., Hofmann, U. K. Assessment of biomechanical properties of the extracellular and pericellular matrix and their interconnection throughout the course of osteoarthritis. *Journal of Biomechanics.* **19**, 109409 (2019).
38. Houtman, E. et al. Human osteochondral explants: Reliable biomimetic models to investigate disease mechanisms and develop personalized treatments for osteoarthritis. *Rheumatology and Therapy.* **8** (1), 499-515 (2021).
39. Anderson, J. R., Phelan, M. M., Foddy, L., Clegg, P. D., Peffers, M. J. Ex vivo equine cartilage explant osteoarthritis model: A metabolomics and proteomics study. *Journal of Proteome Research.* **19** (9), 3652-3667 (2020).
40. Chen, C. T., Torzilli, P. A. In vitro cartilage explant injury models. In *Post-Traumatic Arthritis: Pathogenesis, Diagnosis and Management.*, edited by Olson, S. A., Guilak, F., 29-40. Springer. New York, NY (2015).
41. Thudium, C. S., Engstrom, A., Groen, S. S., Karsdal, M. A., Bay-Jensen, A.-C. An ex vivo tissue culture model of

cartilage remodeling in bovine knee explants. *Journal of Visualized Experiments.* (153), e59467 (2019).

42. Rolauffs, B., Williams, J., Grodzinsky, A., E Kuettner, K., A Cole, A. Distinct horizontal patterns in the spatial organization of superficial zone chondrocytes of human joints. *Journal of Structural Biology.* **162** (2), 335-344 (2008).
43. Deveza, L. A., Loeser, R. F. Is osteoarthritis one disease or a collection of many? *Rheumatology.* **57** (suppl_4), iv34-iv42 (2018).
44. Stolz, M. et al. Dynamic elastic modulus of porcine articular cartilage determined at two different levels of tissue organization by indentation-type atomic force microscopy. *Biophysical Journal.* **86** (5), 3269-3283 (2004).
45. Sicard, D., Fredenburgh, L. E., Tschumperlin, D. J. Measured pulmonary arterial tissue stiffness is highly sensitive to AFM indenter dimensions. *Journal of the Mechanical Behavior of Biomedical Materials.* **74**, 118-127 (2017).
46. Krieg, M. et al. Atomic force microscopy-based mechanobiology. *Nature Reviews Physics.* **1** (1), 41-57 (2019).
47. Gavara, N. Combined strategies for optimal detection of the contact point in AFM force-indentation curves obtained on thin samples and adherent cells. *Scientific Reports.* **6**, 21267 (2016).
48. Mow, V. C., Kuei, S. C., Lai, W. M., Armstrong, C. G. Biphasic creep and stress relaxation of articular cartilage in compression? Theory and experiments. *Journal of Biomechanical Engineering.* **102** (1), 73-84 (1980).
49. Armstrong, C. G., Lai, W. M., Mow, V. C. An analysis of the unconfined compression of articular cartilage. *Journal of Biomechanical Engineering.* **106** (2), 165-173 (1984).
50. Deng, L. et al. Fast and slow dynamics of the cytoskeleton. *Nature Materials.* **5** (8), 636-640 (2006).
51. Fischer-Friedrich, E. et al. Rheology of the active cell cortex in mitosis. *Biophysical Journal.* **111** (3), 589-600 (2016).
52. Gould, T. E., Jesunathadas, M., Nazarenko, S., Piland, S. G. Chapter 6 - Mouth Protection in Sports. In *Materials in Sports Equipment (Second Edition).*, edited by Subic, A., 199-231. Woodhead Publishing. Sawston, Cambridge (2019).
53. Kontomaris, S. V., Malamou, A. Hertz model or Oliver & Pharr analysis? Tutorial regarding AFM nanoindentation experiments on biological samples. *Materials Research Express.* **7** (3), 033001 (2020).
54. Guz, N., Dokukin, M., Kalaparthi, V., Sokolov, I. If cell mechanics can be described by elastic modulus: study of different models and probes used in indentation experiments. *Biophysical Journal.* **107** (3), 564-575 (2014).
55. Wu, C.-E., Lin, K.-H., Juang, J.-Y. Hertzian load-displacement relation holds for spherical indentation on soft elastic solids undergoing large deformations. *Tribology International.* **97**, 71-76 (2016).
56. Westbrook, J. H., Conrad, H. *The Science of Hardness Testing and its Research Applications.* American Society for Metal. Metals Park, Ohio (1973).

57. Pritzker, K. P. H. et al. Osteoarthritis cartilage histopathology: Grading and staging. *Osteoarthritis and Cartilage.* **14** (1), 13-29 (2006).

58. Stylianou, A., Kontomaris, S. V., Grant, C., Alexandratou, E. Atomic force microscopy on biological materials related to pathological conditions. *Scanning.* **2019**, 8452851 (2019).

59. Sokolov, I. Atomic force microscopy in cancer cell research. *Cancer Nanotechnology.* **1**, 1-17 (2007).

60. Emad, A. et al. Relative microelastic mapping of living cells by atomic force microscopy. *Biophysical Journal.* **74** (3), 1564-1578 (1998).

61. Crick, S. L., Yin, F. C. Assessing micromechanical properties of cells with atomic force microscopy: Importance of the contact point. *Biomechanics and Modeling in Mechanobiology.* **6** (3), 199-210 (2007).

62. Shoelson, B., Dimitriadis, E. K., Cai, H., Kachar, B., Chadwick, R. S. Evidence and implications of inhomogeneity in tectorial membrane elasticity. *Biophysical Journal.* **87** (4), 2768-2777 (2004).

63. Lin, D. C., Dimitriadis, E. K., Horkay, F. Robust strategies for automated AFM force curve analysis--I. Non-adhesive indentation of soft, inhomogeneous materials. *Journal of Biomechanical Engineering.* **129** (3), 430-440 (2007).

64. Rudoy, D., Yuen, S. G., Howe, R. D., Wolfe, P. J. Bayesian change-point analysis for atomic force microscopy and soft material indentation. *Journal of the Royal Statistical Society: Series C (Applied Statistics).* **59** (4), 573-593 (2010).

65. Benítez, R., Moreno-Flores, S., Bolós, V. J., Toca-Herrera, J. L. A new automatic contact point detection algorithm for AFM force curves. *Microscopy Research and Technique.* **76** (8), 870-876 (2013).

66. Timashev, P. S. et al. Cleaning of cantilevers for atomic force microscopy in supercritical carbon dioxide. *Russian Journal of Physical Chemistry B.* **8** (8), 1081-1086 (2014).

2.2 An exploratory study of cell stiffness as a mechanical label-free biomarker across multiple musculoskeletal sarcoma cells

Daniel *et al. BMC Cancer* (2023) 23:862
https://doi.org/10.1186/s12885-023-11375-3

BMC Cancer

RESEARCH Open Access

An exploratory study of cell stiffness as a mechanical label-free biomarker across multiple musculoskeletal sarcoma cells

Cyril Daniel[1,2*], Frank Traub[2,3], Saskia Sachsenmaier[1,2], Rosa Riester[1], Moritz Mederake[4], Christian Konrads[5] and Marina Danalache[1,2]

Abstract

Background Cancer cells are characterized by changes in cell cytoskeletal architecture and stiffness. Despite advances in understanding the molecular mechanisms of musculoskeletal cancers, the corresponding cellular mechanical properties remain largely unexplored. The aim of this study was to investigate the changes in cellular stiffness and the associated cytoskeleton configuration alterations in various musculoskeletal cancer cells.

Methods Cell lines from five main sarcoma types of the musculoskeletal system (chondrosarcoma, osteosarcoma, Ewing sarcoma, fibrosarcoma and rhabdomyosarcoma) as well as their healthy cell counterparts (chondrocytes, osteoblasts, mesenchymal stem cells, fibroblasts, skeletal muscle cells) were subjected to cell stiffness measurements via atomic force microscopy (AFM). Biochemical and structural changes of the cytoskeleton (F-actin, β-tubulin and actin-related protein 2/3) were assessed by means of fluorescence labelling, ELISA and qPCR.

Results While AFM stiffness measurements showed that the majority of cancer cells (osteosarcoma, Ewing sarcoma, fibrosarcoma and rhabdomyosarcoma) were significantly less stiff than their corresponding non-malignant counterparts ($p < 0.001$), the chondrosarcoma cells were significant stiffer than the chondrocytes ($p < 0.001$). Microscopically, the distribution of F-actin differed between malignant entities and healthy counterparts: the organisation in well aligned stress fibers was disrupted in cancer cell lines and the proteins was mainly concentrated at the periphery of the cell, whereas β-tubulin had a predominantly perinuclear localization. While the F-actin content was lower in cancer cells, particularly Ewing sarcoma ($p = 0.018$) and Fibrosarcoma ($p = 0.023$), this effect was even more pronounced in the case of β-tubulin for all cancer-healthy cell duos. Interestingly, chondrosarcoma cells were characterized by a significant upregulation of β-tubulin gene expression ($p = 0.005$) and protein amount ($p = 0.032$).

Conclusion Modifications in cellular stiffness, along with structural and compositional cytoskeleton rearrangement, constitute typical features of sarcomas cells, when compared to their healthy counterpart. Notably, whereas a decrease in stiffness is typically a feature of malignant entities, chondrosarcoma cells were stiffer than chondrocytes, with chondrosarcoma cells exhibiting a significantly upregulated β-tubulin expression. Each Sarcoma entity may have

*Correspondence:
Cyril Daniel
cyril.daniel@med.uni-tuebingen.de

Full list of author information is available at the end of the article

his own cellular-stiffness and cytoskeleton organisation/composition fingerprint, which in turn may be exploited for diagnostic or therapeutic purposes.

Keywords Cancer, Musculoskeletal sarcomas, Atomic force microscopy, Stiffness, Biomarker, Cytoskeleton

Introduction

Cancer cells differ from normal cells and these differences refer to alterations in cell morphology, cell-cell and cell-extracellular matrix (ECM) interactions, cell invasion and adhesion, as well as cell death [1]. Sarcomas of the musculoskeletal system are a heterogeneous group of malignant tumors, including over 80 different histological diagnoses [2]. Commonly, sarcomas are categorized into two main categories: bone sarcomas and soft tissue sarcomas. With diagnostic means getting better constantly, more and more subtypes are characterized, thus, steadily increasing the number of possible different diagnoses [3]. The majority of sarcoma subtypes continue to pose a significant diagnostic and treatment challenge, with overall survival rates falling between 20 and 30% [4]. Due to the high degree of heterogeneity in their genetic profile, histology, as well as clinical features, the implementation of specific biomarkers, could function as a diagnosis and therapeutic Achilles' heel [5].

Cell stiffness has previously been proposed to serve as a label-free biomarker for cancer detection [6–8], and refers to a cell's ability to deform in response to external stress. It has recently been emphasized that alterations in the mechanical properties of cells and the surrounding environment (i.e. extracellular matrix (ECM)) play a decisive role during malignant transformation and cancer progression [9]. In fact, several studies have shown that cells derived from primary tumors as well as metastatic cells (e.g., lung, breast, and pancreatic neoplasia) are more elastic than their benign counterparts [6, 10]. Such changes in cellular stiffness may be a feature of carcinogenesis or even part of cancer cell's survival strategy to adapt to new environments. The cytoskeleton is the cell's primary mechanical structure; it is a complex, dynamic biopolymer network composed of microtubules, actin, and intermediate filaments [11]. Actin filaments (F-actin) along with multi-protein actin complexes (i.e. ARPC2/3) dictate the directionality, orientation, and large-scale architecture of the cytoskeleton framework [12], and are thought to be major contributors to cell stiffness [13]. The close link between actin filaments and cell stiffness is well documented by the use of disruptive pharmacological agents such as cytochalasin D [14]. Microtubules, like actin, play also an important role, with magnetic twisting cytometry studies showing that destabilizing microtubules decreased cell stiffness while stabilizing them increased it [15].

The advancement of technology in measuring stiffness of individual cells has resulted in powerful techniques capable of bridging the gap between mechanical properties and cellular functioning and structures. Pioneering research over two decades ago demonstrated the importance of mechanical properties in characterizing cancerous cells [16]. Various techniques for probing the mechanics of tumors have been developed, with atomic force microscopy (AFM) emerging as an excellent platform for simultaneously characterizing the structures and mechanical properties of living biological systems [17]. It has a phenomenal spatiotemporal resolution, opening up new avenues for understanding tumor physics and contributing significantly to cancer research. Indeed, AFM-stiffness assessment has been demonstrated to be useful not only for early cancer diagnosis by measuring cancer-specific proteins, but also for cancer progression monitoring by correlating the amount of cancer-specific proteins with cancer progression [18]. This seems logical given that metastatic cells require the ability to deform in order to metastasize and infiltrate, and several studies have shown that cells with higher elasticity have increased invasiveness and metastatic potential [19, 20]. Cell mechanical properties in mammalian cells are primarily determined by the cell cytoskeleton network, where the density and arrangement of filaments, the number of cross-links, activity, and stress generation all influence elastic properties [21–23].

The aim of this study was to investigate the mechanical characteristic alterations (i.e. stiffness) that occur at the cellular level of a wide range of tissue sarcoma types (i.e. chondrosarcoma, osteosarcoma, fibrosarcoma, Ewing sarcoma, rhabdomyosarcoma) as well as their healthy counterparts and to gain insight into the cytoskeleton changes (actin and microtubules), that may cause such changes.

Materials and methods

Cell lines and culture

Five different sarcoma cell lines: chondrosarcoma (SW1353, #HTB-94, American Type Culture Collection (ATCC), Manassas, Virginia, USA)), osteosarcoma (SaOs-2, #HTB-85, ATCC), Ewing sarcoma (RD-ES, #HTB-166, ATCC), fibrosarcoma (HT-1080, #CCL-121, ATCC) and rhabdomyosarcoma (RD, #CCL-136, ATCC) were used in this study. SW1353 and SaOs-2 cells were cultured in Dulbecco's Modified Eagle Medium DMEM/F12 (Gibco, Darmstadt, Germany) with 5% (v/v) FCS (fetal bovine serum; Gibco) and 1% (v/v) penicillin/streptomycin (Biochrom, Berlin, Germany), RD-ES cells in RPMI-1640 with L-glutamine (Gibco) media,

supplemented with 15% (v/v) FCS (Gibco) and 1% (v/v) penicillin/streptomycin (Biochrom), while HT-1080 cells and RD were cultured in DMEM with GlutaMAX, 4.5 g/l D-glucose (Gibco) supplemented with 10% (v/v) FCS (Gibco) and 1% (v/v) penicillin/streptomycin (Biochrom). Chondrocytes isolated from femoral condyles collected from patients undergoing total knee arthroplasty were used as healthy control cells (for comparison with chondrosarcoma). As a control group for the osteosarcoma, human bone marrow- mesenchymal stem cells (MSC) were isolated, differentiated and propagated into osteoblasts as previously described [24]. Adult human fibroblasts (#PCS-201-012, ATCC) were used as a control for the fibrosarcoma, MSC for the Ewing sarcoma and primary human skeletal muscle cells (SKMC, #PCS-950-010, ATCC) for the rhabdomyosarcoma. Chondrocytes, fibroblasts, skeletal muscle cells were cultured in RPMI 1640 with L-glutamine (Gibco) supplemented with 10% (v/v) FCS with 1% (v/v) penicillin/streptomycin (Biochrom), while MSC were cultured in DMEM (Gibco) media containing 10% (v/v) human platelet lysate (hPL) and 1% (v/v) amphotericin B and penicillin/streptomycin (Biochrom), 200mM glutamine (Sigma-Adrich, St. Louis, Missouri, USA), 1 IU heparin (AppliChem GmbH, Darmstadt, Germany). The hPL was purchased from the Tübingen Centre for Clinical Transfusion Medicine; it did not contain heparin and was referred to as a research lysate due to the absence of a quarantine period. All cells were cultured at 37 °C in the incubator supplied with 5% CO_2 and trypsin-versene EDTA (1X, Lonza, Basel, Switzerland) was used to passage cells.

Cell stiffness assessment - atomic force microscopy

All cell types were seeded at a density of 3×10^4 in petri dishes (TPP Techno Plastic Products AG, Trasadingen, Switzerland) and covered with Leibovitz's L-15 medium w/o l-glutamine (Merck KGaA, Darmstadt, Germany) media. The stiffness of living cells was assessed using a CellHesion200 (Bruker, Billerica, Massachusetts, USA) atomic force microscope (AFM) system, mounted onto an inverted light microscope (AxioObserver D1, Carl Zeiss Microscopy, Jena, Germany). A 5 µm radius spherical tip (model: SAA-SPH-5 µm, k=0.2 N/m, Bruker) was used for microscale indentation (Fig. 1 - A). The cantilever was calibrated on the extended curve, and the spring constant was determined using the thermal noise method built into the device software (Bruker, Fig. 1 - B). In force spectroscopy mode, force-distance curves were sampled at 2 kHz, with a force trigger of 3nN and a velocity of 2 µm/sec. To assess the stiffness of the cells, we performed indentations on selected cells identified by microscopic examination (3 repetitions/cell; 90 cells per each cancer entity, Fig. 1 - C). Using the Hertz-fit model for spherical intenders included in the data processing software (Version 5.0.86, Bruker), the cell stiffness in the form of the Young's modulus or elastic modulus (EM) was calculated from the force-distance curves. The Hertzian model's equations are shown in Eq. 1 and Eq. 2.

$$F = \frac{E}{1-v^2}\left[\frac{a^2+R_s^2}{2} ln \frac{R_s+a}{R_s-a} - aR_s\right] \quad (1)$$

$$\delta = \frac{a}{2} ln \frac{R_s+a}{R_s-a} \quad (2)$$

Where F=Force; E=Young's Modulus; ν=Poisson's ratio (which was set at 0.5); δ=indentation; a=radius of contact circle; R_s = radius of the sphere.

Cytoskeleton structural investigation – immunolabelling

Following AFM measurements, the cell lines were labeled with F-actin and β-tubulin. Briefly, the cells were fixed for 10 min with 4% (v/v) paraformaldehyde (PFA, Sigma-Adrich) in PBS at room temperature and then washed three times with PBS. For F-actin, a solution of 1µM CellMask™ Green Actin Tracking Stain (#A57243; Thermo Scientific, Waltham, Massachusetts, USA) in 1% (w/v) bovine serum albumin (BSA) in PBS was used for 1 h. For β-tubulin, the cells were then incubated with anti-β-tubulin (rabbit, 1:100, #2129 9F3, Cell Signaling, Danvers, MA, United States) in 1% (w/v) BSA-PBS overnight at 4 °C in a humidity chamber. Afterward, the cells were washed three times with PBS and incubated with a secondary conjugated antibody (Alexa Fluor-594 goat anti-rabbit IgG, #a21429, Thermo Scientific) at a dilution of 1:200 in 1% (w/v) BSA-PBS for 2 h at room temperature in the dark. Nuclear staining was performed with 2 µg/ml DAPI (4′,6-diamidino-2-phenylindole, Thermo Fisher Scientific). The cells were washed three times for 5 min each in PBS. Images were acquired using a Leica DMi8 microscope (Leica, Wetzlar, Germany) at a 40x objective.

Cytoskeleton biochemical investigation - ELISA

The changes in F-actin and β-tubulin content were analyzed by means of enzyme-linked immunosorbent assay (ELISA). For protein isolation, cells (density 1×10^6) were washed with PBS and lysed in protein lysis buffer (40 mM Tris/HCl pH 7.4, 300 mM NaCl, 2 mM EDTA, 20% (v/v) glycerol, 2% (v/v) Triton X-100) supplemented with 1X proteinase inhibitor (Halt™ Protease-Inhibitor-Cocktail, Thermo Scientific) at 4 °C. A soluble fraction was obtained by centrifugation at 15,000 *g* for 15 min at 4° C. Protein aliquots were first tested for total protein concentration using the Bradford protein assay before being normalized (Bio-Rad Laboratories, Richmond, CA, USA). A total of 20 µg of protein for each cell type was subjected

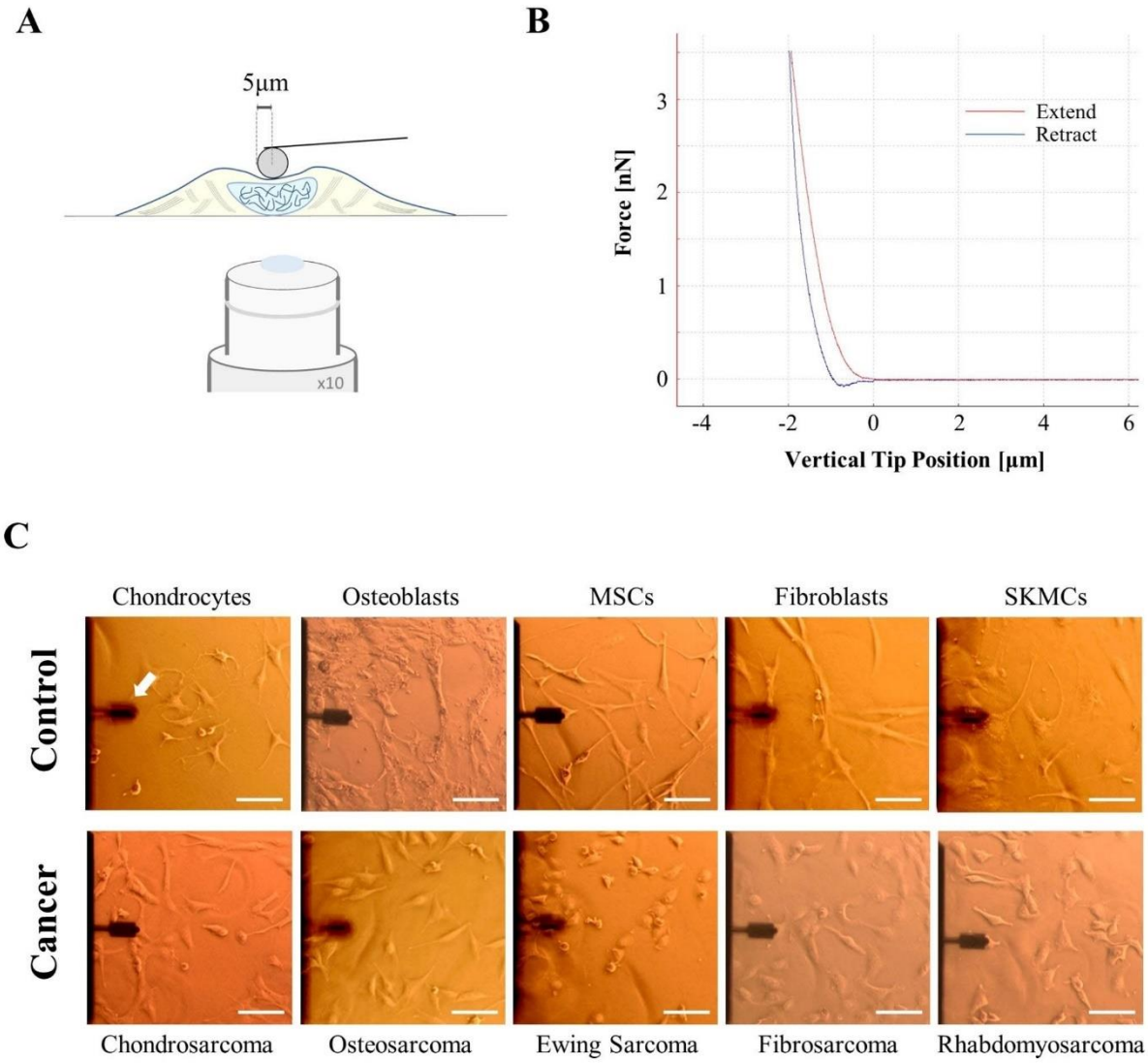

Fig. 1 Experimental settings for cell stiffness assessment. (**A**) Schematic representation of cell micro-indentations using a 5 µm radius spherical cantilever. (**B**) Representative force-distance curve obtained from AFM indentations for cells. The extend curve that is used for fitting of the Hertz fit model is shown in red. (**C**) Microscopic pictures of AFM measured cancer cell lines and their corresponding non-malignant counterparts. The cantilever used for measurements is also shown (white arrow). Scale bar (white) represents 100 µm. Abbreviations: AFM – atomic force microscopy

to F-actin ELISA (#CSB-E13678h, Cusabio Technology LLC, Houston, Texas, USA) and β-tubulin ELISA (#RD-TuBb1-Hu, Reddot Biotech, Kelowna, Canada) following the manufacturer's protocol. Absorbance was recorded at 450 nm by using an EL 800 reader (BioTek Instruments GmbH, Bad Friedrichshall, Germany). Three independent measurements of the ELISA assays were performed for each cell type.

Cytoskeleton gene analysis

RNA was isolated from the cells (1×10^6) using the RNeasy Mini kit (Qiagen, Hilden, Germany). Using the innuSCRIPT reverse transcriptase (Analytik Jena, Jena, Germany), 1 µg of RNA was reverse transcribed. A NanoDrop™ (Thermo Scientific) spectrophotometer was used to determine the purity and concentration of RNA. In a total volume of 10 µl, cDNA (50ng) was analyzed in duplicate reactions by quantitative-real-time-PCR (qRT-PCR) using gene-specific primers and 1X SYBR select master mix for CFX (Life Technologies GmbH). Primer pairs: F-actin (for: 5´-ACAGAGCCTCGCCTTTG-3´, rev: 5´-CCTTGCACATGCCGGAG-3´), β-tubulin (for: 5´-TCTTGCCCCATACATACCTTG-3´,rev: 5´-TCACTGATCACCTCCCAGAA-3´), ARPC2/3

complex (for: 5´-CTCTGGAGCTGAAAGACACA-3´, rev: 5´-AGGTTGATGGTGTTGTCTCG-3´), were purchased from Eurofins Genomics (Ebersberg, Germany). qRT-PCR was carried out in a QuantStudio3 (Thermo Scientific) and was analyzed using data analysis software incorporated in the device (Thermo Scientific). Relative expression levels were calculated using the ΔΔCt ($2^{-\Delta\Delta Ct}$) method as previously described [25], using GAPDH as reference gene.

Statistical analysis

The data is either graphically displayed as the median in a boxplot, or as mean with standard deviation (SD) in a bar diagram. Normality of the data was assessed by histograms and Shapiro-Wilk test. Depending on the normality, the comparison between experimental results was performed either by a Kruskal-Wallis with Mann-Whitney-U test as a post hoc test (AFM data) or t-test as a post hoc test (ELISA and qRT-PCR). Statistical analysis was performed with SPSS Statistics 22 (version 280.0.0.0 (190), IBM Corp., Armonk, NY, USA).

Results

For each cell type, 270 AFM measurements were conducted (n=3 biological replicates, 30 cells/ replicate, 3 repetitions/ cell) and Fig. 2 displays the computed Young's moduli. Cancer cells were significantly less stiff (more elastic) than their corresponding non-malignant counterparts (osteosarcoma cells - osteoblasts: $p<0.001$, Ewing sarcoma cells - MSC: $p<0.001$, fibrosarcoma cells - fibroblasts: $p<0.001$, rhabdomyosarcoma cells - SKMC: $p<0.001$) with the exception of chondrosarcoma cells and chondrocytes, where the trend was the opposite ($p<0.001$, Fig. 2). Absolute values were thereby reduced

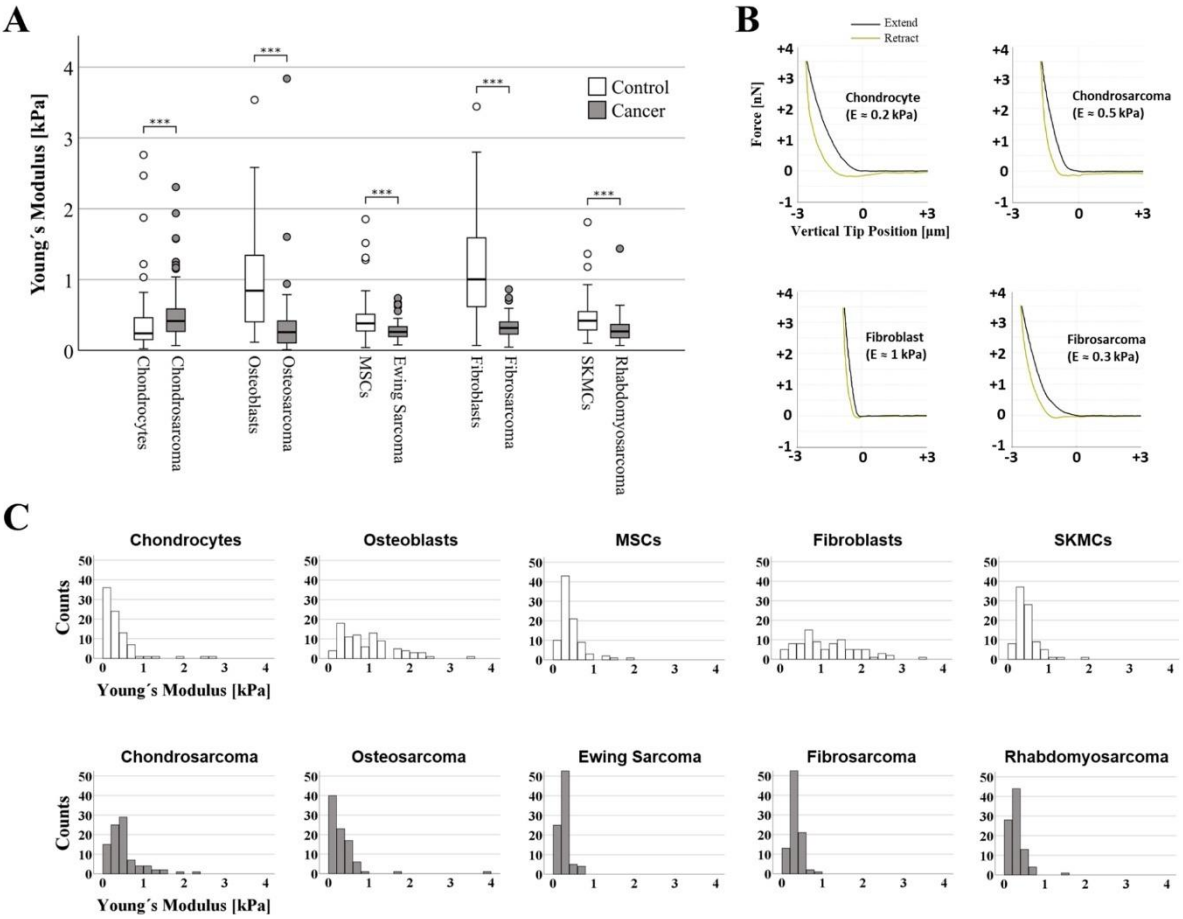

Fig. 2 Analysis of Young's modulus of musculoskeletal cancer cell lines and heathy controls. (**A**) Box plots (medians, first and third quartiles, minimum, maximum) of the cellular stiffness (kPa) for each cell line is displayed. Outliers are depicted by circles. Healthy control cells were stiffer than their corresponding neoplastic cell line ($p<0.001$), only exception being the chondrocytes that exhibited a lower stiffness than the chondrosarcoma cell line ($p<0.001$). (**B**) Representative force-distance curves for various cell types. (**C**) Images showing histogram distribution of elastic modulus of all cell types.*** $p<0.001$. Abbreviations: MSC- mesenchymal stem cells, SKMC - skeletal muscle cells

by 69% for the osteoblast - osteosarcoma group (median: 0.842 kPa to 0.256 kPa), 31% for the MSC - Ewing sarcoma (median: 0.381 kPa to 0.260 kPa), 70% for the fibroblasts - fibrosarcoma (median: 1.008 kPa to 0.315 kPa) and 36% for the SKMC- rhabdomyosarcoma group (median: 0.418 kPa to 0.267 kPa), while for the chondrocyte - chondrosarcoma group a notable increase in stiffness (i.e. a lower elastic profile) was observed (median: 0.239 kPa to 0.414 kPa corresponding to a 73% increase). In terms of stiffness distribution, malignant cells showed a unimodal skewed to the left distribution, while for normal cells the distribution is broader and have a higher stiffness. The chondrosarcoma cells exhibited a bimodal stiffness distribution with two prominent peaks at 0.29 ± 0.05 kPa ('peak 1') and 0.48 ± 0.06 kPa ('peak 2').

Since cytoskeletal remodeling may be a major contributor to the observed differences in cell stiffness [26] between cancer cells and their healthy counterparts, we examined the cytoskeletal structure by F-actin and β-tubulin labelling. The results presented in Fig. 3A-J show that in comparison to all cancer cells (Fig. 3 - B, D, F, H, J), healthy cells show denser, better-aligned F-actin with longer stress fibers. Chondrocytes (Fig. 3 - A) showed a similar actin pattern, however at a lower density. For the stiffer healthy cells (Fig. 3 - C, E, G, I) the actin filaments are dispersed throughout the cell body, with actin bundles aligned along the long axis of the cell with well-defined stress fibers. Actin filaments in the softer cancer cells, in contrast, are less organized and F-actin bundles are oriented randomly with short segments, forming a tangled network (Fig. 3 - D, F, H, J). All cancer cells showed a predominant cortical F-actin structure, with the majority of filament lying in the cell's periphery (Fig. 3 - B, D, F, H, J).

All of the cancer cell lines- healthy controls duo had a strong perinuclear presence of β-tubulin, forming a tortuous microtubular structure with longitudinally and obliquely concentrated crossed filaments, with a decreasing tendency toward the cytoplasm's periphery. This effect was especially noticeable in cancer cells (Fig. 3 - D, F, H, J), where the β-tubulin presence was reduced in F-actin enriched areas of the cell periphery. The chondrosarcoma cells (Fig. 3 - B) exhibited a similar β-tubulin distribution to their healthy counterparts (Fig. 3 - A), with long, rich, well defined, and elongated microtubule networks, a feature shared by the rest of the healthy cells (Fig. 3 - E, G, I).

We further looked into the cytoskeleton composition to get a better understanding of the changes we saw at the structural level. To this end we quantitatively analyzed actin filaments (F-actin), microtubules (β-tubulin) and actin-related protein 2/3 (ARPC 2/3) complex known to act as a nucleus for actin polymerization (Fig. 4).

While there was a significant difference in F-actin protein content between osteoblasts and osteosarcoma ($p=0.020$), fibroblasts and fibrosarcoma ($p=0.004$), and SKMC and rhabdomyosarcoma ($p=0.016$), no other cancer-healthy duo group showed a substantial difference in the F-actin protein content (Fig. 4 - A). At the gene-expression level, a similar trend was seen, between MSCs and Ewing sarcoma ($p=0.018$) and fibrocytes and fibrosarcoma ($p=0.023$, Fig. 4 - B).

The total protein content of β-tubulin was significantly lower in sarcoma cell lines compared to controls (osteoblasts – osteosarcoma, $p=0.001$; MSC - Ewing sarcoma, $p=0.001$, fibroblasts - fibrosarcoma $p=0.001$; respectively SKMC – rhabdomyosarcoma, $p=0.002$, Fig. 4 - C). In contrast, the opposite trend was observed for the chondrocyte – chondrosarcoma duo, with the chondrosarcoma cells exhibiting significantly more β-tubulin ($p=0.032$). A similar trend was seen at the gene level, where β-tubulin expression was significantly upregulated in chondrosarcoma cells ($p=0.005$), while the remaining difference between the other cancer-control duos did not reach statistical significance.

The ARPC2/3 expression (Fig. 4 - E) was tendentially elevated in cancer cells relative to their healthy counterparts, except for the fibroblasts-fibrosarcoma group in which the opposite trend was significantly observed ($p=0.038$).

Discussion

Due to the wide range of histological subtypes and clinical and histopathological characteristics that are not always distinct, musculoskeletal sarcomas remain a diagnosis challenge [27]. To date, there are still no reliable biomarkers that can be used for disease surveillance and screening. With the advent of quick biomechanical assaying techniques, stiffness may become a particularly important biomarker [28, 29] for load bearing tissues. In our study, we sought to determine whether cell stiffness is a valid, universal biomarker for different musculoskeletal sarcoma cell entities. Our study was designed as a large-scale exploratory one, in which we used the same AFM method and micro-mechanical indentation analysis on some of the major sarcoma entities to compare 10 cell lines, including 5 distinct sarcoma cell lines and 5 controls (healthy cells).

Our AFM results showed that, in four of our five experimental groups, the heathy cells were significantly stiffer than their corresponding cancer cell lines (osteosarcoma, Ewing sarcoma, fibrosarcoma, rhabdomyosarcoma). These results are in line with previous research showing reduced elastic moduli values of cancer cells compared to healthy cells [7, 8, 26]. Healthy and non-invasive cells are thought to have bulk stiffnesses far from the critical range, whereas cancerous and invasive cells are thought

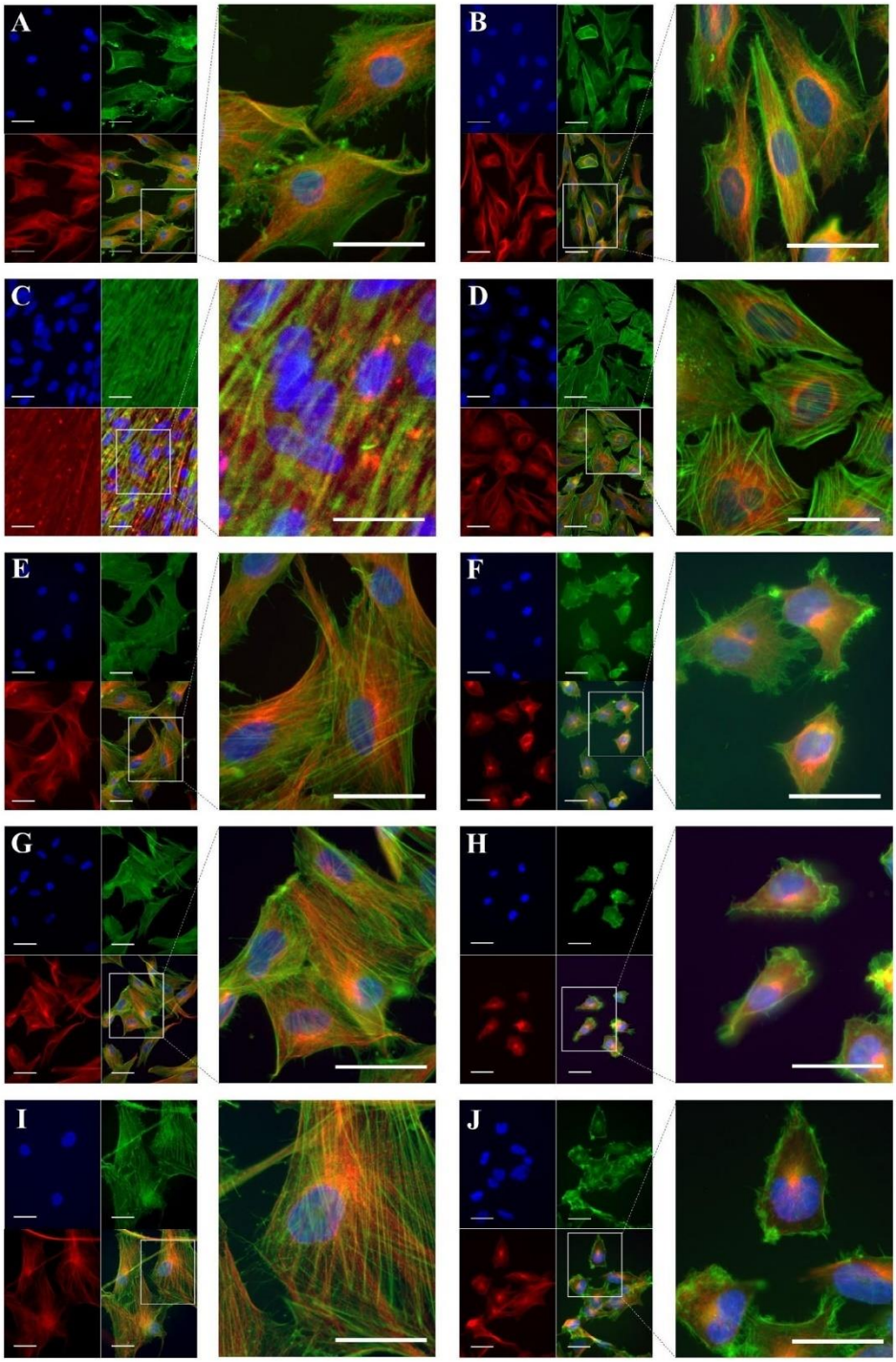

Fig. 3 Cytoskeleton structure in musculoskeletal cancer lines and healthy cells. Healthy cells: (**A**) chondrocytes, (**C**) osteoblasts, (**E**) MSC, (**G**) fibroblasts, (**I**) SKMC and their corresponding cancer cell line: (**B**) chondrosarcoma, (**D**) osteosarcoma, (**F**) Ewing sarcoma, (**H**) fibrosarcoma and (**J**) rhabdomyosarcoma were subjected to β-tubulin immunolabelling (red) coupled with fluorescence labeling of F-actin (green). Cell nuclei are depicted in blue. Pictures taken at a 40x objective and scale bars (white) represent 50 µm. Abbreviations: MSC - mesenchymal stem cells, SKMC - skeletal muscle cells

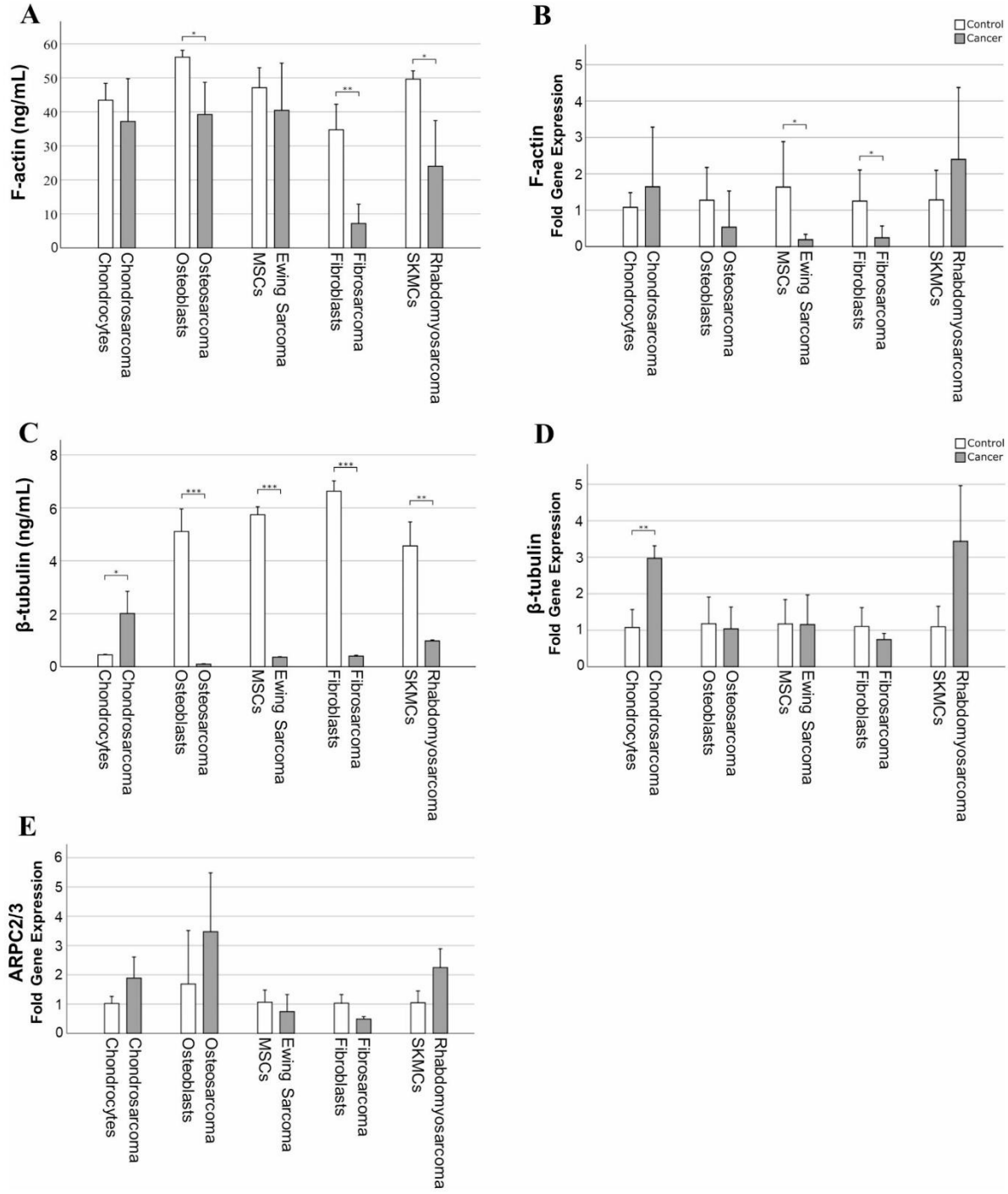

Fig. 4 Quantification of cytoskeleton composition in musculoskeletal cancer lines and corresponding healthy cells. (**A**) F-actin protein (ELISA) and (**B**) gene expression (qPCR), (**C**) β-tubulin protein and (**D**) gene expression, (**E**) ARPC 2/3 complex gene expression. Data presented as bar diagram ± SD (n = 3). *p < 0.05, **p < 0.01, ***p < 0.001. Abbreviations: ARPC 2/3 - actin-related protein 2/3 complex, MSC- mesenchymal stem cells, SKMC - skeletal muscle cells

to modulate their stiffness to a value near the critical range in order to maximize the migratory potential required for tumor progression [30]. Softening tumor cells boost their ability to self-renew [31]. Although a correlation has been established between cell stiffness and tumor cell malignancy [32], the link between cellular mechanical properties and metastatic preference remains inconclusive.

One of the most interesting findings of our study was that the chondrosarcoma cell line had the exact opposite elastic fingerprint as the other sarcoma cell lines we looked at - it was much stiffer than the healthy control - chondrocytes. This interesting observation might be attributed to the molecular fingerprint of the neoplastic entity, and the nuanced differences between the cancer cell and the healthy control cell: chondrocytes. Chondrosarcomas have been shown to express several proteins known as MSC markers [33]. In fact, two cell types with distinct marker expression signatures have been isolated from primary conventional chondrosarcomas: one group of multipotent MSC origins (CD49b high/CD10 low/CD221 high), and another that resembled fibroblastic lineage (CD49b low/CD10 high/CD221 low) [34], suggesting that both chondrosarcoma cell types arose from multipotent MSC origins, the presumed origin of chondrosarcomas [34]. In fact, when looking at the elastic profile obtained in our study of the chondrosarcoma (median of 0.414 kPa) it resembles closely the MSC elastic profile (0.381 kPa) ($p=0.358$). While adult chondrocytes also express MSC markers (CD105/CD166) [35] that increase with osteoarthritic driven degeneration of the articular cartilage [36], it is unclear whether this increase in MSC markers is an attempt at cartilage repair or a prerequisite for macroscopic cartilage degradation due to a lack of extracellular matrix maintenance. The differences between the two cell lines were also corroborated by a study done by Gabauer et al. which found only very limited similarities between SW1353 chondrosarcoma cells and chondrocytes, implying that the SW1353 cell line has a very limited potential to mimic chondrocytes [37].

Reorganization of the cytoskeleton, particularly actin microfilaments, has been shown to play a critical role in all aspects of cancer pathomechanism, including cell invasion and metastasis [38–40]. As such, we examined the organization of F-actin both qualitatively and quantitatively in these cell lines and compared their cytoskeletal architecture. All musculoskeletal cancer cells (chondrosarcoma, osteosarcoma, fibrosarcoma, Ewing sarcoma and rhabdomyosarcoma) exhibited a distinct F-actin arrangement pattern, barely displaying organized actin stress fibers (Fig. 3). This is consistent with previous research that also found actin stress fibers in the apical regions of healthy cells, but not in cancerous cells, suggesting that there fibers cannot contribute to stiffness [41]. This peculiar cytoskeletal reorganization might represent an adaptation mechanism used by the cancerous cells to adjust their stiffness to match the compliance of their substrates [42, 43]. The organization of the actin network can be altered by actin-binding proteins, among which is the ARPC2/3 that induces the formation of branched filaments, affecting actin dynamics [44]. Deregulation of the ARPC 2/3 regulatory framework has previously been described in cancer migration [45]. Our results showed that it is mainly expressed in cancer entities as well as in fibroblasts. The ARPC 2/3 complexes has been detected in both filopodia and lamellipodia of spreading fibroblasts, and their interplay is considered a significant factor in determining the motility choices made by the cells [46].

Also, in the healthy - cancer cell group where the cancer cells showed a lower stiffness (osteosarcoma, fibrosarcoma, Ewing sarcoma, and rhabdomyosarcoma), there was a decrease in the quantity of filamentous actin (F-actin) fibers, albeit to a lesser extent in the chondrosarcoma cell line (SW1335). These features reinforced the notion that the chondrosarcoma cell line has a distinct molecular, structural and mechanical fingerprint. In fact, previous research found an inverse relationship between the malignancy of chondrosarcoma cells and their degree of chondrocytic differentiation, implying, thus, that their metastatic ability was more dependent on the expression of specific matrix metalloproteases, that are required for egress from the tumor matrix and invasion into the extracellular matrix [47, 48]. Similarly a study done by Calzado-Martín et al. showed that although actin stress fibers contribute significantly to stiffness in healthy breast cells, the elasticity in tumorigenic cells does not appear to be primarily determined by these structures [41].

It is also conceivable that in chondrosarcomas, actin stress fibers are not the primary candidates responsible for changes in the stiffness profile. Interestingly, when looking at the cytoskeleton from the microtubules perspective, β-tubulin was significantly upregulated in this cell line (SW1335) when compared to chondrocytes (Fig. 4- C, D). The remaining cancer-healthy cell duos showed an exact opposite trend. Moreover, the beta-tubulin data seems to be consistent with the AFM stiffness data (Fig. 2), which showed that for all cancer cells-healthy controls duos, the healthy cells were significantly stiffer than the cancer cells, with the exception of chondrocytes-chondrosarcoma, where the opposite effect was observed. In fact, prior studies have demonstrated that microtubules possess a similar elastic modulus as actin filaments, measuring around 1 GPa, however, they also exhibit a bending rigidity approximately 100 times greater than that of actin [49, 50]. As dynamic components, microtubules also have the ability to form bundles with the aid of other proteins, consequently

enhancing their stiffness. Remarkably, cross-linking two microtubules leads to a four-fold increase in stiffness, a considerable alteration that highlights their substantial role in cellular mechanics [51].

The presence of tumor cells with varying degrees of stiffness within the same tumor tissue may be due to the heterogeneity of the tumor mechanical microenvironment [52]. As a result, it is unclear whether the unique cell cytoskeleton arrangement, composition and stiffness are due to their adaptation to the particular mechanical microenvironment of the targeted organ or to their intrinsic features independent of extracellular factors. Also, it should be noted that because we only studied one chondrosarcoma cell line - SW1335, thus, it is highly conceivable that the elastic behavior varies between cell lines from the same cancer entity, as chondrosarcoma is known to be a highly heterogeneous disease [53]. Darling et al., showed that among 3 different grade II chondrosarcoma cells lines (JJ012, FS090, and 105KC) the mechanical properties differ significantly [54], which also exhibit different levels of aggressiveness and metastatic potential. The authors also suggested that cell deformability may reflect certain phenotypic characteristics associated with the metastatic process [54].

Overall, we found that most sarcoma cell lines from the musculoskeletal neoplastic family are associated with significant stiffness decrease at a cellular level coupled with a specific structural and compositional rearrangement of the cytoskeleton. Together with previous biochemical findings, these results could lead to new diagnostic or prognostic approaches at a cellular level for determining the metastatic potential of musculoskeletal sarcomas. Recent studies, for example, have reported a microfluidic cell sorting approach based on cell stiffness that can identify molecular mechanisms of drug resistance and examine the heterogeneous responses of cancers to therapies [55]. Moreover, a better understanding of the mechanisms underlying these mechanical changes coupled with tumorigenic transformation could lead to the development of new pharmacological approaches (i.e. inhibiting metastasis by chemically targeting cytoskeletal structures that regulate cell stiffness and its subsequent motility).

Conclusion

This study suggests that changes in cellular stiffness are a peculiar feature found in the majority of musculoskeletal sarcomas investigated. The mechanical properties of chondrosarcoma cell lines show a distinct mechanical fingerprint, that potentially may vary substantially depending on the cell line tested. The structural rearrangement and composition of the cell cytoskeleton are also distinguishing features of these cell lines. These findings highlight the importance of cell stiffness in musculoskeletal sarcomas, which may not only reflect but also influence metastatic potential, and may be utilized for diagnostic, prognostic or therapeutic purposes.

Study limitations

Cellular heterogeneity in tumors is a well-established phenomenon [56, 57] that is thought to be an important cause of drug resistance that impedes treatment outcome [58, 59]. Since, we only examined one patient-derived cell line for each neoplasia type in our study, the entire neoplastic cell population may not be represented. Our findings are, however, highly consistent with the previous publications that analyzed and showed a loss of stiffness in cancer cells coupled with a structural rearrangement of the cytoskeleton [8, 26, 30, 31]. It also has to be noted that our heathy control for the chondrosarcoma – the chondrocytes, were isolated from osteoarthritic cartilage samples received from patients receiving total knee replacement surgery. Thus, it is possible that, several cellular and molecular features of these cells may be altered when compared to chondrocytes derived from completely healthy cartilage samples.

List of abbreviations

AFM	Atomic force microscopy
BSA	Bovine serum albumin
DMEM	Dulbecco´s modified eagle medium
ECM	Extracellular matrix
ELISA	Enzyme-linked immunosorbent assay
EM	Elastic modulus
FCS	Fetal bovine serum
MSC	Mesenchymal stem cells
PBS	Phosphate buffered saline
PFA	Paraformaldehyde
qRT-PCR	Real-time quantitative polymerase chain reaction
SD	Standard deviation
SKMC	Skeletal muscle cells

Acknowledgements

For removal of the cartilage tissue samples, we thank the orthopedic surgeons from the Department of Orthopedic Surgery at the University Hospital in Tübingen. We also acknowledge the support by the Open Access Publishing Fund of the University of Tübingen. We would also like to thank Magdalena Sady-Janczak for performing some of the F-actin labelling.

Authors' contributions

C.D. performed the experiments, statistical analyses and co-wrote the manuscript; F.T. helped with the statistical analysis, interpret the data and critically revised the manuscript S.S. helped interpret the data and critically revised the manuscript; R.R. performed the cell culture and qRT-PCR experiments; M.M. helped interpret the data and co-wrote the manuscript; C.K. helped with the statistical analysis, data interpretation and critically revised the manuscript; M.D. designed and supervised the study, helped with the statistical analyses, data interpretation and co-wrote the manuscript. All authors read and approved the final manuscript.

Funding

No funding was received for the current study.
Open Access funding enabled and organized by Projekt DEAL.

Data Availability

The dataset used and/or analysed during the current study are available from the correcponding author on reasonable request.

Declarations

Ethics approval and consent to participate

The study was conducted according to local and national regulations and according to the declaration of Helsinki. The MSCs were isolated from human bone marrow and the femoral condyles used for chondrocyte isolation were collected from patients undergoing total knee arthroplasty at the University Hospital of Tübingen, Germany. Written informed consent was obtained from all patients and the study and all the experimental protocols were approved by the Ethical Committee of the Medicine Faculty of Tübingen (Project no. 885/2021BO2 and Project no. 674/2016BO2).

Consent for publication

Not applicable.

Competing interests

The authors declare no competing interests.

Author details

[1]Laboratory of Cell Biology, Department of Orthopedic Surgery, University Hospital of Tübingen, 72076 Tübingen, Germany
[2]Department of Orthopedic Surgery, University Hospital of Tübingen, 72076 Tübingen, Germany
[3]Department of Orthopedics and Traumatology, University Medical Center Mainz, Johannes Gutenberg-University Mainz, 55122 Mainz, Germany
[4]Department of Trauma and Reconstructive Surgery, BG Clinic, University of Tübingen, 72076 Tübingen, Germany
[5]Department of Orthopedics and Traumatology, Hanseatic Hospital Stralsund, 18437 Stralsund, Germany

Received: 5 June 2023 / Accepted: 5 September 2023
Published online: 12 September 2023

References

1. Stylianou A, Stylianopoulos T. Atomic Force Microscopy probing of Cancer cells and Tumor Microenvironment Components. BioNanoScience. 2016;6(1):33–46.
2. Casali PG, Abecassis N, Aro HT, Bauer S, Biagini R, Bielack S, Bonvalot S, Boukovinas I, Bovee J, Brodowicz T, Broto JM, Buonadonna A, De Álava E, Dei Tos AP, Del Muro XG, Dileo P, Eriksson M, Fedenko A, Ferraresi V, Ferrari A, Ferrari S, Frezza AM, Gasperoni S, Gelderblom H, Gil T, Grignani G, Gronchi A, Haas RL, Hassan B, Hohenberger P, Issels R, Joensuu H, Jones RL, Judson I, Jutte P, Kaal S, Kasper B, Kopeckova K, Krákorová DA, Le Cesne A, Lugowska I, Merimsky O, Montemurro M, Pantaleo MA, Piana R, Picci P, Piperno-Neumann S, Pousa AL, Reichardt P, Robinson MH, Rutkowski P, Safwat AA, Schöffski P, Sleijfer S, Stacchiotti S, Sundby Hall K, Unk M, Van Coevorden F, van der Graaf J, Wardelmann E, Zaikova O, Blay JY. Soft tissue and visceral sarcomas: ESMO-EURACAN Clinical Practice Guidelines for diagnosis, treatment and follow-up. *Ann Oncol* 2018, 29, (Suppl 4), iv51-iv67.
3. Italiano A, Di Mauro I, Rapp J, Pierron G, Auger N, Alberti L, Chibon F, Escande F, Voegeli AC, Ghnassia JP, Keslair F, Laé M, Ranchère-Vince D, Terrier P, Baffert S, Coindre JM, Pedeutour F. Clinical effect of molecular methods in sarcoma diagnosis (GENSARC): a prospective, multicentre, observational study. Lancet Oncol. 2016;17(4):532–8.
4. Voltan K, Baptista AM, Etchebehere M. Extremities soft tissue sarcomas, more common and as dangerous as bone sarcomas. Rev Bras Ortop (Sao Paulo). 2021;56(4):419–24.
5. Genadry KC, Pietrobono S, Rota R, Linardic CM. Soft tissue Sarcoma Cancer Stem cells: an overview. Front Oncol. 2018;8:475–5.
6. Hayashi K, Iwata M. Stiffness of cancer cells measured with an AFM indentation method. J Mech Behav Biomed Mater. 2015;49:105–11.
7. Kwon S, Yang W, Moon D, Kim KS. Comparison of Cancer Cell elasticity by cell type. J Cancer. 2020;11(18):5403–12.
8. Xu W, Mezencev R, Kim B, Wang L, McDonald J, Sulchek T. Cell stiffness is a biomarker of the metastatic potential of ovarian cancer cells. 2012.
9. Kumar S, Weaver VM. Mechanics, malignancy, and metastasis: the force journey of a tumor cell. Cancer Metastasis Rev 2009, 28, (1–2), 113 – 27.
10. Cross SE, Jin YS, Rao J, Gimzewski JK. Nanomechanical analysis of cells from cancer patients. Nat Nanotechnol. 2007;2(12):780–3.
11. Fletcher DA, Mullins RD. Cell mechanics and the cytoskeleton. Nature. 2010;463(7280):485–92.
12. Zhang S, Vavylonis D. Steps of actin filament branch formation by Arp2/3 complex investigated with coarse-grained molecular dynamics. Front Cell Dev Biol. 2023;11:1071977.
13. Gavara N, Chadwick RS. Relationship between cell stiffness and stress fiber amount, assessed by simultaneous atomic force microscopy and live-cell fluorescence imaging. Biomech Model Mechanobiol. 2016;15(3):511–23.
14. Wakatsuki T, Schwab B, Thompson NC, Elson EL. Effects of cytochalasin D and latrunculin B on mechanical properties of cells. J Cell Sci. 2001;114(Pt 5):1025–36.
15. Wang N. Mechanical interactions among cytoskeletal filaments. Hypertension. 1998;32(1):162–5.
16. Lekka M, Laidler P, Gil D, Lekki J, Stachura Z, Hrynkiewicz AZ. Elasticity of normal and cancerous human bladder cells studied by scanning force microscopy. Eur Biophys J. 1999;28(4):312–6.
17. Li M, Xi N, Wang Y-c, Liu L. -q., atomic force microscopy for revealing micro/nanoscale mechanics in tumor metastasis: from single cells to microenvironmental cues. Acta Pharmacol Sin. 2021;42(3):323–39.
18. Kwon T, Gunasekaran S, Eom K. Atomic force microscopy-based cancer diagnosis by detecting cancer-specific biomolecules and cells. Biochim Biophys Acta Rev Cancer. 2019;1871(2):367–78.
19. Xu W, Mezencev R, Kim B, Wang L, McDonald J, Sulchek T. Cell stiffness is a biomarker of the metastatic potential of ovarian cancer cells. PLoS ONE 2012, 7, (10), e46609.
20. Swaminathan V, Mythreye K, O'Brien ET, Berchuck A, Blobe GC, Superfine R. Mechanical stiffness grades metastatic potential in patient tumor cells and in cancer cell lines. Cancer Res. 2011;71(15):5075–80.
21. Schäfer A, Radmacher M. Influence of myosin II activity on stiffness of fibroblast cells. Acta Biomater. 2005;1(3):273–80.
22. Moeendarbary E, Harris AR. Cell mechanics: principles, practices, and prospects. 2014, 6, (5), 371–388.
23. Rotsch C, Radmacher M. Drug-induced changes of cytoskeletal structure and mechanics in fibroblasts: an atomic force microscopy study. Biophys J. 2000;78(1):520–35.
24. Baghaei K, Hashemi SM, Tokhanbigli S, Asadi Rad A, Assadzadeh-Aghdaei H, Sharifian A, Zali MR. Isolation, differentiation, and characterization of mesenchymal stem cells from human bone marrow. Gastroenterol Hepatol Bed Bench. 2017;10(3):208–13.
25. Livak KJ, Schmittgen TD. Analysis of relative gene expression data using real-time quantitative PCR and the 2(-Delta Delta C(T)) Method. *Methods* 2001, 25, (4), 402-8.
26. Grady ME, Composto RJ, Eckmann DM. Cell elasticity with altered cytoskeletal architectures across multiple cell types. J Mech Behav Biomed Mater. 2016;61:197–207.
27. Pillozzi S, Bernini A, Palchetti I, Crociani O, Antonuzzo L, Campanacci D, Scoccianti G. Soft tissue sarcoma: an insight on biomarkers at Molecular, Metabolic and Cellular Level. Cancers (Basel) 2021, 13, (12).
28. Gossett DR, Tse HTK, Lee SA, Ying Y, Lindgren AG, Yang OO, Rao J, Clark AT, Di Carlo D. Hydrodynamic stretching of single cells for large population mechanical phenotyping. *Proceedings of the National Academy of Sciences* 2012, 109, (20), 7630–7635.
29. Runel G, Lopez-Ramirez N, Chlasta J, Masse I. Biomechanical Properties of Cancer cells. Cells 2021, 10, (4).
30. Kashani AS, Packirisamy M. Cancer cells optimize elasticity for efficient migration. Royal Soc Open Sci. 2020;7(10):200747.
31. Luo Q, Kuang D, Zhang B, Song G. Cell stiffness determined by atomic force microscopy and its correlation with cell motility. Biochim Biophys Acta. 2016;1860(9):1953–60.
32. Lv J, Liu Y, Cheng F, Li J, Zhou Y, Zhang T, Zhou N, Li C, Wang Z, Ma L, Liu M, Zhu Q, Liu X, Tang K, Ma J, Zhang H, Xie J, Fang Y, Zhang H, Wang N, Liu Y, Huang B. Cell softness regulates tumorigenicity and stemness of cancer cells. Embo j 2021, 40, (2), e106123.
33. Boehme KA, Schleicher SB, Traub F, Rolauffs B. Chondrosarcoma: A Rare Misfortune in Aging Human Cartilage? The Role of Stem and Progenitor Cells in Proliferation, Malignant Degeneration and Therapeutic Resistance. *Int J Mol Sci* 2018, 19, (1).
34. Diaz-Romero J, Romeo S, Bovée JV, Hogendoorn PC, Heini PF, Mainil-Varlet P. Hierarchical clustering of flow cytometry data for the study of conventional central chondrosarcoma. J Cell Physiol. 2010;225(2):601–11.

35. Mazor M, Cesaro A, Ali M, Best TM, Lespessaille E, Toumi H. Progenitor Cells from Cartilage: Grade Specific Differences in Stem Cell Marker Expression. *Int J Mol Sci* 2017, 18, (8).
36. Fickert S, Fiedler J, Brenner RE. Identification of subpopulations with characteristics of mesenchymal progenitor cells from human osteoarthritic cartilage using triple staining for cell surface markers. Arthritis Res Ther. 2004;6(5):R422.
37. Gebauer M, Saas J, Sohler F, Haag J, Söder S, Pieper M, Bartnik E, Beninga J, Zimmer R, Aigner T. Comparison of the chondrosarcoma cell line SW1353 with primary human adult articular chondrocytes with regard to their gene expression profile and reactivity to IL-1β. Osteoarthr Cartil. 2005;13(8):697–708.
38. Yamazaki D, Kurisu S, Takenawa T. Regulation of cancer cell motility through actin reorganization. Cancer Sci. 2005;96(7):379–86.
39. Izdebska M, Zielińska W, Hałas-Wiśniewska M, Grzanka A. Involvement of Actin and Actin-Binding Proteins in Carcinogenesis. *Cells* 2020, 9, (10).
40. Donald CD, Cooper CR, Harris-Hooker S, Emmett N, Scanlon M, Cooke DB 3. Cytoskeletal organization and cell motility correlates with metastatic potential and state of differentiation in prostate cancer. Cell Mol Biol (Noisy-le-grand). 2001;47(6):1033–8.
41. Calzado-Martín A, Encinar M, Tamayo J, Calleja M, San Paulo A. Effect of actin Organization on the stiffness of living breast Cancer cells revealed by peak-force Modulation Atomic Force Microscopy. ACS Nano. 2016;10(3):3365–74.
42. Rianna C, Radmacher M. Influence of microenvironment topography and stiffness on the mechanics and motility of normal and cancer renal cells. Nanoscale. 2017;9(31):11222–30.
43. Solon J, Levental I, Sengupta K, Georges PC, Janmey PA. Fibroblast adaptation and stiffness matching to soft elastic substrates. Biophys J. 2007;93(12):4453–61.
44. Liman J, Bueno C, Eliaz Y, Schafer NP, Waxham MN, Wolynes PG, Levine H, Cheung MS. The role of the Arp2/3 complex in shaping the dynamics and structures of branched actomyosin networks. *Proceedings of the National Academy of Sciences* 2020, 117, (20), 10825–10831.
45. Molinie N, Gautreau A. The Arp2/3 Regulatory System and its Deregulation in Cancer. Physiol Rev. 2018;98(1):215–38.
46. Johnston SA, Bramble JP, Yeung CL, Mendes PM, Machesky LM. Arp2/3 complex activity in filopodia of spreading cells. BMC Cell Biol. 2008;9:65.
47. Jiang X, Dutton CM, Qi WN, Block JA, Garamszegi N, Scully SP. siRNA mediated inhibition of MMP-1 reduces invasive potential of a human chondrosarcoma cell line. J Cell Physiol. 2005;202(3):723–30.
48. Scully SP, Berend KR, Toth A, Qi WN, Qi Z, Block JA. Marshall Urist Award. Interstitial collagenase gene expression correlates with in vitro invasion in human chondrosarcoma. Clin Orthop Relat Res 2000, (376), 291–303.
49. Gittes F, Mickey B, Nettleton J, Howard J. Flexural rigidity of microtubules and actin filaments measured from thermal fluctuations in shape. J Cell Biol. 1993;120(4):923–34.
50. Hawkins T, Mirigian M, Selcuk Yasar M, Ross JL. Mechanics of microtubules. J Biomech. 2010;43(1):23–30.
51. Matis M. The mechanical role of Microtubules in tissue remodeling. BioEssays 2020, 42, (5), e1900244.
52. Plodinec M, Loparic M, Monnier CA, Obermann EC, Zanetti-Dallenbach R, Oertle P, Hyotyla JT, Aebi U, Bentires-Alj M, Lim RY, Schoenenberger CA. The nanomechanical signature of breast cancer. Nat Nanotechnol. 2012;7(11):757–65.
53. Zając A, Król SK, Rutkowski P, Czarnecka AM. Biological Heterogeneity of Chondrosarcoma: From (Epi) Genetics through Stemness and Deregulated Signaling to Immunophenotype. *Cancers (Basel)* 2021, 13, (6).
54. Darling EM, Zauscher S, Block JA, Guilak F. A thin-layer model for viscoelastic, stress-relaxation testing of cells using atomic force microscopy: do cell properties reflect metastatic potential? Biophys J. 2007;92(5):1784–91.
55. Islam M, Mezencev R, McFarland B, Brink H, Campbell B, Tasadduq B, Waller EK, Lam W, Alexeev A, Sulchek T. Microfluidic cell sorting by stiffness to examine heterogenic responses of cancer cells to chemotherapy. Cell Death Dis. 2018;9(2):239.
56. Huxley J. Biological aspects of cancer: Harcourt, Brace. 1958.
57. Alizadeh AA, Aranda V, Bardelli A, Blanpain C, Bock C, Borowski C, Caldas C, Califano A, Doherty M, Elsner M. Toward understanding and exploiting tumor heterogeneity. Nat Med. 2015;21(8):846–53.
58. McGranahan N, Swanton C. Clonal heterogeneity and Tumor Evolution: past, Present, and the future. Cell. 2017;168(4):613–28.
59. Dai Z, Gu X-y, Xiang S-y, Gong D-d, Man C-f:,, Fan Y, editors. Research and application of single-cell sequencing in tumor heterogeneity and drug resistance of circulating tumor cells. *Biomarker Research* 2020, 8, (1), 60.

Publisher's Note

3 Discussion

The biomechanical properties of a tissue are shaped by a multitude of dynamic processes that take place at the cellular level and within the ECM. The type and amount of collagen, the diversity of proteoglycans and their capacity to bind water, and the presence of particular enzymes that support regeneration or degradation are the main variables that will influence the stiffness of a tissue (Panwar et al., 2015; Thibbotuwawa et al., 2021). All of these parameters are highly dependent on the synthesis function of the on-site settled cells (Lu et al., 2011). In turn, those cells display a broad array of sensing mechanisms, in the form of membrane channels, metabolic pathways, cytoskeleton constructs or nuclear force-transmission systems (Burridge and Guilluy, 2016; Lee et al., 2014), which impact gene expression and protein synthesis. Hence, the whole acts as a feedback loop, where both the ECM and the cells have the possibility to transmit information to each other and remodel. All of these complex mechanisms represent as many putative targets for therapy.

Tissue and cell stiffness shape the interaction with the environment and can determine the frontier between health and disease. As is apparent in both of the presented works, stiffness can be a good indicator of the pathological state of a biological system. Consequently, the mechanical properties of tissue/cells may offer a great opportunity to improve existing diagnostic procedures or develop new therapeutical methods. As the field of mechanobiology represent a relatively recent discipline, the need for mechanical characterizations of biological systems and the creation of appropriate models to study them remains considerable.

3.1 Cartilage stiffness: a biological marker throughout the course of osteoarthritis

At the present time, although many of the factors leading to OA are known, our understanding of the key components involved in the modulation of the disease remains limited and the treatment options are poor. Since decades, the field of regenerative medicine has explored the possibilities to comprehend cartilage regeneration (Guilak et al., 2022; Sittinger et al., 1999). The growth of the tissue, its sustainment in a particular environment and its transfer to the in-vivo milieu have revealed themselves to be

remarkably difficult. Some techniques (e.g. microfracture, mosaicplasty, autologous chondrocyte implantation) are applied clinically, principally to attempt reappearing focal damages, and show varying degrees of success (Bentley et al., 2012; van Assche et al., 2010). However, those approaches are not adapted to treat patients suffering from extensive tissue degeneration. Besides cartilage engineering and the use of auto-/allograft to reimplant tissue-depleted regions, another strategy is giving hope to significantly improve the condition of OA patients, namely the use of DMDs. This therapy option relies on the fact that OA is a slowly developing disease that gradually progresses over many years or even decades. Articular cartilage degeneration occurs as the result of prolonged exposure of the tissue to inappropriate mechanical stress (Lee et al., 2017), inflammation (Scanzello, 2017), and uncontrolled enzymatic digestion (Troeberg and Nagase, 2012), with the whole leading to an imbalance between anabolic and catabolic processes. The "re-equilibration" of this fragile balance may participate to tissue protection and lead to a significant slowdown of OA progression. Indeed, several serious candidates have already been identified for a targeted pharmacological modulation. These include the large family of matrix metalloproteinases (MMPs) and A disintegrin and metalloproteinase with thrombospondin motifs (ADAMTSs). For instance, MMP-13 and ADAMTS-5 are known to be closely involved in articular cartilage degradation (Jiang et al., 2021; Mitchell et al., 1996) and have already been targeted by inhibitors as a part of clinical trials (Krzeski et al., 2007; Larkin et al., 2015). Like many other studies using enzyme inhibitors, the beneficial outcome for the patients ranges from moderate to non-significant and the adverse side effects constitute a serious concern, both indicating that further investigations are needed. Another limitation of these studies is that the articular cartilage of the selected patients may have already reached an advanced level of degeneration. It is conceivable that at later OA stages, the damage induced to the tissue may be irreversible, masking a potential effect of the DMDs. Yet, it is complicated to determine a pool of participant manifesting the adequate advancement in the disease, since the early stages of OA cannot be assessed precisely in vivo.

Overall, there are several indications that the modern field of orthopedic research requires new reliable models to develop the most promising technic in terms of diagnostic and therapy for OA. In the present study, we propose the use of cartilage discs that are easy to generate, simple to handle, compatible with standard laboratory methods, and can be

submitted to mechanical measurements. This model may be used to test different diagnostic and therapeutical approaches of OA in vitro and monitor them at the biomechanical level. The fact that the tissue stems from patients undergoing total knee arthroplasty ensure wide availability, which is convenient to conduct routine experiments. On the other hand, it has to be kept in mind that the cartilage originates from osteoarthritic joints. For this reason, it is questionable that the samples labeled as SS effectively represent the healthiest state of the tissue. This fact leads to the limitation that the ideal controls (i.e. SS cartilage discs originating from subjects with healthy joints) may be missing in this model. In the case of our mechanical measurements, it is conceivable that the stiffness measured by the SS discs may already be reduced in comparison to fully healthy cartilage samples.

One of the main advantages of the depicted cartilage discs is their large diameter and their thickness. This allows for the original properties of the tissue to be relatively well preserved and probably makes them comparable to those of the native cartilage in the joint. The exact limits between the different zones in the tissue (superficial, transitional, deep) cannot be clearly drawn, since they are overlapping at their point of transition. In the literature, the proportion of each zone is typically given as the percentage (Ulrich-Vinther et al., 2003) of a total cartilage thickness, therefore varying depending on the investigated specie, the nature of the joint, the location on the articular surface, and the degree of erosion. The discs are 1mm thick, which implies that the superficial zone (≈300µm) is definitely encompassed and a large portion of the transitional zone is also included. Additionally, the original surface of the cartilage systematically remains. This means that the mechanical measurements could be directly performed on the authentic surface, which is naturally exposed to strain within the joint. Other works employed fine cartilage slices processed with microtome (Danalache et al., 2019; Wilusz et al., 2012b). This approach permits removing the eroded cartilage surface and directly exposing a deeper part of the tissue, whose architecture has been better preserved. For instance, this technique enables specifically targeting a desired location (e.g. the PCM). This would not be possible with the actual 1mm discs, unless confocal microscopy is used. On the other hand, with slices in the micrometer range, the bulk of the tissue present in the deep of the indentation point is limited and cannot account for the determination of the stiffness, as is the case in situ. Yet, this may be only a minor concern in the case of AFM indentations

of very few micrometers, but would definitely impact the outcome if the model was submitted to mechanical measurements using indenters working at a larger indentation depth. The need for devices that are able to measure cartilage stiffness in vivo in clinical settings is presently unmet. AFM and numerous other possible candidate techniques (Cykowska et al., 2022) seem to be difficult to implement in clinical settings due to their complex handling and the voluminous aspect of the setups. In this context, fiber Bragg grating (FBG) appears as one of the most promising methods. This optical-fiber based indenter could be used in minimal invasive settings (i.e. could be introduced in an arthroscope) and directly probe patients' cartilage in vivo. The capacity of FBG to discern between different grades of cartilage stiffness using AFM as a reference has already been experimented (Hartmann et al., 2020). Since FBG has a probe diameter of ≈125µm and works at an indentation depth up to 300µm (Marchi et al., 2017), the cartilage discs presented in this protocol would offer the perfect condition for such mechanical trials. Additionally, it would be interesting to test if this device could – based on the measured stiffness similarly to AFM – discriminate between cartilage explants exhibiting different cellular organization patterns.

Concerning the analysis of the data generated with AFM indentation, a disc thickness of 1mm also averts certain shortfalls of the fitting models used to extract the Young's modulus from the force-distance curves. In the case of the present study, a cantilever with a 5µm radius spherical tip was used and the model employed to fit the curves was the classical Hertz model. This model implies several assumptions about the experimental settings, one of which is that the indentation depth remains under 10% of the total thickness of the sample (Krieg et al., 2019). A thickness of 1mm hence permits satisfying this assumption for absolutely any AFM measurements. Another recommendation in order for the model to yield the most accurate estimation of the stiffness is that the indentation depth should not overcome 10% of the indenter's diameter. This is a common problem in the field of mechanical characterization of soft tissue, since a sufficient indentation depth must be reached to gain a representative estimation of the stiffness. Hence, a compromise has to be found. In the present study, the indentation depth ranged up to 3µm for a minority of measurements. Principally the cartilage samples with a high degeneration stage (i.e. BC) were concerned. This rely on the fact that due to the relative softness of altered cartilage, the resistance to indentation is reduced. For this reason, in

order for the tissue to offer a sufficient opposite force to reach the established setpoint (4.477nN in the case of the present study), the compression has to be amplified and the indentation depth increased. There is already evidence in the literature that a higher indentation depth/indenter diameter ratio is still being relatively well supported by the model, if the investigated sample is not too thin (Wu et al., 2016). Nonetheless, to test for the solidity of the fit model on those measurements, we separately performed a data analysis based only on the first 1µm of indentation of such force-distance curves. The results showed that the resulting Young's moduli differed by maximally a few tens of pascals in comparison to the analysis conducted on the totality of the curve (Figure 2 in appendix). These differences can be considered as negligeable and should not interfere with the determination of a trend between the experimental groups, since intervals of up to several kilopascals can be observed between the medians of those groups (e.g. between SS and BC). This information additionally indicates that the experiments could probably also be conducted successfully using a given/fixed indentation depth as a setpoint (e.g. 1µm for all measurements) instead of using a predefined force like in the present case. This would have the advantage to keep the ratio indentation depth/indenter diameter at 10%, thereby better satisfying the theoretical assumptions of the Hertz model.

Alternatively, a cantilever with a larger tip size could be employed in order to minimize the indentation depth/probe-diameter ratio. The choice of the cantilever depends principally on the nature of the sample (e.g. tissue vs cells) and the scale at which the sample should be investigated. Articular cartilage can be mechanically investigated at the micro- or nanoscale. For nanoscale measurements, pyramidal cantilevers with a tip radius in the nanometer range are typically used. With this technique, it is assumed that different molecular territories of the tissue can even be distinguished (Loparic et al., 2010). Given the size of the nano-probe compared to the size and the arrangement of the ECM components (Chen and Broom, 1998; Roughley and Lee, 1994), collagen microfibrils or proteoglycan networks can be encountered separately, hence returning two distinct profiles of stiffness within the same sample. On the other hand, microscale measurements represent an averaged value of those two populations (collagen microfibrils + proteoglycan networks) since the indented surface encompasses both the collagen and the proteoglycans. With a radius of 5µm and a spring constant of 0.15N/m, the cantilever used in the present study is of intermediate size and rigidity in comparison to the probes

typically used for microscale AFM measurements in the literature (Danalache et al., 2020; Stolz et al., 2009; Wilusz et al., 2012b). The fact that the native surface of degenerated cartilage was investigated led to the problem that the texture that directly entered in contact with the cantilever was not plane. Superficial fibrillation and clefting of the tissue complicated the measurements and in the worst case led to substantial artifacts, such as multiple contact points in the force-distance curves. The purpose of the wide cantilever tip used in the present work was hence not only to average the molecular components of the matrix but also the irregularities protruding on the surface of the cartilage. It is conceivable that the fulfillment of this objective could be further refined by the use of a cantilever with a tip radius superior to the actual 5µm in order to average a larger amount of the discontinuous surface. Additionally, the use of a cantilever with a higher spring constant would allow applying a greater force thereby compressing the superficial protrusions to reach a deeper, more representative portion of the tissue.

In the literature, a broad range of values have been described for the stiffness of human articular cartilage, fluctuating from kPa (Darling et al., 2010; Wilusz et al., 2013) to mPa (Loparic et al., 2010; Stolz et al., 2009). In the present study, >90% of the Young's moduli were comprised between 300Pa and 6kPa, which is fairly low compared to the values generally reported, inclusive in comparison to those obtained in previous works of our group (Danalache et al., 2019). From our experience, processed cartilage slices (e.g. 35µm thick sections prepared with a microtome) exhibit a higher stiffness than cartilage samples where the original surface is still preserved. This observation probably relies on the fact that in resected tissue, a relatively flat surface is created, as it is cleanly sliced by the cutting device. Conversely, on a native eroded cartilage surface the fibrillation of the ECM render a loser structure that contributes to weaken its resistance to applied forces. Yet, higher stiffness values also have been reported in a study using similar settings as our (Tschaikowsky et al., 2021). In this work, a cantilever with a 5µm in radius spherical tip was used, the native surface of the cartilage was indented, and the indentation depth was settled to 1µm. The most notable difference to our study design was the thickness of the samples. The discs investigated by Tschaikowsky et al. (2021) were only 300µm thick, although this should not affect the measured stiffness given the comparatively low indentation depth. Particularly for samples classified as healthy (i.e. SS), stiffness maps with Young's moduli of several hundreds of kPa were recorded. We tested our AFM

equipment on commercially available Petri dishes, with a ground stiffness (of several tens of kPa) nominally specified by the manufacturer. The measured Young's moduli were always comparable to the specified values, so that we are confident that our data depict the genuine stiffness of the studied samples.

Real artifacts compromising the reliability of the data are typically detectable by analyzing critically the force-distance curves. This is the case – for instance – when an undesired motion of the disc occurs during the measurement. Hence, an apparently trivial yet decisive aspect of the protocol was the fixation of the disc in its AFM-compatible environment. Following resection, the tissue had generally the tendency to retract slightly, so that the discs were not completely flat but tended to bend at their extremities. Furthermore, due to their thickness, these samples were rather rigid macroscopically and did not always line closely with the bottom of the Petrie dish like – for example – a fine slice of flexible tissue would have done. The result was that the piece of cartilage was sometimes holding in balance into the fluid. In this situation, the fixation of the discs required particular attention. For this purpose, diverse commercially available glues were tested. We deduced that the most appropriate adhesive should present itself in a liquid form in order to line all of the borders of the disc and penetrate in the empty interstices between the sample and the Petri dish. Thus, the glue finally formed a compact block, containing the embedded section of interest after drying. During the indentation measurements, the stability of the disc had to be systematically controlled. This was principally enabled by the observation of the focal plan in the optical microscopy, whose shift would reveal a movement of the sample. Additionally, an unstable disc could commonly be detected in the related force-distance curves, since those displayed a biphasic slope, with an initial portion accounting for the compression of the disc against the ground and a second for the actual indentation of the resulting firmly held tissue.

These concerns related to the physical aspect of the discs may account for the drawback of the model. Although these issues may be further assessed – for instance – by re-sectioning the bottom of the disc to flatten the contact spot with the ground, or diminishing the thickness to facilitate the fit with the Petri dish, any further processing of the tissue was avoided. The two reasons for this were the need to keep the sample as close as possible to the in-situ situation, and avert any supplemental damages of the cells. Further resection of cartilage typically requires to freeze the tissue and the subsequent use

of a cryotome. Although cryotome processed slices have been broadly employed in the literature, the effect on the integrity of the tissue and the cells is uncertain. Our model intends to induce only a minimal traumatic handling of the cartilage, since there are only few processing steps between the harvest and the mechanical measurements. Additionally, the samples can be kept for almost the entire procedure (except the few minutes required to resect the disc to the correct diameter/thickness and glue it to the bottom of the AFM-compatible Petri dish) in medium and at a constant temperature. As the produced discs display a fairly healthy and unaltered tissue, it is conceivable that not only its passive but also dynamic physiological properties can be studied. The samples can be kept in culture for several days and be monitored again at any time point. As an example, the ECM/PCM remodeling which occurs during OA could be investigated. With the development of OA, a decrease in aggrecan amount coupled with a switch from collagen type II to collagen type I content (type II degradation and type I overproduction) can be observed in the ECM (Lahm et al., 2010; Maldonado and Nam, 2013). Subsequently, the water content in the tissue increases. With modern imaging and spectroscopy technics, these parameters can be measured in an atraumatic manner in living tissue (e.g. Fowkes et al., 2022; Padalkar et al., 2013; Ross et al., 2013). A study design including correlation of such relevant parameters with the stiffness of the tissue would be conceivable. Similarly, the critical processes of enzymatic digestions that take place alongside with OA progression could be further investigated, if desired. During cartilage degeneration, a myriad of proteases are active at different time points, different localizations, and target different substrates (Rose and Kooyman, 2016), and these processes can be studied in vitro (Park et al., 2008; Wilusz et al., 2012a). The present model would offer the perfect platform to monitor selective enzymatic digestion optically and at the biomechanical level. Similarly, as the pathways underlying mechanosensing are starting to be elucidated, mainly through experiments being conducted at the level of single cells (Lee et al., 2014), the next step could possibly be carried out in an environment nearing the physiological conditions, on cells embedded in their native PCM, hence enabling all extracellular components to play their important role in filtering the mechanical inputs.

3.2 Mechanical- and cytoskeletal characterization of bone- and soft-tissue cancer cell lines

As interest in mechanobiology within the field of oncology grows, the need for biomechanical characterization of the various tumor entities gains in importance. If this characterization occurred to a certain extent for the "classical"/most common cancer types, the actual available data on this subject concerning the bone and soft-tissue sarcomas remains very scarce. In the presented study, we propose expanding this knowledge by investigating five cell lines that are representative of some of the clinically most relevant sarcomas. Cells from chondrosarcoma, osteosarcoma, Ewing sarcoma, fibrosarcoma and rhabdomyosarcoma lineage were subjected to stiffness measurements with AFM, the organization of their intracellular scaffolding was revealed by microscopical imaging, and gene expression as well as protein levels of some of the most relevant cytoskeleton components were quantified. As controls, the healthy cells corresponding to the different malignant cell lines were used, namely chondrocytes, osteoblasts, MSCs, fibrocytes and SKMCs respectively.

Regarding the cell stiffness, osteosarcomas, Ewing sarcoma, fibrosarcoma and rhabdomyosarcoma appeared less stiff than their corresponding controls. This observation is in line with the established notion that malignant cells are typically less stiff than their healthy counterpart of the originating tissue, a fact that has already been demonstrated for numerous cancer entities of all kinds (e.g. Hayashi and Iwata, 2015, Li et al., 2008, Lekka and Pabijan, 2019). Interestingly, on the other hand, chondrosarcoma cells displayed the opposite characteristic, namely that their stiffness was significantly higher when compared to the obtained values for the chondrocytes. To put this finding into perspective, it first has to be noted that few publications exist in which some cancer cells were indeed reported to be stiffer than their healthy controls. Using AFM indentation, Rosenbluth et al. (2006) found that HL-60 cells (myeloblast isolated from a leukemia patient) were approximately six times stiffer than normal human neutrophils. However liquid tumors represent a peculiar entity, particularly regarding the exposure to stress/strain forces, since those cells – once evaded from the bone marrow – are continuously left to mercy of the blood flow. Another group found that the stiffness of hepatocellular carcinoma (HCC) cells (SMMC 7721 cell line) – measured as the viscoelastic coefficient using micropipette aspiration – was higher than that of normal

hepatocytes (Zhang et al., 2002). However, these results are to be interpreted carefully, since it seemed that the trend could not be observed in every experimental groups. In addition, a recent study using AFM indentation was not able to reproduce those findings: Zeng et al. (2023) explored the stiffness of normal human hepatocytes (HL-7702) and two HCC cell lines (SMMC-7721 and HepG2), yet the malignant cells appeared to be consistently less stiff than the healthy controls. In this last work, it also becomes apparent that albeit derived from the same tumor entity, different tumor cell lines may display a distinct stiffness range. In this case, the HepG2 cells were less stiff than the HL-7702. This fact was also observed for numerous other tumor cell lines of diverse origin, such as between different cell lines of breast cancer (Omidvar et al., 2014), ovarian cancer (Xu et al., 2012), prostate cancer (Lekka and Pabijan, 2019), osteosarcoma (Kita et al., 2021) and even chondrosarcoma themselves (Darling et al., 2007). Darling et al. (2017) investigated the stiffness of FS090, 105KC and JJ012 cells, all of chondrosarcoma origins, with AFM. The reported averaged stiffnesses were 1.27 kPa, 0.78 kPa and 0.34 kPa respectively, but no comparison to control cells of any kind were presented in this publication.

The chondrosarcoma cell line that we choose to conduct our experiments was the SW1353. The median of the measured Young´s moduli in our settings was 0.41 kPa (against 0.24 kPa for the chondrocytes). The SW1353 is a well-established cell line, initially isolated from the tumor of a 72-year-old white female. SW1353 cells have been used for experimental research in the field of oncology to study chondrosarcoma biology (e.g. Jeong et al., 2020) diagnosis (e.g. Lohberger et al., 2012) and response to putative treatment (e.g. Reumann et al., 2016, Veys et al., 2021). Furthermore, the SW1353 have also been employed as a model of OA in the field of orthopedic research because of their demonstrated similarities with chondrocytes (e.g. Pang et al., 2021, Welhaven et al., 2022). However, because of the lacking resemblances between the SW1353 cells and chondrocytes in terms of gene expression and response to particular mediator/transcription factors, the use of this cell line for the purpose of OA research has been questioned (Gebauer et al., 2005). Currently, it is not completely clear from which cells chondrosarcoma primarily originate, although accumulating evidence indicates that it may be MSCs (Boehme et al., 2018). Supporting this hypothesis, an interesting study from Diaz-Romero et al. (2010) investigated the expression of eleven surface markers (=

clusters of differentiation (CDs)) that are relevant for mesenchymal lineage, among human chondrocytes, MSCs, malignant cell lines of different origins, fibrocytes and cells extracted from tumors of chondrosarcoma patients. The different entities were compared using hierarchical clustering, which revealed that chondrosarcoma cells clustered strongly with MSCs but poorly with chondrocytes (Diaz-Romero et al., 2010). Together those findings raise the question of the appropriate control for tumor entities of uncertain origin. In our results, MSCs and SW1353 cells appeared to have a resembling stiffness range (0.38 kPa and 0.41 kPa respectively), with the chondrosarcoma cell line thereby remaining slightly stiffer.

To further investigate the reasons for the changes in stiffness observed with AFM, the main actor responsible for the biomechanical properties of the cell was examined, namely the cytoskeleton. The cytoskeleton is recognized to be the principal contributor to the overall cell stiffness (Galie et al., 2022). Principally actin microfilaments have been shown to be of prime relevance in this regard. Inhibition of actin filament formation by cytochalasin B or latrunculin led to a considerable decrease in cell stiffness (Moeendarbary et al., 2013; Rotsch and Radmacher, 2000), whereas the repression of the FAK-ERK1/2 pathway by salinomycin that led to an accumulation of F-actin in the cell is correlated with stiffness increase (Sun et al., 2017). Additionally, the same authors compared two cell lines of close lineage (liver cancer stem-like cells (LCSCs)) and a human hepatoma cell line (MHCC97H)) and found that the cell stiffness positively correlated with the actin content (Sun et al., 2016). Studies investigating the microtubule´s contribution to the cell´s biomechanical properties are rather inconclusive. Notably, pharmacological disruption (polymerization hindrance) using nocodazole had no significant effect on the stiffness of the cells, as reported by Moeendarbary et al. (2013). On the other hand, using the same drug, Kasas et al. (2005) suggested that only the deeper layers of the cell (i.e. the layer that are dominated by tubulin presence) may be affected by this microtubule destabilization. Our immunostainings against F-actin and β-tubulin revealed evident differences in the cytoskeleton organization between the malignant cells and their healthy counterpart. Concretely, actin forms a clearly discernible structure in controls, such as stress fibers and bundles of appreciable thickness dispersed throughout the cytoplasm, an observation in accordance with previous findings (Li et al., 2008; Stricker et al., 2010). By contrast, the protein was rather confined to the periphery

in a bulky manner in Ewing sarcoma, fibrosarcoma and rhabdomyosarcoma cells. Chondrosarcoma and osteosarcoma displayed an actin organization closer to that of the controls. β-tubulin presented a strong perinuclear presence with decreasing staining intensity towards the cytoplasm's periphery. This pattern was particularly marked in the malignant cells where the boundaries between tubulin- and actin-rich areas were strongly pronounced, except for the chondrosarcoma cells, where a more diffuse repartition could be observed.

To explore the most relevant cytoskeleton components in a quantitative manner, the protein and gene expression levels of F-actin and β-tubulin were determined. The enzyme-linked immunosorbent assays (ELISA) for F-actin revealed a decreased protein amount in malignant cells for the osteosarcomas/osteoblasts, fibrosarcoma/fibroblasts and rhabdomyosarcoma/SKMCs pairs, consolidating the disturbances in the actin scaffold as a putative reason for the observed reduced stiffness in those cancer cell lines. The chondrosarcoma/chondrocytes and Ewing sarcoma/MSCs pairs showed a similar yet statistically not significant trend. The quantitative polymerase chain reaction (qPCR) results indicated a significantly reduced F-actin gene expression in Ewing sarcoma/MSCs and fibrosarcoma/fibroblasts duos. It should be noted that if it is true that the level of gene expression (i.e. mRNA amount) correlates with the effective protein amount in many cases, this does not constitute an absolute rule (Buccitelli and Selbach, 2020). β-tubulin protein levels were substantially decreased in all cancer cells compared to the control, except for the chondrosarcoma group, where a higher amount of the microtubule structural protein was detected. An increased β-tubulin gene expression was also observed in chondrosarcoma cells, whereas no significant differences appeared in the remaining cancer/control pairs. The interesting results of the microtubule quantification may provide an explanation to justify the elevated stiffness in chondrosarcoma cells, and would warrant further exploration by focusing on this particular component of the cytoskeleton. For instance, new series of AFM measurement of the SW1353 cell line under pharmacological disturbance of the microtubules (e.g. with nocodazole) could be considered.

Overall, the presented work investigated the stiffness of five of the most relevant bone and soft-tissue cancers compared to their respective control cells. For most of the malignant/healthy pairs studied, a classical constellation of decreased stiffness and

reduced F-actin content in the cancer cells was observed. However, the chondrosarcoma cell line displayed a surprising profile, with a stiffness superior to chondrocytes (and all other measured sarcoma cell lines) and a marked increase in β-tubulin protein content and gene expression. These results illustrate the relevance of a thorough characterization of the individual cancer entities, particularly when such heterogenous groups as the bone and soft-tissue sarcomas are considered. While in some cases a decrease in the stiffness can be regarded as a common feature of malignancy, certain tumor cells may not follow this precept. The cellular and molecular correlates of the mechanical properties of cells/tissues may be utilized as a label-free biomarker and a putative therapeutic target in the field of oncology. Researchers are currently attempting to use the stiffness shift observed in cancer cells/tissue to develop new diagnostic methods. The idea of taking advantage of stiffness disparities to identify diseased state is not new: for example, more than 20 years ago, macroscopical indentation was successfully employed to distinguish breast tumor from healthy tissue in experimental settings (Wellman et al., 1999). With the advance of stiffness measuring tools and computational methods, the precision of tissue recognition based on mechanical properties has increased. It is now possible using indentation techniques to even distinguish between single components of a tissue (i.e. blood vessels, fat, collagens of different kinds, tumor cells, duct cells of the breast) with a high precision and use this information to identify tumorous structures (Sneider et al., 2022). Furthermore, the accuracy of cell-type differentiation can be increased when mechanical properties are combined with the analysis of additional characteristics of rheological and morphological nature (Nyberg et al., 2018). From a therapeutical point of view, the tumor microenvironment – which encompasses the ECM, stroma cells (i.e. CAFs), immune cells and blood vessels – has stand in the focus of recent research. It is known that the tumor microenvironment is establishing favorable conditions for the development and protection of malignant cells. Particularly, it hinders drug penetration towards the location of interest (Papavassiliou et al., 2023). Targeting CAFs with saridegib – an hedgehog pathway inhibitor – lowers the ECM induced solid stress, allows a better perfusion of the tumorous tissue and hence a better drug penetration (Stylianopoulos et al., 2012). Similarly, reducing collagen type I using angiotensin inhibitors led to a blood vessel decompression and enhanced drug delivery in animal models of pancreatic tumors (Chauhan et al., 2013). Aside from tumor microenvironment

modulation, malignant cells can also be directly targeted. Increasing the membrane stiffness of melanoma cells in vitro by the use of a cholesterol depleter (methyl-β-cyclodextrin) considerably augmented their susceptibility to be killed by T-cells (Lei et al., 2021). This finding could be reproduced in vivo, in an animal model inoculated with tumor cells engineered to over-express a membrane-cholesterol regulator (acyl-CoA:cholesterol acyltransferase 1). The tumor developing from those modified cells, could be better controlled by adoptive T-cell transfer therapy (Lei et al., 2021). Finally, mechanosensors that guarantee the mechanical interface between the cell and its environment also represent an additional element that may be therapeutically addressed. For instance, pharmacologically inhibiting ezrin – a protein linking the actin cytoskeleton to the ECM – significantly reduced the metastasis formation from osteosarcoma in animal models (Bulut et al., 2012). The Yes-associated protein 1 and WW-domain-containing transcription regulator 1 (YAP/TAZ) are a pair of transcriptional factors which are activated by mechanical stress (Dupont, 2016). These two proteins have been shown to be upregulated in several cancer entities, where they confer drug resistance to the malignant cells (Gargalionis et al., 2018). Experimentally shutting down the YAP/TAZ pathway has been shown to restore drug sensitivity in overwise resistant melanomas and non-small cell lung cancers (Kim et al., 2016; Lin et al., 2015). Mechanoreceptors of the piezo family are mechanosensitive ion channels regulating the intracellular calcium concentration. They have been shown to support malignant processes in various cancer types. With a growing array of new drugs targeting the piezo1 and piezo2 channels, those mechanoreceptors represent additional potential targets to hinder cancer growth, local migration of cancer cells and metastasis (Felice and Alaimo, 2020).

Mechanobiology of cancer is a fast-developing field because of the great perspectives it offers with regard to clinical applications. With the goal of improving the diagnostic and therapy options by sensing/modifying the physical properties of tumor cells and environment, the need for a precise characterization of the different malignant entities is growing. The present work aspires to contribute to the effort of investigation of the mechanical properties from bone and soft-tissue sarcomas, a large and diverse group of diseases, with the hope of identifying putative candidates as biomarkers or therapeutical targets.

3.3 Conclusion

The transition from health to disease is characterized by a number of changes at the cellular, tissue and whole organ level. Identifying those changes and attempting to make them reversible – namely the diagnostic process and the therapy initiation – are the successive steps to clinically address a disorder. Aside from morphological, biochemical, and genetical alterations, biomechanical remodeling is nowadays a well-recognized parameter providing important information about the pathology. To sense biomechanical alterations up to the nanoscopic scale, AFM is currently established as the most powerful method.

In a first study, we presented a new in-vitro model to study cartilage alteration during the course of OA. The 4mm in diameter and 1mm thick cartilage discs extracted from femoral condyles of patients undergoing total knee arthroplasty could be successfully classified according to their chondrocytes organization patterns and their stiffness was subsequently measured using AFM indentation. The inherent difficulties in the mechanical investigation of tissue probes of this thickness could be overcome, and a stiffness decrease was reliably observed along with each stage of OA progression.

In a second study, the mechanical properties of five cell lines of five different bone and soft-tissue cancer entities were investigated. The stiffness of the osteosarcoma, Ewing sarcoma, fibrosarcoma, and rhabdomyosarcoma cells showed a substantial decrease in comparison to their respective healthy controls. However, chondrosarcoma cells displayed the opposite trend and were significantly stiffer than chondrocytes. The F-actin and β-tubulin staining revealed a less disorganized cytoskeleton structure in the chondrosarcoma compared to the other malignant groups. Finally, while most of the investigated sarcoma cell lines displayed decreased protein levels of both F-actin and β-tubulin, chondrosarcoma cells appeared to substantially over-express β-tubulin. These findings support the notion that cell stiffness is an appropriate parameter to dissociate between healthy and malignant cells and that the changes in cytoskeleton organization are responsible for this observation. However, if a stiffness decrease associated with disturbance of the actin structure is the most common feature of malignant cells, the stiffness shift may occur in the opposite direction (increase in tumor cells) in some cases, with the microtubule potentially playing a central role in this process.

4 Summary

Mechanobiology encompasses all of the mechanical processes that influence the cell and its environment. Thereby, the major actors are the cell´s structural components (i.e. cell membrane, cytoskeleton), the components of the extracellular matrix (ECM), and the interface between both (i.e. mechanosensors, adhesion molecules). It is well established that biomechanics plays a critical role in the homeostasis of living tissue, but the concrete mechanisms by which mechanical cues are assimilated and regulate the balance between health and disease are not yet fully understood. In recent decades, atomic force microscopy (AFM) has emerged as the gold standard to measure the foremost mechanical marker of a tissue/cell, namely the stiffness (measured as the Young´s modulus). This parameter provides important information about the state of a living entity, and can be used to investigate a diseased/degenerative condition. In the present work, AFM was employed to characterize the biomechanical alterations occurring during two major disorders from the orthopedic field: osteoarthritis (OA) and bone/soft-tissue cancers.

OA is defined as a degenerative joint condition, characterized by articular cartilage destruction. With progression of the disease the chondrocyte organization pattern is evolving, from single string (SS) in healthy cartilage to double string (DS), small cluster (SC), big cluster (BC) and finally diffuse pattern in the most advanced arthritic state. Cartilage discs of 1mm thickness and 4mm diameter were generated from condyles of patient undergoing total knee arthroplasty and were sorted according to the aforementioned cellular patterns. Subsequently the stiffness of the discs was measured with AFM. A stepwise stiffness decrease was observed with an increasing degeneration level, except for the group of the diffuse pattern, which displayed a large data spread with a relatively high stiffness on average. The discs used for those experiments have the advantage of being of appreciable thickness, they exhibit the native cartilage surface at their upmost side and the cells within the tissue are kept alive. They hence represent a suitable model to further investigate articular cartilage degenerative processes in situ.

Bone and soft-tissue sarcomas represent a group of diverse cancer entities from mesenchymal origin, with overall poor prognosis. The stiffness of malignant cells of five different bone and soft-tissue sarcoma cell lines were investigated using AFM and were compared to their respective healthy control cells. Osteosarcoma, Ewing sarcoma, fibrosarcoma and rhabdomyosarcoma cells were significantly less stiff than osteoblasts,

Mesenchymal stem cells (MSCs), fibroblasts and skeletal muscle cells (SKMCs) respectively, reflecting a typical feature observed in most of the neoplastic transformation. However, chondrosarcoma cells appeared to be stiffer than chondrocytes and the other malignant cell lines. Further cytoskeleton examination using fluorescence microscopy, ELISA and qPCR revealed that if most of the malignant cells displayed a disorganized internal scaffold and a decreased F-actin content, chondrosarcoma maintained a cytoskeletal structure relatively close to the one of the healthy cells, with the microtubule being the most affected components (increase in the β-tubulin gene expression and protein content). These results define the biomechanical fingerprints of the investigated cancer cell lines and expose the related molecular mechanisms.

Overall, the work presented in this thesis contributes to the effort of mechanical characterization of the biological systems respectively addressed in the disclosed studies. Understanding the processes underlying the biomechanical properties of cells and tissue is of upmost importance for the development of novel diagnostic and therapy approaches.

5 Zusammenfassung

Die Mechanobiologie bezeichnet alle mechanischen Prozesse, die die Zellen und deren Umfeld beeinflussen. Die Hauptakteure dabei sind die zellulären Gerüstkomponenten (i.e. Zellmembrane, Zytoskelett), die extrazelluläre Matrix und die Verbindung zwischen beiden (i.e. Mechanosensoren, Adhäsionsmoleküle). Es ist anerkannt, dass die Biomechanik eine wichtige Rolle bei der Gewebehomöostase spielt, dennoch sind die konkreten Mechanismen, die der Assimilation von mechanischen Signalen unterliegen und deren Rolle in der Beeinflussung der Gesundheit und von Krankheiten, noch nicht völlig geklärt. In den letzten Jahren, setzte sich die Rasterkraftmikroskopie (AFM) als Goldstandard für die Messung der Steifigkeit (als Young´s Modulus gemessen) von Gewebe und Zellen durch. Dieser Parameter kann relevante Informationen über den Zustand von lebenden Entitäten aufzeigen und kann angewendet werden, um pathologische/degenerative Zustände zu untersuchen. In der vorliegenden Arbeit wurde AFM benutzt, um die biomechanischen Veränderungen, zwei der bedeutendsten Krankheitsspektren in der Orthopädie zu untersuchen: Arthrose und Knochen-/Weichteilsarkome.

Arthrose ist eine degenerative Gelenkerkrankung, gekennzeichnet durch die Zerstörung des hyalinen Knorpels. Mit dem Fortschreiten der Krankheit, Chondrozyten-Organisationsmuster entwickelt sich von single string (SS) im gesunden Knorpel, zu double string (DS), small cluster (SC), big cluster (BC) und letztendlich diffusen Mustern im fortgeschrittenen arthrotischen Zustand. Es wurden Knorpelscheiben, von 1 Millimeter Dicke und 4 Millimeter im Diameter aus Kondylen von Patienten, die für eine Operation zur totalen Knie- Endoprothese geplant waren, herauspräpariert. Die Scheiben wurden je nach ihrem Chondrozyten-Organisationsmuster sortiert und deren Steifigkeit wurde anschließend mit AFM gemessen. Eine schrittweise Reduzierung der Steifigkeit konnte mit steigenden Degenerationsstufen festgestellt werden, außer für die diffuse Mustergruppe, die eine etwas breitere Verteilung der Messwerte und eine relativ hohe durchschnittliche Steifigkeit zeigte. Die für diese Experimente verwendeten Knorpelscheiben boten die Vorteile einer ausgeprägten Dicke, einer verbleibenden nativen Knorpeloberfläche und weiterhin lebendigen Zellen im Gewebe. Dieses Modell eignet sich deshalb besonders gut zur in-situ- Untersuchung der degenerativen Prozesse im Gelenkknorpel.

Knochen- und Weichteilsarkome sind eine sehr heterogene Gruppe von Krebsentitäten mesenchymaler Herkunft, mit insgesamt schlechten Prognosen. Die Steifigkeit bösartiger Zellen von fünf verschiedenen Knochen- und Weichteilsarkomen-Zelllinien wurden mit AFM untersucht und gegenüber deren respektiven gesunden Kontrollzellen verglichen. Osteosarkom-, Ewing-Sarkom-, Fibrosarkom- und Rhabdomyosarkom- Zellen waren signifikant weicher als jeweils Osteoblasten, Mesenchymale Stammzellen (MSCs), Fibroblasten und skelettale Muskelzellen (SKMCs); eine typische Eigenschaft, die bei den meisten malignen Transformationen beobachtet werden kann. Chondrosarkom-Zellen allerdings, zeigten sich steifer als Chondrozyten und die anderen malignen Zelllinien. Die weitere Zytoskelettuntersuchungen anhand fluoreszenter Mikroskopie, ELISA und qPCR zeigten, dass die meisten malignen Zellen ein desorganisiertes, internes Gerüst und einen reduzierten F-Aktin-Gehalt aufwiesen. Jedoch das Chondrosarkom dahingegen erhielt eine zytoskelettale Struktur, relativ ähnlich zu der von gesunden Zellen, mit den Mikrotubuli als die am meisten betroffenen Komponenten (Anstieg der β-Tubulin Genexpression und Proteinmenge). Diese Ergebnisse ermitteln die biomechanischen Eigenschaften der geprüften Tumorzellinien und bestimmen die zugrundeliegenden molekularen Mechanismen.

Die hier vorgestellte Arbeit trägt zu den wissenschaftlichen Bemühungen bei, die jeweils untersuchten biologischen Systeme, mechanisch zu charakterisieren. Das Verständnis der grundlegenden biomechanischen Prozesse in Zellen und Geweben ist von höchster Relevanz für die Entwicklung neuer diagnostischer und therapeutischer Methoden.

6 References

Abidine, Y., Laurent, V. M., Michel, R., Duperray, A. and Verdier, C. (2015) 'Local mechanical properties of bladder cancer cells measured by AFM as a signature of metastatic potential', *The European Physical Journal Plus*, vol. 130, no. 10.

Allison, D. P., Mortensen, N. P., Sullivan, C. J. and Doktycz, M. J. (2010) 'Atomic force microscopy of biological samples', *Wiley interdisciplinary reviews. Nanomedicine and nanobiotechnology*, vol. 2, no. 6, pp. 618–634.

Anderson, N. M. and Simon, M. C. (2020) 'The tumor microenvironment', *Current biology : CB*, vol. 30, no. 16, R921-R925.

Aszódi, A., Legate, K. R., Nakchbandi, I. and Fässler, R. (2006) 'What mouse mutants teach us about extracellular matrix function', *Annual review of cell and developmental biology*, vol. 22, pp. 591–621.

Badylak, S. F. (2007) 'The extracellular matrix as a biologic scaffold material', *Biomaterials*, vol. 28, no. 25, pp. 3587–3593.

Bentley, G., Biant, L. C., Vijayan, S., Macmull, S., Skinner, J. A. and Carrington, R. W. J. (2012) 'Minimum ten-year results of a prospective randomised study of autologous chondrocyte implantation versus mosaicplasty for symptomatic articular cartilage lesions of the knee', *The Journal of bone and joint surgery. British volume*, vol. 94, no. 4, pp. 504–509.

Binnig, Quate and Gerber (1986) 'Atomic force microscope', *Physical review letters*, vol. 56, no. 9, pp. 930–933.

Boehme, K. A., Schleicher, S. B., Traub, F. and Rolauffs, B. (2018) 'Chondrosarcoma: A Rare Misfortune in Aging Human Cartilage? The Role of Stem and Progenitor Cells in Proliferation, Malignant Degeneration and Therapeutic Resistance', *International journal of molecular sciences*, vol. 19, no. 1.

Bos, J. L. (1989) 'ras oncogenes in human cancer: a review', *Cancer research*, vol. 49, no. 17, pp. 4682–4689.

Buccitelli, C. and Selbach, M. (2020) 'mRNAs, proteins and the emerging principles of gene expression control', *Nature reviews. Genetics*, vol. 21, no. 10, pp. 630–644.

Bulut, G., Hong, S.-H., Chen, K., Beauchamp, E. M., Rahim, S., Kosturko, G. W., Glasgow, E., Dakshanamurthy, S., Lee, H.-S., Daar, I., Toretsky, J. A., Khanna, C. and Uren, A. (2012) 'Small molecule inhibitors of ezrin inhibit the invasive phenotype of osteosarcoma cells', *Oncogene*, vol. 31, no. 3, pp. 269–281.

Burridge, K. and Guilluy, C. (2016) 'Focal adhesions, stress fibers and mechanical tension', *Experimental cell research*, vol. 343, no. 1, pp. 14–20.

Butcher, D. T., Alliston, T. and Weaver, V. M. (2009) 'A tense situation: forcing tumour progression', *Nature reviews. Cancer*, vol. 9, no. 2, pp. 108–122.

Cai, X., Yuan, S., Zeng, Y., Wang, C., Yu, N. and Ding, C. (2021) 'New Trends in Pharmacological Treatments for Osteoarthritis', *Frontiers in pharmacology*, vol. 12, p. 645842.

Cameron, M. L., Briggs, K. K. and Steadman, J. R. (2003) 'Reproducibility and reliability of the outerbridge classification for grading chondral lesions of the knee arthroscopically', *The American journal of sports medicine*, vol. 31, no. 1, pp. 83–86.

Chauhan, V. P., Martin, J. D., Liu, H., Lacorre, D. A., Jain, S. R., Kozin, S. V., Stylianopoulos, T., Mousa, A. S., Han, X., Adstamongkonkul, P., Popović, Z., Huang, P., Bawendi, M. G., Boucher, Y. and Jain, R. K. (2013) 'Angiotensin inhibition enhances drug delivery and potentiates chemotherapy by decompressing tumour blood vessels', *Nature communications*, vol. 4, p. 2516.

Chen, M. H. and Broom, N. (1998) 'On the ultrastructure of softened cartilage: a possible model for structural transformation', *Journal of anatomy*, 192 (Pt 3), pp. 329–341.

Cross, S. E., Jin, Y.-S., Rao, J. and Gimzewski, J. K. (2007) 'Nanomechanical analysis of cells from cancer patients', *Nature nanotechnology*, vol. 2, no. 12, pp. 780–783.

Cykowska, A., Danalache, M., Bonnaire, F. C., Feierabend, M. and Hofmann, U. K. (2022) 'Detecting early osteoarthritis through changes in biomechanical properties - A review of recent advances in indentation technologies in a clinical arthroscopic setup', *Journal of biomechanics*, vol. 132, p. 110955.

Danalache, M., Beutler, K. R., Rolauffs, B., Wolfgart, J. M., Bonnaire, F. C., Fischer, S., Greving, I. and Hofmann, U. K. (2021) 'Exploration of changes in spatial chondrocyte organisation in human osteoarthritic cartilage by means of 3D imaging', *Scientific reports*, vol. 11, no. 1, p. 9783.

Danalache, M., Jacobi, L. F., Schwitalle, M. and Hofmann, U. K. (2019) 'Assessment of biomechanical properties of the extracellular and pericellular matrix and their interconnection throughout the course of osteoarthritis', *Journal of biomechanics*, vol. 97, p. 109409.

Danalache, M., Tiwari, A., Sigwart, V. and Hofmann, U. K. (2020) 'Application of Atomic Force Microscopy to Detect Early Osteoarthritis', *Journal of visualized experiments : JoVE*, no. 159.

Darling, E. M., Wilusz, R. E., Bolognesi, M. P., Zauscher, S. and Guilak, F. (2010) 'Spatial mapping of the biomechanical properties of the pericellular matrix of articular cartilage measured in situ via atomic force microscopy', *Biophysical journal*, vol. 98, no. 12, pp. 2848–2856.

Darling, E. M., Zauscher, S., Block, J. A. and Guilak, F. (2007) 'A thin-layer model for viscoelastic, stress-relaxation testing of cells using atomic force microscopy: do cell properties reflect metastatic potential?', *Biophysical journal*, vol. 92, no. 5, pp. 1784–1791.

Deng, B., Zhao, Z., Kong, W., Han, C., Shen, X. and Zhou, C. (2022) 'Biological role of matrix stiffness in tumor growth and treatment', *Journal of translational medicine*, vol. 20, no. 1, p. 540.

Deng, H., Shu, X., Wang, Y., Zhang, J., Yin, Y., Wu, F. and He, J. (2023) 'Matrix Stiffness Regulated Endoplasmic Reticulum Stress-mediated Apoptosis of Osteosarcoma Cell through Ras Signal Cascades', *Cell biochemistry and biophysics*, vol. 81, no. 4, pp. 839–850.

Deng, X., Xiong, F., Li, X., Xiang, B., Li, Z., Wu, X., Guo, C., Li, X., Li, Y., Li, G., Xiong, W. and Zeng, Z. (2018) 'Application of atomic force microscopy in cancer research', *Journal of nanobiotechnology*, vol. 16, no. 1, p. 102.

Deutsches Kinderkrebsregister (2019) 'DKKR_Jahresbericht_2019' [Online]. Available at https://www.kinderkrebsregister.de/dkkr/ergebnisse/jahresberichte/jahresbericht-2019.html.

Diaz-Romero, J., Romeo, S., Bovée, J. V. M. G., Hogendoorn, P. C. W., Heini, P. F. and Mainil-Varlet, P. (2010) 'Hierarchical clustering of flow cytometry data for the study of conventional central chondrosarcoma', *Journal of cellular physiology*, vol. 225, no. 2, pp. 601–611.

D'Lima, D. D., Patil, S., Steklov, N., Chien, S. and Colwell, C. W. (2007) 'In vivo knee moments and shear after total knee arthroplasty', *Journal of biomechanics*, 40 Suppl 1, S11-7.

Dufrêne, Y. F., Ando, T., Garcia, R., Alsteens, D., Martinez-Martin, D., Engel, A., Gerber, C. and Müller, D. J. (2017) 'Imaging modes of atomic force microscopy for application in molecular and cell biology', *Nature nanotechnology*, vol. 12, no. 4, pp. 295–307.

Dupont, S. (2016) 'Role of YAP/TAZ in cell-matrix adhesion-mediated signalling and mechanotransduction', *Experimental cell research*, vol. 343, no. 1, pp. 42–53.

Eschweiler, J., Horn, N., Rath, B., Betsch, M., Baroncini, A., Tingart, M. and Migliorini, F. (2021) 'The Biomechanics of Cartilage-An Overview', *Life (Basel, Switzerland)*, vol. 11, no. 4.

Esiashvili, N., Goodman, M. and Marcus, R. B. (2008) 'Changes in incidence and survival of Ewing sarcoma patients over the past 3 decades: Surveillance Epidemiology and End Results data', *Journal of pediatric hematology/oncology*, vol. 30, no. 6, pp. 425–430.

Eyre, D. (2002) 'Collagen of articular cartilage', *Arthritis research*, vol. 4, no. 1, pp. 30–35.

Eyre, D. R. (2004) 'Collagens and cartilage matrix homeostasis', *Clinical orthopaedics and related research*, 427 Suppl, S118-22.

Felice, D. de and Alaimo, A. (2020) 'Mechanosensitive Piezo Channels in Cancer: Focus on altered Calcium Signaling in Cancer Cells and in Tumor Progression', *Cancers*, vol. 12, no. 7.

Felka, T., Rothdiener, M., Bast, S., Uynuk-Ool, T., Zouhair, S., Ochs, B. G., Zwart, P. de, Stoeckle, U., Aicher, W. K., Hart, M. L., Shiozawa, T., Grodzinsky, A. J., Schenke-Layland, K., Venkatesan, J. K., Cucchiarini, M., Madry, H., Kurz, B. and Rolauffs, B. (2016) 'Loss of spatial organization and destruction of the pericellular matrix in early osteoarthritis in vivo and in a novel in vitro methodology', *Osteoarthritis and cartilage*, vol. 24, no. 7, pp. 1200–1209.

Felson, D. T., Niu, J., Guermazi, A., Sack, B. and Aliabadi, P. (2011) 'Defining radiographic incidence and progression of knee osteoarthritis: suggested modifications of the Kellgren and Lawrence scale', *Annals of the rheumatic diseases*, vol. 70, no. 11, pp. 1884–1886.

Ferguson, J. L. and Turner, S. P. (2018) 'Bone Cancer: Diagnosis and Treatment Principles', *American family physician*, vol. 98, no. 4, pp. 205–213.

Fiorica, J. (2001) 'Prevention and treatment of breast cancer', *Obstetrics and gynecology clinics of North America*, vol. 28, no. 4, pp. 711–726.

Fletcher, D. A. and Mullins, R. D. (2010) 'Cell mechanics and the cytoskeleton', *Nature*, vol. 463, no. 7280, pp. 485–492.

Fowkes, M. M., Das Neves Borges, P., Cacho-Nerin, F., Brennan, P. E., Vincent, T. L. and Lim, N. H. (2022) 'Imaging articular cartilage in osteoarthritis using targeted peptide radiocontrast agents', *PloS one*, vol. 17, no. 5, e0268223.

Fuchs, J., Kuhnert, R. and Scheidt-Nave, C. (2017) *12-Monats-Prävalenz von Arthrose in Deutschland: Journal of Health Monitoring 2(3). RKI*.

Galie, P. A., Georges, P. C. and Janmey, P. A. (2022) 'How do cells stiffen?', *The Biochemical journal*, vol. 479, no. 17, pp. 1825–1842.

Gargalionis, A. N., Basdra, E. K. and Papavassiliou, A. G. (2018) 'Tumor mechanosensing and its therapeutic potential', *Journal of cellular biochemistry*, vol. 119, no. 6, pp. 4304–4308.

Gebauer, M., Saas, J., Sohler, F., Haag, J., Söder, S., Pieper, M., Bartnik, E., Beninga, J., Zimmer, R. and Aigner, T. (2005) 'Comparison of the chondrosarcoma cell line SW1353 with primary human adult articular chondrocytes with regard to their gene expression profile and reactivity to IL-1beta', *Osteoarthritis and cartilage*, vol. 13, no. 8, pp. 697–708.

Gerber, C. and Lang, H. P. (2006) 'How the doors to the nanoworld were opened', *Nature nanotechnology*, vol. 1, no. 1, pp. 3–5.

Gronchi, A., Miah, A. B., Dei Tos, A. P., Abecassis, N., Bajpai, J., Bauer, S., Biagini, R., Bielack, S., Blay, J. Y., Bolle, S., Bonvalot, S., Boukovinas, I., Bovee, J. V. M. G., Boye, K., Brennan, B., Brodowicz, T., Buonadonna, A., Álava, E. de, Del Muro, X. G., Dufresne, A., Eriksson, M., Fagioli, F., Fedenko, A., Ferraresi, V., Ferrari, A., Frezza, A. M., Gasperoni, S., Gelderblom, H., Gouin, F., Grignani, G., Haas, R., Hassan, A. B., Hecker-Nolting, S., Hindi, N., Hohenberger, P., Joensuu, H., Jones, R. L., Jungels, C., Jutte, P., Kager, L., Kasper, B., Kawai, A., Kopeckova, K., Krákorová, D. A., Le Cesne, A., Le Grange, F., Legius, E., Leithner, A., Lopez-Pousa, A., Martin-Broto, J., Merimsky, O., Messiou, C., Mir, O., Montemurro, M., Morland, B., Morosi, C., Palmerini, E., Pantaleo, M. A., Piana, R., Piperno-Neumann, S., Reichardt, P., Rutkowski, P., Safwat, A. A., Sangalli, C., Sbaraglia, M., Scheipl, S., Schöffski, P., Sleijfer, S., Strauss, D., Strauss, S., Sundby Hall, K., Trama, A., Unk, M., van de Sande, M. A. J., van der Graaf, W. T. A., van Houdt, W. J., Frebourg, T., Casali, P. G. and Stacchiotti, S. (2021) 'Soft tissue and visceral sarcomas: ESMO-EURACAN-GENTURIS Clinical Practice Guidelines for diagnosis, treatment and follow-up☆', *Annals of oncology : official journal of the European Society for Medical Oncology*, vol. 32, no. 11, pp. 1348–1365.

Guilak, F. (2011) 'Biomechanical factors in osteoarthritis', *Best practice & research. Clinical rheumatology*, vol. 25, no. 6, pp. 815–823.

Guilak, F., Alexopoulos, L. G., Upton, M. L., Youn, I., Choi, J. B., Cao, L., Setton, L. A. and Haider, M. A. (2006) 'The pericellular matrix as a transducer of biomechanical and biochemical signals in articular cartilage', *Annals of the New York Academy of Sciences*, vol. 1068, pp. 498–512.

Guilak, F., Estes, B. T. and Moutos, F. T. (2022) 'Functional tissue engineering of articular cartilage for biological joint resurfacing-The 2021 Elizabeth Winston Lanier Kappa Delta Award', *Journal of orthopaedic research : official publication of the Orthopaedic Research Society*, vol. 40, no. 8, pp. 1721–1734.

Guilak, F., Nims, R. J., Dicks, A., Wu, C.-L. and Meulenbelt, I. (2018) 'Osteoarthritis as a disease of the cartilage pericellular matrix', *Matrix biology : journal of the International Society for Matrix Biology*, 71-72, pp. 40–50.

Hardingham, T. E. and Fosang, A. J. (1992) 'Proteoglycans: many forms and many functions', *FASEB journal : official publication of the Federation of American Societies for Experimental Biology*, vol. 6, no. 3, pp. 861–870.

Hartmann, B., Marchi, G., Alberton, P., Farkas, Z., Aszodi, A., Roths, J. and Clausen-Schaumann, H. (2020) 'Early Detection of Cartilage Degeneration: A Comparison of Histology, Fiber Bragg Grating-Based Micro-Indentation, and Atomic Force Microscopy-Based Nano-Indentation', *International journal of molecular sciences*, vol. 21, no. 19.

Hayashi, K. and Iwata, M. (2015) 'Stiffness of cancer cells measured with an AFM indentation method', *Journal of the mechanical behavior of biomedical materials*, vol. 49, pp. 105–111.

Hunter, D. J. and Bierma-Zeinstra, S. (2019) 'Osteoarthritis', *The Lancet*, vol. 393, no. 10182, pp. 1745–1759.

Ingber, D. E., Wang, N. and Stamenovic, D. (2014) 'Tensegrity, cellular biophysics, and the mechanics of living systems', *Reports on progress in physics. Physical Society (Great Britain)*, vol. 77, no. 4, p. 46603.

Iozzo, R. V. and Schaefer, L. (2015) 'Proteoglycan form and function: A comprehensive nomenclature of proteoglycans', *Matrix biology : journal of the International Society for Matrix Biology*, vol. 42, pp. 11–55.

Jeong, J. Y., Jeong, W. and Kim, H.-J. (2020) 'Promotion of Chondrosarcoma Cell Survival, Migration and Lymphangiogenesis by Periostin', *Anticancer research*, vol. 40, no. 10, pp. 5463–5469.

Jiang, L., Lin, J., Zhao, S., Wu, J., Jin, Y., Yu, L., Wu, N., Wu, Z., Wang, Y. and Lin, M. (2021) 'ADAMTS5 in Osteoarthritis: Biological Functions, Regulatory

Network, and Potential Targeting Therapies', *Frontiers in molecular biosciences*, vol. 8, p. 703110.

Jiang, T., Zhao, J., Yu, S., Mao, Z., Gao, C., Zhu, Y., Mao, C. and Zheng, L. (2019) 'Untangling the response of bone tumor cells and bone forming cells to matrix stiffness and adhesion ligand density by means of hydrogels', *Biomaterials*, vol. 188, pp. 130–143.

Jin, P., Jan, L. Y. and Jan, Y.-N. (2020) 'Mechanosensitive Ion Channels: Structural Features Relevant to Mechanotransduction Mechanisms', *Annual review of neuroscience*, vol. 43, pp. 207–229.

Karoutsos, V. (2009) 'Scanning probe microscopy: instrumentation and applications on thin films and magnetic multilayers', *Journal of nanoscience and nanotechnology*, vol. 9, no. 12, pp. 6783–6798.

Kasas, S., Wang, X., Hirling, H., Marsault, R., Huni, B., Yersin, A., Regazzi, R., Grenningloh, G., Riederer, B., Forrò, L., Dietler, G. and Catsicas, S. (2005) 'Superficial and deep changes of cellular mechanical properties following cytoskeleton disassembly', *Cell motility and the cytoskeleton*, vol. 62, no. 2, pp. 124–132.

Keene, D. R., Jordan, C. D., Reinhardt, D. P., Ridgway, C. C., Ono, R. N., Corson, G. M., Fairhurst, M., Sussman, M. D., Memoli, V. A. and Sakai, L. Y. (1997) 'Fibrillin-1 in human cartilage: developmental expression and formation of special banded fibers', *The journal of histochemistry and cytochemistry : official journal of the Histochemistry Society*, vol. 45, no. 8, pp. 1069–1082.

KELLGREN, J. H. and LAWRENCE, J. S. (1957) 'Radiological assessment of osteo-arthrosis', *Annals of the rheumatic diseases*, vol. 16, no. 4, pp. 494–502.

Kikuchi, A. (2003) 'Tumor formation by genetic mutations in the components of the Wnt signaling pathway', *Cancer science*, vol. 94, no. 3, pp. 225–229.

Kim, M. H., Kim, J., Hong, H., Lee, S.-H., Lee, J.-K., Jung, E. and Kim, J. (2016) 'Actin remodeling confers BRAF inhibitor resistance to melanoma cells through YAP/TAZ activation', *The EMBO journal*, vol. 35, no. 5, pp. 462–478.

Kita, K., Asanuma, K., Okamoto, T., Kawamoto, E., Nakamura, K., Hagi, T., Nakamura, T., Shimaoka, M. and Sudo, A. (2021) 'Cytoskeletal Actin Structure

in Osteosarcoma Cells Determines Metastatic Phenotype via Regulating Cell Stiffness, Migration, and Transmigration', *Current issues in molecular biology*, vol. 43, no. 3, pp. 1255–1266.

Krieg, M., Fläschner, G., Alsteens, D., Gaub, B. M., Roos, W. H., Wuite, G. J. L., Gaub, H. E., Gerber, C., Dufrêne, Y. F. and Müller, D. J. (2019) 'Atomic force microscopy-based mechanobiology', *Nature Reviews Physics*, vol. 1, no. 1, pp. 41–57.

Krzeski, P., Buckland-Wright, C., Bálint, G., Cline, G. A., Stoner, K., Lyon, R., Beary, J., Aronstein, W. S. and Spector, T. D. (2007) 'Development of musculoskeletal toxicity without clear benefit after administration of PG-116800, a matrix metalloproteinase inhibitor, to patients with knee osteoarthritis: a randomized, 12-month, double-blind, placebo-controlled study', *Arthritis research & therapy*, vol. 9, no. 5, R109.

Lahm, A., Mrosek, E., Spank, H., Erggelet, C., Kasch, R., Esser, J. and Merk, H. (2010) 'Changes in content and synthesis of collagen types and proteoglycans in osteoarthritis of the knee joint and comparison of quantitative analysis with Photoshop-based image analysis', *Archives of orthopaedic and trauma surgery*, vol. 130, no. 4, pp. 557–564.

Larkin, J., Lohr, T. A., Elefante, L., Shearin, J., Matico, R., Su, J.-L., Xue, Y., Liu, F., Genell, C., Miller, R. E., Tran, P. B., Malfait, A.-M., Maier, C. C. and Matheny, C. J. (2015) 'Translational development of an ADAMTS-5 antibody for osteoarthritis disease modification', *Osteoarthritis and cartilage*, vol. 23, no. 8, pp. 1254–1266.

Lee, W., Guilak, F. and Liedtke, W. (2017) 'Role of Piezo Channels in Joint Health and Injury', *Current topics in membranes*, vol. 79, pp. 263–273.

Lee, W., Leddy, H. A., Chen, Y., Lee, S. H., Zelenski, N. A., McNulty, A. L., Wu, J., Beicker, K. N., Coles, J., Zauscher, S., Grandl, J., Sachs, F., Guilak, F. and Liedtke, W. B. (2014) 'Synergy between Piezo1 and Piezo2 channels confers high-strain mechanosensitivity to articular cartilage', *Proceedings of the National Academy of Sciences of the United States of America*, vol. 111, no. 47, E5114-22.

Lei, K., Kurum, A., Kaynak, M., Bonati, L., Han, Y., Cencen, V., Gao, M., Xie, Y.-Q., Guo, Y., Hannebelle, M. T. M., Wu, Y., Zhou, G., Guo, M., Fantner, G. E., Sakar, M. S. and Tang, L. (2021) 'Cancer-cell stiffening via cholesterol depletion enhances adoptive T-cell immunotherapy', *Nature biomedical engineering*, vol. 5, no. 12, pp. 1411–1425.

Lekka, M. and Pabijan, J. (2019) 'Measuring Elastic Properties of Single Cancer Cells by AFM', *Methods in molecular biology (Clifton, N.J.)*, vol. 1886, pp. 315–324.

Li, Q. S., Lee, G. Y. H., Ong, C. N. and Lim, C. T. (2008) 'AFM indentation study of breast cancer cells', *Biochemical and biophysical research communications*, vol. 374, no. 4, pp. 609–613.

Lin, H.-H., Ng, K.-F., Chen, T.-C. and Tseng, W.-Y. (2022) 'Ligands and Beyond: Mechanosensitive Adhesion GPCRs', *Pharmaceuticals (Basel, Switzerland)*, vol. 15, no. 2.

Lin, L., Sabnis, A. J., Chan, E., Olivas, V., Cade, L., Pazarentzos, E., Asthana, S., Neel, D., Yan, J. J., Lu, X., Pham, L., Wang, M. M., Karachaliou, N., Cao, M. G., Manzano, J. L., Ramirez, J. L., Torres, J. M. S., Buttitta, F., Rudin, C. M., Collisson, E. A., Algazi, A., Robinson, E., Osman, I., Muñoz-Couselo, E., Cortes, J., Frederick, D. T., Cooper, Z. A., McMahon, M., Marchetti, A., Rosell, R., Flaherty, K. T., Wargo, J. A. and Bivona, T. G. (2015) 'The Hippo effector YAP promotes resistance to RAF- and MEK-targeted cancer therapies', *Nature genetics*, vol. 47, no. 3, pp. 250–256.

Lo, C. M., Wang, H. B., Dembo, M. and Wang, Y. L. (2000) 'Cell movement is guided by the rigidity of the substrate', *Biophysical journal*, vol. 79, no. 1, pp. 144–152.

Lohberger, B., Rinner, B., Stuendl, N., Absenger, M., Liegl-Atzwanger, B., Walzer, S. M., Windhager, R. and Leithner, A. (2012) 'Aldehyde dehydrogenase 1, a potential marker for cancer stem cells in human sarcoma', *PloS one*, vol. 7, no. 8, e43664.

Loparic, M., Wirz, D., Daniels, A. U., Raiteri, R., Vanlandingham, M. R., Guex, G., Martin, I., Aebi, U. and Stolz, M. (2010) 'Micro- and nanomechanical

analysis of articular cartilage by indentation-type atomic force microscopy: validation with a gel-microfiber composite', *Biophysical journal*, vol. 98, no. 11, pp. 2731–2740.

Lu, P., Takai, K., Weaver, V. M. and Werb, Z. (2011) 'Extracellular matrix degradation and remodeling in development and disease', *Cold Spring Harbor perspectives in biology*, vol. 3, no. 12.

Luyten, F. P., Denti, M., Filardo, G., Kon, E. and Engebretsen, L. (2012) 'Definition and classification of early osteoarthritis of the knee', *Knee surgery, sports traumatology, arthroscopy : official journal of the ESSKA*, vol. 20, no. 3, pp. 401–406.

Makale, M. (2007) 'Cellular mechanobiology and cancer metastasis', *Birth defects research. Part C, Embryo today : reviews*, vol. 81, no. 4, pp. 329–343.

Makris, E. A., Gomoll, A. H., Malizos, K. N., Hu, J. C. and Athanasiou, K. A. (2015) 'Repair and tissue engineering techniques for articular cartilage', *Nature reviews. Rheumatology*, vol. 11, no. 1, pp. 21–34.

Maldonado, M. and Nam, J. (2013) 'The Role of Changes in Extracellular Matrix of Cartilage in the Presence of Inflammation on the Pathology of Osteoarthritis', *BioMed Research International*, vol. 2013, pp. 1–10.

Mammoto, A., Mammoto, T. and Ingber, D. E. (2012) 'Mechanosensitive mechanisms in transcriptional regulation', *Journal of cell science*, vol. 125, Pt 13, pp. 3061–3073.

Marchi, G., Baier, V., Alberton, P., Foehr, P., Burgkart, R., Aszodi, A., Clausen-Schaumann, H. and Roths, J. (2017) 'Microindentation sensor system based on an optical fiber Bragg grating for the mechanical characterization of articular cartilage by stress-relaxation', *Sensors and Actuators B: Chemical*, vol. 252, pp. 440–449.

Martino, F., Perestrelo, A. R., Vinarský, V., Pagliari, S. and Forte, G. (2018) 'Cellular Mechanotransduction: From Tension to Function', *Frontiers in physiology*, vol. 9, p. 824.

Melrose, J., Hayes, A. J., Whitelock, J. M. and Little, C. B. (2008) 'Perlecan, the "jack of all trades" proteoglycan of cartilaginous weight-bearing connective

tissues', *BioEssays : news and reviews in molecular, cellular and developmental biology*, vol. 30, no. 5, pp. 457–469.

Miosge, N., Flachsbart, K., Goetz, W., Schultz, W., Kresse, H. and Herken, R. (1994) 'Light and electron microscopical immunohistochemical localization of the small proteoglycan core proteins decorin and biglycan in human knee joint cartilage', *The Histochemical journal*, vol. 26, no. 12, pp. 939–945.

Mirabello, L., Troisi, R. J. and Savage, S. A. (2009) 'Osteosarcoma incidence and survival rates from 1973 to 2004: data from the Surveillance, Epidemiology, and End Results Program', *Cancer*, vol. 115, no. 7, pp. 1531–1543.

Mitchell, P. G., Magna, H. A., Reeves, L. M., Lopresti-Morrow, L. L., Yocum, S. A., Rosner, P. J., Geoghegan, K. F. and Hambor, J. E. (1996) 'Cloning, expression, and type II collagenolytic activity of matrix metalloproteinase-13 from human osteoarthritic cartilage', *The Journal of clinical investigation*, vol. 97, no. 3, pp. 761–768.

Moeendarbary, E., Valon, L., Fritzsche, M., Harris, A. R., Moulding, D. A., Thrasher, A. J., Stride, E., Mahadevan, L. and Charras, G. T. (2013) 'The cytoplasm of living cells behaves as a poroelastic material', *Nature materials*, vol. 12, no. 3, pp. 253–261.

Müller, D. J., Schabert, F. A., Büldt, G. and Engel, A. (1995) 'Imaging purple membranes in aqueous solutions at sub-nanometer resolution by atomic force microscopy', *Biophysical journal*, vol. 68, no. 5, pp. 1681–1686.

Naji, L., Randhawa, H., Sohani, Z., Dennis, B., Lautenbach, D., Kavanagh, O., Bawor, M., Banfield, L. and Profetto, J. (2018) 'Digital Rectal Examination for Prostate Cancer Screening in Primary Care: A Systematic Review and Meta-Analysis', *Annals of family medicine*, vol. 16, no. 2, pp. 149–154.

Nandi, T. and Ainavarapu, S. R. K. (2021) 'Applications of atomic force microscopy in modern biology', *Emerging topics in life sciences*, vol. 5, no. 1, pp. 103–111.

Nyberg, K. D., Bruce, S. L., Nguyen, A. V., Chan, C. K., Gill, N. K., Kim, T.-H., Sloan, E. K. and Rowat, A. C. (2018) 'Predicting cancer cell invasion by single-

cell physical phenotyping', *Integrative biology : quantitative biosciences from nano to macro*, vol. 10, no. 4, pp. 218–231.

Omidvar, R., Tafazzoli-Shadpour, M., Shokrgozar, M. A. and Rostami, M. (2014) 'Atomic force microscope-based single cell force spectroscopy of breast cancer cell lines: an approach for evaluating cellular invasion', *Journal of biomechanics*, vol. 47, no. 13, pp. 3373–3379.

OUTERBRIDGE, R. E. (1961) 'The etiology of chondromalacia patellae', *The Journal of bone and joint surgery. British volume*, 43-B, pp. 752–757.

Padalkar, M. V., Spencer, R. G. and Pleshko, N. (2013) 'Near infrared spectroscopic evaluation of water in hyaline cartilage', *Annals of biomedical engineering*, vol. 41, no. 11, pp. 2426–2436.

Pang, K.-L., Chow, Y. Y., Leong, L. M., Law, J. X., Ghafar, N. A., Soelaiman, I. N. and Chin, K.-Y. (2021) 'Establishing SW1353 Chondrocytes as a Cellular Model of Chondrolysis', *Life (Basel, Switzerland)*, vol. 11, no. 4.

Panwar, P., Lamour, G., Mackenzie, N. C. W., Yang, H., Ko, F., Li, H. and Brömme, D. (2015) 'Changes in Structural-Mechanical Properties and Degradability of Collagen during Aging-associated Modifications', *The Journal of biological chemistry*, vol. 290, no. 38, pp. 23291–23306.

Papavassiliou, K. A., Basdra, E. K. and Papavassiliou, A. G. (2023) 'The emerging promise of tumour mechanobiology in cancer treatment', *European journal of cancer (Oxford, England : 1990)*, vol. 190, p. 112938.

Park, S., Nicoll, S. B., Mauck, R. L. and Ateshian, G. A. (2008) 'Cartilage mechanical response under dynamic compression at physiological stress levels following collagenase digestion', *Annals of biomedical engineering*, vol. 36, no. 3, pp. 425–434.

Paszek, M. J., Zahir, N., Johnson, K. R., Lakins, J. N., Rozenberg, G. I., Gefen, A., Reinhart-King, C. A., Margulies, S. S., Dembo, M., Boettiger, D., Hammer, D. A. and Weaver, V. M. (2005) 'Tensional homeostasis and the malignant phenotype', *Cancer cell*, vol. 8, no. 3, pp. 241–254.

Payen, T., Oberstein, P. E., Saharkhiz, N., Palermo, C. F., Sastra, S. A., Han, Y., Nabavizadeh, A., Sagalovskiy, I. R., Orelli, B., Rosario, V., Desrouilleres, D.,

Remotti, H., Kluger, M. D., Schrope, B. A., Chabot, J. A., Iuga, A. C., Konofagou, E. E. and Olive, K. P. (2020) 'Harmonic Motion Imaging of Pancreatic Tumor Stiffness Indicates Disease State and Treatment Response', *Clinical cancer research : an official journal of the American Association for Cancer Research*, vol. 26, no. 6, pp. 1297–1308.

Pepin, K. M. and McGee, K. P. (2018) 'Quantifying Tumor Stiffness With Magnetic Resonance Elastography: The Role of Mechanical Properties for Detection, Characterization, and Treatment Stratification in Oncology', *Topics in magnetic resonance imaging : TMRI*, vol. 27, no. 5, pp. 353–362.

Plodinec, M., Loparic, M., Monnier, C. A., Obermann, E. C., Zanetti-Dallenbach, R., Oertle, P., Hyotyla, J. T., Aebi, U., Bentires-Alj, M., Lim, R. Y. H. and Schoenenberger, C.-A. (2012) 'The nanomechanical signature of breast cancer', *Nature nanotechnology*, vol. 7, no. 11, pp. 757–765.

Poole, C. A., Ayad, S. and Gilbert, R. T. (1992) 'Chondrons from articular cartilage. V. Immunohistochemical evaluation of type VI collagen organisation in isolated chondrons by light, confocal and electron microscopy', *Journal of cell science*, 103 (Pt 4), pp. 1101–1110.

Poole, C. A., Gilbert, R. T., Herbage, D. and Hartmann, D. J. (1997) 'Immunolocalization of type IX collagen in normal and spontaneously osteoarthritic canine tibial cartilage and isolated chondrons', *Osteoarthritis and cartilage*, vol. 5, no. 3, pp. 191–204.

Provenzano, P. P. and Keely, P. J. (2011) 'Mechanical signaling through the cytoskeleton regulates cell proliferation by coordinated focal adhesion and Rho GTPase signaling', *Journal of cell science*, vol. 124, Pt 8, pp. 1195–1205.

Quillen, D. M., Wuchner, M. and Hatch, R. L. (2004) 'Acute shoulder injuries', *American family physician*, vol. 70, no. 10, pp. 1947–1954.

Reumann, S., Shogren, K. L., Yaszemski, M. J. and Maran, A. (2016) 'Inhibition of Autophagy Increases 2-Methoxyestradiol-Induced Cytotoxicity in SW1353 Chondrosarcoma Cells', *Journal of cellular biochemistry*, vol. 117, no. 3, pp. 751–759.

Riedl, J. M., Moik, F., Esterl, T., Kostmann, S. M., Gerger, A. and Jost, P. J. (2023) 'Molecular diagnostics tailoring personalized cancer therapy-an oncologist's view', *Virchows Archiv : an international journal of pathology*.

RKI (2023) *Krebs in Deutschland für 2019/2020: Journal of health Monitoring 2(3).*

Rodriguez-Merchan, E. C. (2023) 'The Current Role of Disease-modifying Osteoarthritis Drugs', *The archives of bone and joint surgery*, vol. 11, no. 1, pp. 11–22.

Rolauffs, B., Williams, J. M., Aurich, M., Grodzinsky, A. J., Kuettner, K. E. and Cole, A. A. (2010) 'Proliferative remodeling of the spatial organization of human superficial chondrocytes distant from focal early osteoarthritis', *Arthritis and rheumatism*, vol. 62, no. 2, pp. 489–498.

Rolauffs, B., Williams, J. M., Grodzinsky, A. J., Kuettner, K. E. and Cole, A. A. (2008) 'Distinct horizontal patterns in the spatial organization of superficial zone chondrocytes of human joints', *Journal of structural biology*, vol. 162, no. 2, pp. 335–344.

Rose, B. J. and Kooyman, D. L. (2016) 'A Tale of Two Joints: The Role of Matrix Metalloproteases in Cartilage Biology', *Disease markers*, vol. 2016, p. 4895050.

Ross, K. A., Williams, R. M., Schnabel, L. V., Mohammed, H. O., Potter, H. G., Bradica, G., Castiglione, E., Pownder, S. L., Satchell, P. W., Saska, R. A. and Fortier, L. A. (2013) 'Comparison of Three Methods to Quantify Repair Cartilage Collagen Orientation', *Cartilage*, vol. 4, no. 2, pp. 111–120.

Rotsch, C. and Radmacher, M. (2000) 'Drug-induced changes of cytoskeletal structure and mechanics in fibroblasts: an atomic force microscopy study', *Biophysical journal*, vol. 78, no. 1, pp. 520–535.

Roughley, P. J. and Lee, E. R. (1994) 'Cartilage proteoglycans: structure and potential functions', *Microscopy research and technique*, vol. 28, no. 5, pp. 385–397.

(2022) 'S3-Leitlinie „Adulte Weichgewebesarkome“', *Der Chirurg; Zeitschrift fur alle Gebiete der operativen Medizin*, vol. 93, no. 5, p. 520.

Safiri, S., Kolahi, A.-A., Smith, E., Hill, C., Bettampadi, D., Mansournia, M. A., Hoy, D., Ashrafi-Asgarabad, A., Sepidarkish, M., Almasi-Hashiani, A., Collins, G., Kaufman, J., Qorbani, M., Moradi-Lakeh, M., Woolf, A. D., Guillemin, F., March, L. and Cross, M. (2020) 'Global, regional and national burden of osteoarthritis 1990-2017: a systematic analysis of the Global Burden of Disease Study 2017', *Annals of the rheumatic diseases*, vol. 79, no. 6, pp. 819–828.

Sahin, N. and Yesil, H. (2023) 'Regenerative methods in osteoarthritis', *Best practice & research. Clinical rheumatology*, vol. 37, no. 2, p. 101824.

Scanzello, C. R. (2017) 'Role of low-grade inflammation in osteoarthritis', *Current opinion in rheumatology*, vol. 29, no. 1, pp. 79–85.

Sittinger, M., Perka, C., Schultz, O., Häupl, T. and Burmester, G. R. (1999) 'Joint cartilage regeneration by tissue engineering', *Zeitschrift fur Rheumatologie*, vol. 58, no. 3, pp. 130–135.

Slattery, C. and Kweon, C. Y. (2018) 'Classifications in Brief: Outerbridge Classification of Chondral Lesions', *Clinical orthopaedics and related research*, vol. 476, no. 10, pp. 2101–2104.

Sneider, A., Kiemen, A., Kim, J. H., Wu, P.-H., Habibi, M., White, M., Phillip, J. M., Gu, L. and Wirtz, D. (2022) 'Deep learning identification of stiffness markers in breast cancer', *Biomaterials*, vol. 285, p. 121540.

Stiller, C. A., Trama, A., Serraino, D., Rossi, S., Navarro, C., Chirlaque, M. D. and Casali, P. G. (2013) 'Descriptive epidemiology of sarcomas in Europe: report from the RARECARE project', *European journal of cancer (Oxford, England : 1990)*, vol. 49, no. 3, pp. 684–695.

Stolz, M., Gottardi, R., Raiteri, R., Miot, S., Martin, I., Imer, R., Staufer, U., Raducanu, A., Düggelin, M., Baschong, W., Daniels, A. U., Friederich, N. F., Aszodi, A. and Aebi, U. (2009) 'Early detection of aging cartilage and osteoarthritis in mice and patient samples using atomic force microscopy', *Nature nanotechnology*, vol. 4, no. 3, pp. 186–192.

Stricker, J., Falzone, T. and Gardel, M. L. (2010) 'Mechanics of the F-actin cytoskeleton', *Journal of biomechanics*, vol. 43, no. 1, pp. 9–14.

Stylianopoulos, T., Martin, J. D., Chauhan, V. P., Jain, S. R., Diop-Frimpong, B., Bardeesy, N., Smith, B. L., Ferrone, C. R., Hornicek, F. J., Boucher, Y., Munn, L. L. and Jain, R. K. (2012) 'Causes, consequences, and remedies for growth-induced solid stress in murine and human tumors', *Proceedings of the National Academy of Sciences of the United States of America*, vol. 109, no. 38, pp. 15101–15108.

Sun, J., Luo, Q., Liu, L., Yang, X., Zhu, S. and Song, G. (2017) 'Salinomycin attenuates liver cancer stem cell motility by enhancing cell stiffness and increasing F-actin formation via the FAK-ERK1/2 signalling pathway', *Toxicology*, vol. 384, pp. 1–10.

Sun, J., Luo, Q., Liu, L., Zhang, B., Shi, Y., Ju, Y. and Song, G. (2016) 'Biomechanical profile of cancer stem-like cells derived from MHCC97H cell lines', *Journal of biomechanics*, vol. 49, no. 1, pp. 45–52.

Thibbotuwawa, N., Singh, S. and Gu, Y. (2021) 'Proteoglycan and collagen contribution to the strain-rate-dependent mechanical behaviour of knee and shoulder cartilage', *Journal of the mechanical behavior of biomedical materials*, vol. 124, p. 104733.

Tilghman, R. W., Cowan, C. R., Mih, J. D., Koryakina, Y., Gioeli, D., Slack-Davis, J. K., Blackman, B. R., Tschumperlin, D. J. and Parsons, J. T. (2010) 'Matrix rigidity regulates cancer cell growth and cellular phenotype', *PloS one*, vol. 5, no. 9, e12905.

Troeberg, L. and Nagase, H. (2012) 'Proteases involved in cartilage matrix degradation in osteoarthritis', *Biochimica et biophysica acta*, vol. 1824, no. 1, pp. 133–145.

Tschaikowsky, M., Selig, M., Brander, S., Balzer, B. N., Hugel, T. and Rolauffs, B. (2021) 'Proof-of-concept for the detection of early osteoarthritis pathology by clinically applicable endomicroscopy and quantitative AI-supported optical biopsy', *Osteoarthritis and cartilage*, vol. 29, no. 2, pp. 269–279.

Tsiambas, E., Lefas, A. Y., Georgiannos, S. N., Ragos, V., Fotiades, P. P., Grapsa, D., Stamatelopoulos, A., Kavantzas, N., Patsouris, E. and Syrigos, K. (2016) 'EGFR gene deregulation mechanisms in lung adenocarcinoma: A

molecular review', *Pathology, research and practice*, vol. 212, no. 8, pp. 672–677.

Ulrich-Vinther, M., Maloney, M. D., Schwarz, E. M., Rosier, R. and O'Keefe, R. J. (2003) 'Articular cartilage biology', *The Journal of the American Academy of Orthopaedic Surgeons*, vol. 11, no. 6, pp. 421–430.

van Assche, D., Staes, F., van Caspel, D., Vanlauwe, J., Bellemans, J., Saris, D. B. and Luyten, F. P. (2010) 'Autologous chondrocyte implantation versus microfracture for knee cartilage injury: a prospective randomized trial, with 2-year follow-up', *Knee surgery, sports traumatology, arthroscopy : official journal of the ESSKA*, vol. 18, no. 4, pp. 486–495.

Vasudevan, J., Jiang, K., Fernandez, J. G. and Lim, C. T. (2023) 'Extracellular matrix mechanobiology in cancer cell migration', *Acta biomaterialia*, vol. 163, pp. 351–364.

Veys, C., Benmoussa, A., Contentin, R., Duchemin, A., Brotin, E., Lafont, J. E., Saintigny, Y., Poulain, L., Denoyelle, C., Demoor, M., Legendre, F. and Galéra, P. (2021) 'Tumor Suppressive Role of miR-342-5p in Human Chondrosarcoma Cells and 3D Organoids', *International journal of molecular sciences*, vol. 22, no. 11.

Vincent, T. L., McLean, C. J., Full, L. E., Peston, D. and Saklatvala, J. (2007) 'FGF-2 is bound to perlecan in the pericellular matrix of articular cartilage, where it acts as a chondrocyte mechanotransducer', *Osteoarthritis and cartilage*, vol. 15, no. 7, pp. 752–763.

Vousden, K. H. and Lane, D. P. (2007) 'p53 in health and disease', *Nature reviews. Molecular cell biology*, vol. 8, no. 4, pp. 275–283.

Wadowska, K., Bil-Lula, I., Trembecki, Ł. and Śliwińska-Mossoń, M. (2020) 'Genetic Markers in Lung Cancer Diagnosis: A Review', *International journal of molecular sciences*, vol. 21, no. 13.

Welhaven, H. D., McCutchen, C. N. and June, R. K. (2022) 'Effects of mechanical stimulation on metabolomic profiles of SW1353 chondrocytes: shear and compression', *Biology open*, vol. 11, no. 1.

Wellman, P. S., Howe, R. D., Dalton, E. and Kern, K. A. (1999) 'The Mechanical Properties of Breast Tissues in Compression is Correlated to Histological Diagnosis' [Online]. Available at https://www.biorobotics.harvard.edu/pubs/1999/mechprops.pdf.

Wilusz, R. E., DeFrate, L. E. and Guilak, F. (2012a) 'A biomechanical role for perlecan in the pericellular matrix of articular cartilage', *Matrix biology : journal of the International Society for Matrix Biology*, vol. 31, no. 6, pp. 320–327.

Wilusz, R. E., DeFrate, L. E. and Guilak, F. (2012b) 'Immunofluorescence-guided atomic force microscopy to measure the micromechanical properties of the pericellular matrix of porcine articular cartilage', *Journal of the Royal Society, Interface*, vol. 9, no. 76, pp. 2997–3007.

Wilusz, R. E., Zauscher, S. and Guilak, F. (2013) 'Micromechanical mapping of early osteoarthritic changes in the pericellular matrix of human articular cartilage', *Osteoarthritis and cartilage*, vol. 21, no. 12, pp. 1895–1903.

Wu, C.-E., Lin, K.-H. and Juang, J.-Y. (2016) 'Hertzian load–displacement relation holds for spherical indentation on soft elastic solids undergoing large deformations', *Tribology International*, vol. 97, pp. 71–76.

Wullkopf, L., West, A.-K. V., Leijnse, N., Cox, T. R., Madsen, C. D., Oddershede, L. B. and Erler, J. T. (2018) 'Cancer cells' ability to mechanically adjust to extracellular matrix stiffness correlates with their invasive potential', *Molecular biology of the cell*, vol. 29, no. 20, pp. 2378–2385.

Xu, W., Mezencev, R., Kim, B., Wang, L., McDonald, J. and Sulchek, T. (2012) 'Cell stiffness is a biomarker of the metastatic potential of ovarian cancer cells', *PloS one*, vol. 7, no. 10, e46609.

Yuan, G., Xie, F., Song, Y., Li, Q., Li, R., Hu, X., Zang, M., Cheng, X., Lu, G., Huang, J., Fan, W., Rong, X., Sun, J. and Chen, J. (2022) 'Hepatic Tumor Stiffness Measured by Shear Wave Elastography Is Prognostic for HCC Progression Following Treatment With Anti-PD-1 Antibodies Plus Lenvatinib: A Retrospective Analysis of Two Independent Cohorts', *Frontiers in immunology*, vol. 13, p. 868809.

Zeng, Y., Liu, X., Wang, Z., Gao, W., Li, L. and Zhang, S. (2023) 'Detection and classification of hepatocytes and hepatoma cells using atomic force microscopy and machine learning algorithms', *Microscopy research and technique*, vol. 86, no. 8, pp. 1047–1056.

Zhang, G., Long, M., Wu, Z.-Z. and Yu, W.-Q. (2002) 'Mechanical properties of hepatocellular carcinoma cells', *World journal of gastroenterology*, vol. 8, no. 2, pp. 243–246.

Zhao, Z., Li, Y., Wang, M., Zhao, S., Zhao, Z. and Fang, J. (2020) 'Mechanotransduction pathways in the regulation of cartilage chondrocyte homoeostasis', *Journal of cellular and molecular medicine*, vol. 24, no. 10, pp. 5408–5419.

7 Declaration of contribution

The dissertation work was carried out at the Department of Orthopedic Surgery, University Hospital of Tübingen, Germany under the supervision of Prof. Dr. Nikolaus Wülker.

The study was designed by the following:

1. Dr. Marina Danalache and myself, Department of Orthopedic Surgery, Tübingen for the 1st publication: Daniel et al. (2022), Addressing Practical Issues in Atomic Force Microscopy-Based Micro-indentation on Human Articular Cartilage Explants. *Journal of visualized experiments.*
2. Dr. Marina Danalache, Department of Orthopedic Surgery, Tübingen for the 2nd publication: Daniel et al. (2023), An exploratory study of cell stiffness as a mechanical label-free biomarker across multiple musculoskeletal sarcoma cells. *BMC cancer.*

I had the major contribution for both of the research papers published, with the collaboration and assistance of the co-authors as indicated in the "Authors contribution sections".
I carried out the majority of the experiments and received assistance from Rosa Riester for the AFM measurements, ELISAs and qPCR experiment on the sarcoma cell lines.
The statistical analysis was carried out independently by myself after consultation with Dr. Marina Danalache and Prof. Dr. Christian Konrads.
I confirm that I wrote the thesis by myself and any additional sources of information have been duly cited.
Proofreading for language errors in spelling and grammar was performed by *Wissenschaftslektorat Kelly GmbH.*

Tübingen, den 27.07.2024

8 Acknowledgements

I would like to express my sincere gratitude to my supervisor, Dr. Marina Danalache, for having offering me the chance to be part of this project, for her time and energy spent on the realization of the two papers and the correction of my thesis, and for always being there whenever I needed help or advice. “There is always a solution”, that´s true. Thank you for your support and the unforgettable moments in the lab.

I would like to thank Rosa Riester for the great technical support and the precious instructions given on the different techniques necessary for the realization of this project.

I would also like to extend my gratitude to Dr. Sebastian Höflsauer for having teaching me patiently the handling of the AFM, Dr. Felix Umrath for always having a valuable advice on every scientific topic, Dr. Chen Liang for the support during the publishing process, and Prof. Dr. Wilhelm Aicher and his group for always being ready to help whenever needed.

9 Appendix

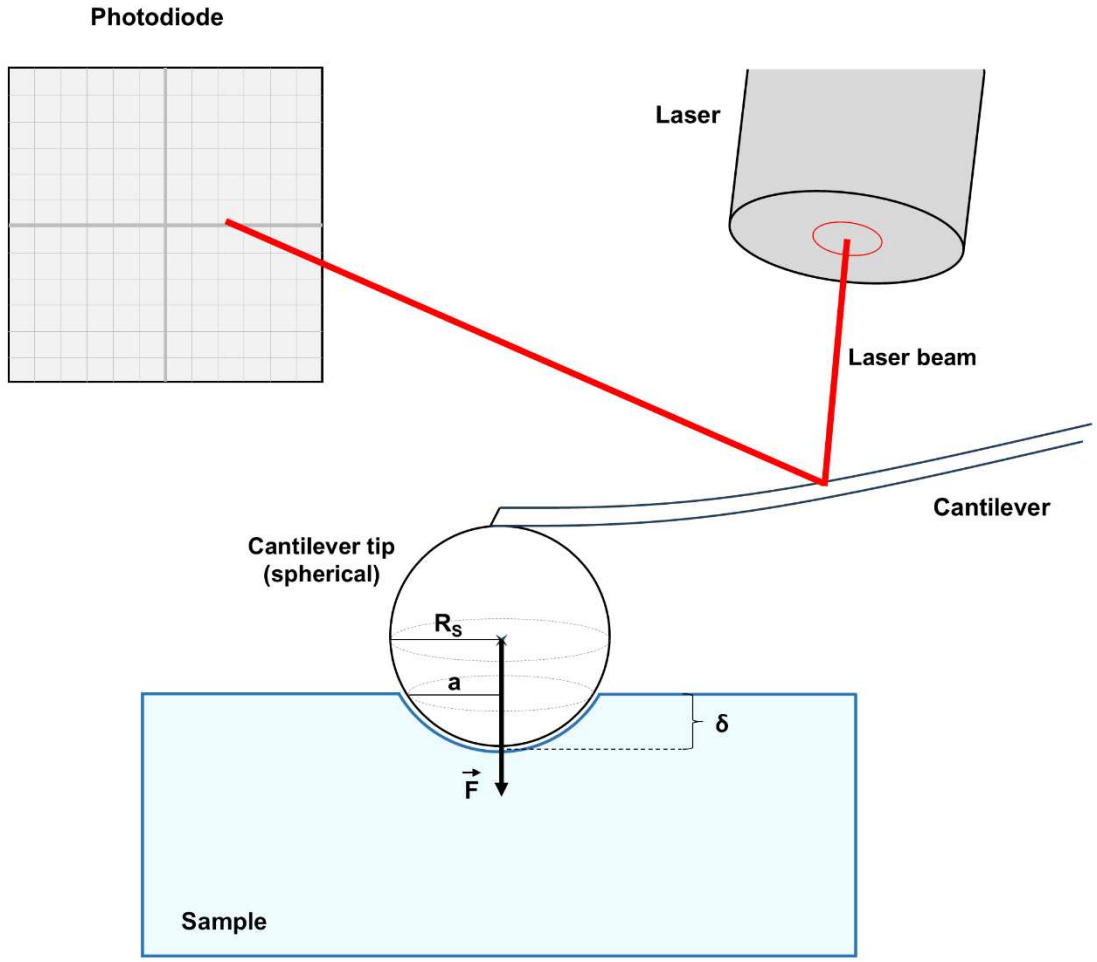

Figure 1 - Principle of stiffness measurement with AFM
The cantilever is represented in deflected state. The laser beam is reflecting at the surface of the cantilever. Variations in the course of the laser beam are monitored using a photodiode panel. The principal variables necessary to calculate the Young´s modulus according to the Hertz-model are indicated in the schema. $\vec{F}$ = vector of the force applied on the sample, δ = indentation depth, R_s = radius spherical cantilever tip, a = radius of contact circle.

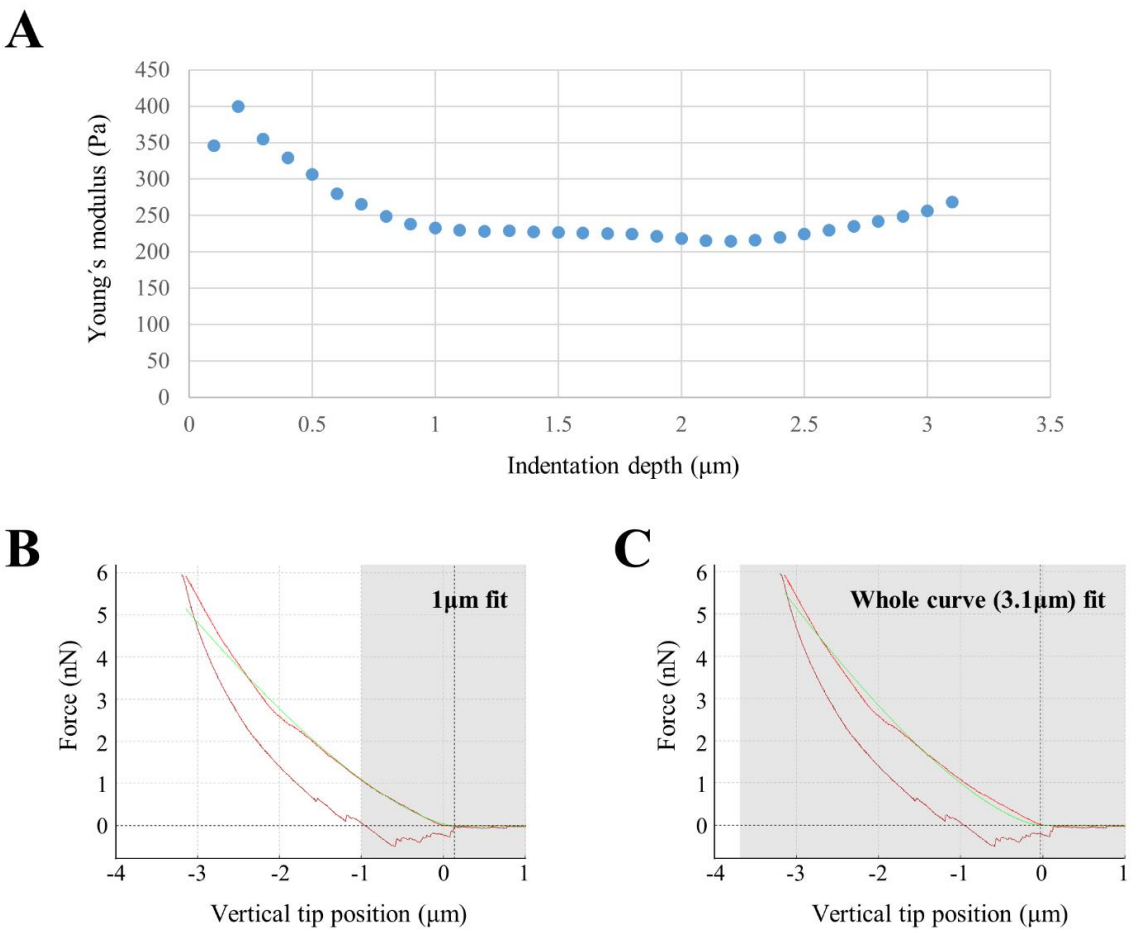

Figure 2 - Impact of the fitted portion of the force-distance curve on the Young´s modulus

The portion of the curve to be fitted using the Hertz-fit-model can be chosen manually. In this figure, the force-distance curve that reached the deepest indentation-depth (one of the measurements performed on a BC cartilage disc) was used to investigate the impact of the of the fitted indentation depth on the calculated Young´s modulus. (**A**) Calculated Young´s modulus as a function of the fitted portion (i.e. indentation depth) of the curve. (**B**) Fit of the extended force-distance curve using only the first 1µm of the indentation depth (the result of the fit is shown in green). (**C**) Fit of the extended force-distance curve using the totality of the indentation depth.